RAY W. HERRICK LABORATORIES

A Graduate Research Facility of The School of Mechanical Engineering

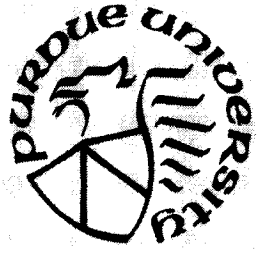

Purdue University

West Lafayette, Indiana 47907

VIBRATIONAL POWER FLOW ANALYSIS OF
RODS AND BEAMS
PRF No. 520 1288-0353

VIBRATIONAL POWER FLOW ANALYSIS OF RODS AND BEAMS

Sponsored by
National Aeronautics And Space Administration

Report No. 0353-12 HL 88-24

Submitted by:

James Christopher Wohlever, Graduate Research Assistant
R. J. Bernhard, Principal Investigator

Approved by:

Raymond Cohen, Director

August, 1988

TABLE OF CONTENTS

LIST OF FIGURES

Figure Page

Figure Page

Figure Page

Figure Page

Figure Page

Figure Page

LIST OF SYMBOLS

Symbol	Description
a	ratio of kinetic energy to total energy
b	ratio of potential energy to total energy
c	phase speed in a rod
c_b	wave velocity in a beam
e	total energy
E	real part of complex modulus E_c
E_c	complex modulus of elasticity
$E_{i,tot}$	total energy in subsystem i
f(x,t)	general forcing function
F	magnitude of general forcing function
I	moment of inertia
j	square root of -1
k	complex wavenumber with hysteretic damping
k_1	real part of k
k_2	imaginary part of k
k_v	complex wavenumber with viscous damping
k_{v1}	real part of k_v
k_{v2}	imaginary part of k_v
L_i	length of rod or beam i
M	moment
n_i	modal density of subsystem i

Symbol	Description
q	vibrational power flow
q_{ij}	vibrational power flow from system i to j
q_{it}	thermal power flow in system i
$q_{i,in}$	power input to system i
S	cross sectional area
t	time
T	kinetic energy
$T(x)$	temperature as a function of position
T_∞	ambient temperature
$u(x)$	position dependent portion of U(x,t)
$U(x,t)$	displacement as a function of position and time
V	potential energy
x	position
$Z_{i,\infty}$	infinite impedance of rod i

Greek Symbols

α_{ij},β_{ij}	mobility functions
$\alpha_\infty,\beta_\infty$	infinite mobility functions
$\bar{\beta}_{ij}$	receptance function
$\delta(x-x_o)$	dirac delta function
η	hysteretic damping coefficient
η_v	viscous damping coefficient
η_{ij}	coupling loss factor
θ_o	angular displacement
$\theta(x)$	$T(x)-T_\infty$
λ	wavelength of vibration
π_{diss}	dissipated power

Symbol	Description
ρ	density
σ_L	linear spring rate
σ_T	torsional spring rate
ω	frequency
Operators	
∂	partial differential
$<>$	time average
$<>_{ff}$	time averaged farfield quantity
$\bar{}$	space average
$()^*$	complex conjugate

ABSTRACT

Wohlever, James Christopher. MSME, Purdue University. August 1988. Vibrational Power Flow Analysis of Rods and Beams. Major Professor: Dr. R.J. Bernhard, School of Mechanical Engineering.

A new method to model vibrational power flow and predict the resulting energy density levels in uniform rods and beams is investigated. This method models the flow of vibrational power in a manner which is analogous to the flow of thermal power in a heat conduction problem.

The classical displacement solutions for harmonically excited, hysteretically damped rods and beams are used to derive expressions for the vibrational power flow and energy density in the rod and beam. Under certain conditions, the power flow in these two structural elements will be shown to be proportional to the gradient of the energy density. Using the relationship between power flow and energy density, an energy balance on differential control volumes in the rod and beam leads to a Poisson's equation which models the energy density distribution in the rod and beam.

Coupling the energy density and power flow solutions for rods and beams is also discussed. It is shown that the resonant behavior of finite structures complicates the coupling of solutions, especially when the excitations are single frequency inputs. Two coupling formulations are discussed. The first coupling

formulation is based on the receptance method. The second coupling scheme is based on the traveling wave approach used in Statistical Energy Analysis. The receptance method is the more computationally intensive method but is capable of analyzing single frequency excitation cases. The traveling wave approach gives a good approximation of the frequency average of energy density and power flow in coupled systems, and thus, is a efficient technique for use with broadband frequency excitation.

CHAPTER 1 - INTRODUCTION

The path by which vibrational (mechanical) power propagates through a structure is an issue of great interest to an engineer concerned with minimizing vibration or noise levels. In many physical situations, vibrations from a remote piece of machinery are transmitted along a structural framework and radiated into an inhabited environment as sound. An example of structure-borne sound is the engine vibrations of an aircraft which travel along the wing and are eventually radiated as sound into the passenger cabin. In a complicated structure, such as an aircraft or building, the ability to map how power flows through the system would greatly facilitate efforts to control structure-borne sound. As discussed by Lu [1], when the main paths of power flow are identified, damping treatments or structural modifications can be optimized to give the highest vibration (acoustic) reductions while minimizing both the cost and weight of the vibration control treatment.

Many complex structures can be modeled as a combination of simple, connected component structures. The dynamic response of a building frame for example, might be analyzed as a system composed of connected beam and plate elements. This type of subdivision is the basis of the popular finite element methods. To study how power flows from one part of the building to another, it

is necessary to understand how an individual beam or plate element conducts mechanical power. Once the power flow in an individual element is understood, it is then necessary to develop a capability to couple the elements into the desired configuration.

Much of the current dynamic structural analysis is done using traditional finite element methods (FEM) [2,3]. However, in complicated acoustic/structural systems the finite element method is usually limited to low frequency analysis. As the frequency increases, the wavelength of vibration decreases. Thus to properly model higher order modes, either the order of the interpolating functions in the FEM must be increased or the size of the elements in the finite element mesh must be decreased [4]. As a result, for accurate high frequency studies, finite element models can quickly become too large for efficient application.

Statistical Energy Analysis (SEA) has become a generally accepted technique for modeling the high frequency, dynamic response of acoustic/structural systems in which high modal density exists. Statistical Energy Analysis treats each component of a built up system as a statistical population of mode groups, and calculates the average dynamic response of the component parts. However, due to simplifying assumptions made in the development of SEA, its accuracy at lower and middle frequencies is limited. In addition, SEA gives no information about the spatial variation of dynamic response within a given subsystem and is generally only valid in the case of a broadband frequency excitation.

The inadequacies of the finite element method and Statistical Energy Analysis have prompted researchers to search for alternative methods of power flow analysis in acoustic/structural systems. This work investigates a new power flow method which could ultimately bridge the mid-frequency range gap where the finite element method is too expensive and Statistical Energy Analysis is unreliable. This alternative power flow method models the flow of mechanical power in a manner which is analogous to the flow of thermal power in a heat conduction problem. The new power flow method has the advantage over the displacement formulations used in the finite element method in that only energy variations are modeled. Since energy variations are simpler than displacement variations, even for higher order modes, the power flow formulation will be an efficient method at high frequency while providing information about the spatial variation of dynamic response within a subsystem. The power flow formulation is also applicable to both single frequency and broadband frequency excitations.

The objectives of this study will be to investigate the power flow in simple one dimensional structures and examine the relationships between energy density and power flow in such structures. In addition, the energy and power flow relationships for coupled simple structures will be studied. Ultimately, these methods should be formulated for numerical methods such that complicated, built-up structures can be modeled. Chapter 2 is a brief literature review of previous work done in vibrational power flow analysis. It will discuss the motivation which led to the development of an alternative power flow

analysis technique. In chapter 3, the classical longitudinal displacement solution of a harmonically excited, hysteretically damped rod is used to develop expressions for the power flow and energy density in a rod. In chapter 4, the classical displacement solution for a transversely vibrating beam is used to develop expressions for the power flow and energy density in a beam. The classical displacement solutions used in chapters 3 and 4 will allow direct assessment of the simplifying assumptions used to develop the governing energy equations for both rods and beams. Chapter 5 will discuss the problems encountered in coupling simple structures using the energy solutions developed in chapters 3 and 4. Some examples comparing the simplified power flow theories developed in chapters 3 and 4 to exact solutions will be presented in chapter 6. Chapter 7 will contain a discussion of results along with recommendations for future research.

CHAPTER 2 - LITERATURE REVIEW

The concept of vibrational power flow through a conductive medium has been considered and utilized for many years. Over one hundred years ago, Lord Rayleigh [5] described the "communication" of vibrational energy between two coupled acoustic systems. However, it has only been in the last twenty five years that the study of vibrational power flow in structural systems has received appreciable attention in the technical literature. This chapter is a short review of some analytical techniques which have been developed for modeling the flow of vibrational power in acoustic/structural systems.

2.1 Statistical Energy Analysis

Statistical Energy Analysis is an analytical technique used to model the flow of power and distribution of vibrational energy in built up acoustic, structural and acoustic/structural systems. SEA models a complex structure as a statistical population of coupled subsystems or mode groups. Each subsystem acts as an energy reservoir with the ability to both store energy and dissipate power. When the power input to each subsystem is a known value, the solution of a SEA model predicts the total energy in each subsystem. The total energy in a subsystem can then be converted into space and time averaged dynamic responses of such physical parameters as displacement, velocity etc.

One of the earliest works in SEA was a study done by Lyon and Maidanik [6] on the power flow between two conservatively coupled, one degree of freedom oscillators (subsystems). Lyon and Maidanik found that when the oscillators were driven by two independent white noise sources (broadband frequency sources):

1) The power flow between the two coupled oscillators is proportional to the difference in the vibrational energies of the two oscillators.

2) The flow of power is from the oscillator of higher energy to the oscillator of lower energy.

3) The power dissipated by an oscillator is proportional to the total energy in that oscillator.

SEA model predictions are based on conservation of power. Power into a subsystem must be dissipated or transmitted to connected subsystems. By predicting power flow from a subsystem of higher energy to a subsystem of lower energy, SEA models the flow of vibrational power in a structure in a manner similar to the flow of heat (thermal energy) in a thermal conduction problem.

SEA was soon extended to multi-degree of freedom and continuous dynamic systems. A complete treatise on Statistical Energy Analysis by Lyon [7], which includes an extensive annotated bibliography on work done in SEA before 1976,

remains the most comprehensive book available, though several other short introductions to SEA have been written by Woodhouse [3], Cremer et al. [8], Maidanik [9] and Fahy [10]. In addition to these introductory guides to Statistical Energy Analysis, several general SEA computer codes, SEAM [11] and COSMIC SEA [12], are available.

Lyon [7] discusses many aspects of SEA, including how built-up systems are modeled, the estimation of dynamical responses from energy values and the evaluation of SEA system parameters. The system parameters in a SEA model include loss factors, modal densities and coupling loss factors. Examples of the evaluation of loss factors and modal densities in plates and shells can be found in work done by Ranky and Clarkson [13] and Clarkson and Pope [14].

A large number of the studies of SEA have been concerned with developing coupling loss factors. The coupling loss factor is a constant of proportionality which models the tendency of power to flow between two connected structures in a SEA model. A common technique to couple structures in SEA is a method known as the "wave transmission approach". The wave transmission approach, introduced by Scharton and Lyon [15], allows the coupling of continuous systems by approximating the frequency averaged, input impedance of a finite structure to be that of an infinite structure. The input impedance of a finite structure is strongly influenced by its resonant behavior. Analytical solutions for the input impedance of finite structures can therefore be quite complex and are generally available only for special cases. The input impedance is also quite

sensitive to slight perturbations in the subsystem. The input impedance of an infinite structure however, exhibits no resonant behavior and is generally a simple function of the material properties and the wave speed in the subsystem. Several authors have presented specific examples which justify modeling finite structures by similar structures of infinite extent. In his book on SEA, Lyon [7] showed the input impedance of a simply supported plate, when averaged over the plate area and over frequency, approached the impedance of an infinite plate. In a separate study, Pinnington and White [16] found that the point mobility of a finite beam, which is the reciprocal of the point impedance, when averaged over frequency is equal to the point mobility of an infinite beam. Cremer et al. [8] generalized the impedance results by showing that for a frequency average, the impedance of a finite structure approaches that of a similar infinite structure. Approximating finite structures by infinite structures greatly simplifies the task of modeling coupled structures.

Remington and Manning [17] calculated the coupling loss factor for two rods vibrating longitudinally, coupled by a linear spring, using the wave transmission approach. Remington and Manning compared their approximate coupling loss factor to an exact closed form solution and found good agreement when the exact solution was averaged over frequency.

Scharton and Lyon [15] also used the wave transmission approach to calculate a coupling loss factor for two simply supported beams coupled by a torsional spring. Newland [18] calculated a coupling loss factor for the same

coupled system studied by Scharton and Lyon. Newland however, calculated his coupling loss factor from a method he introduced known as the "natural frequency shift method" [19]. The natural frequency shift method is a technique by which a coupling loss factor can be calculated for the case of light coupling by evaluating the changes in the natural frequency when two continuous systems are coupled. Crandall and Lotz [20] compared the beam-beam coupling loss factors calculated by Scharton and Lyon and Newland and found that in the case of light coupling the loss factors calculated by each were identical. However, Crandall and Lotz also showed that in the case of strong coupling, the coupling loss factors developed by the two methods did not agree with one another. Crandall and Lotz did not evaluate the accuracy of either method in the case of strong coupling. Later, Davies and Wahab [21], improved the coupling loss factors for strong coupling between the simply supported beams by making approximations on an exact closed form solution based on whether high or low modal overlap existed.

Due to the inherent difficulty involved in their calculation, analytical solutions for the loss factors and coupling loss factors for structural elements may only be partially complete or not available at all. In many applications, the loss factors and coupling loss factors for structural systems must be confirmed or measured experimentally. In comparing SEA predictions with experimental results for cylinder-plate-beam structures, Ghering and Raj [22] concluded that SEA is most reliable when "benchmarked against experimental data so that loss

factors and other parameters can be properly adjusted." In a review of the evaluation of loss and coupling loss factors, Maidanik and Brooks [23] discussed a number of different methods to experimentally determine the loss factors and coupling loss factors for coupled dynamic systems. Maidanik and Brooks explained how loss factors and coupling loss factors could be evaluated by measuring both the input power and resulting energy levels in an experimental set up and back solving for the desired loss parameters. This *in situ* approach of calculating the loss factors and coupling loss factors was demonstrated by Bies and Hamid [24] in calculating the loss factors and coupling loss factors for two coupled plates.

Statistical Energy Analysis has a number of important shortcomings. Since SEA is based on statistical modeling of average system responses, it cannot accurately predict the resonant behavior found in most structures. SEA is generally limited to high frequency, broadband analysis where resonant behavior is less important. In addition, SEA cannot predict the spatial variation of energy in a given subsystem. The output of a SEA model is the total energy which exists in a subsystem. Therefore only average values of displacement, velocity etc. can be calculated. Finally, SEA does not have the capability to model localized or boundary damping mechanisms or local power inputs. These weaknesses in Statistical Energy Analysis have prompted a number of researchers to study vibrational power flow outside the realm of SEA.

2.2 Further Studies in Power Flow

Goyder and White [25] studied the mechanical power flow from machinery into a foundation of beam stiffened plates. Citing work of Skudrzyk [26], Goyder and White modeled the beam-plate foundation as an infinite structure. In effect, Goyder and White assumed that the foundation on which the vibrating machinery was set, was large enough that the propagating waves moving away from the source were attenuated enough so that there were no reflections. Using a spatial Fourier transformation, Goyder and White were able to perform an exact analysis of the infinite model. They found that the power carried by torsional, longitudinal and flexural waves decays exponentially from the source in an infinite, damped beam. Goyder and White also tabulated formulas to calculate the frequencies at which the point mobility of finite beams and plates are well approximated by their infinite counterparts. They found that in a beam-plate foundation, if the input was applied to the beam and was a transverse force or moment, the total power input to the foundation is controlled only by the properties of the beam. As the wave moves away from the power source more power is transmitted by the plate than by the beam.

Pinnington and White [16] continued the work of Goyder and White by investigating the power input to vibration insulators used for vibration control of machinery. Using the mobility model for a beam like insulator, Pinnington and White found that for a force excitation, maximum power is input at the resonant frequencies of the insulator. A velocity excitation has a maximum power input at the antiresonant frequencies.

Independent of the work done by Goyder and White, Belov et al. [27] investigated the optimization of a damping treatment on a beam stiffened plate by modeling the power flow in the plate. To account for the reflections when a wave traveling in a plate encounters a beam, Belov et al. developed reflection coefficients which coupled flexural and longitudinal modes of vibration in the plate. Belov et al. likened the spread of energy in a vibrating structure to the flow of heat in a thermal conduction problem. Using a power balance, Belov et al. developed a set of differential equations "of the heat-conduction type" to model the flow of power in the beam plate structure. Solving this set of differential equations for various arrays of beam patterns Belov et al. optimized the damping treatment on the plate by minimizing the average spectral energy leaving the plate boundaries.

The power flow analyses discussed in this section, though adequate for the specific systems for which they were designed, are not applicable to arbitrary systems. A more useful power flow analysis would be a general method which could be used to accurately model the power flow in a wide range of acoustic/structural systems. The approach to power flow analysis taken by Nefske and Sung, which is discussed in the next section, may be a step in the direction towards a more general and accurate power flow analysis.

2.3 Finite Element Power Flow Analysis

A new method to model the power flow and energy density in structures was recently developed by Nefske and Sung [2]. Nefske and Sung began their

analysis with a simple power balance on a differential control volume in a conductive medium. They based their work on the hypothesis that the power flow in a conductive medium is proportional to the gradient of the energy density. This assumption is analogous to Fourier's law in heat conduction which states that the flow of heat in a material is proportional to the temperature gradient. Using this hypothesis for power flow and assuming that the power dissipated at a point is proportional to the local energy density, Nefske and Sung were able to use a farfield propagating wave analysis to determine energy conduction parameters. These conduction parameters, which are analogous to the thermal conductivity for a heat conduction problem, serve as the constant of proportionality between the power flow and the gradient of energy density. Using these conduction parameters, Nefske and Sung found they could model the power flow and energy density in a simply supported beam with a one dimensional Poisson's equation. The boundary conditions for this problem were known power fluxes. They solved their heat conduction formulation of the vibrating beam problem using a standard MSC/NASTRAN finite element code [28]. Nefske and Sung demonstrated the ability of their power flow method to accurately calculate the displacement of a vibrating beam at frequencies where a traditional displacement finite element formulation could not be used. They also showed how their method could predict the spatial variation of displacement in a beam where SEA could only predict an overall average displacement.

Although Nefske and Sung demonstrated the accuracy of their thermal power flow method for specific cases, the basic premise of their work, which was the relationship between the power flow and energy density in a conductive medium, was never proven explicitly. Thus, there was no way to determine under what conditions the finite element power flow method is valid.

2.4 Summary

As discussed in chapter 1, this study continues the work of analyzing power flow in simple one dimensional structures. In this study however, relationships between the flow of mechanical power and the energy density in rods and beams will be derived from the classical displacement solutions of harmonically excited, hysteretically damped rods and beams. The advantage of deriving the power flow and energy equations from the classical displacement solutions is that the displacement solutions give deterministic relationships which can be used to evaluate the accuracy of the resulting power flow and energy equations. After certain simplifying assumptions are made it will be shown that for certain conditions the power flow in rods and beams can be approximated as being proportional to the gradient in the energy density. The exact nature of the displacement solutions indicate how generally these conditions can be applied. This capability to evaluate the assumptions will give guidelines to determine the conditions for which the analysis is valid. Similarly, the classical displacement solutions will be used to investigate coupling the energy density solutions of rigidly connected, 1-D structures. Local coupling relationships will be explored. In addition, traditional coupling methods will be discussed and evaluated. The

ultimate objective is to implement these coupling methods using numerical methods and thus provide an alternative to FEM and SEA in predicting the energy density levels in built-up, vibrating structures.

CHAPTER 3 - THEORETICAL DEVELOPMENT FOR RODS

3.1 Introduction

In this chapter, the governing equations used to model the power flow through rods will be developed. The power flow and energy density equations will be developed from the classical solutions of displacement in a harmonically driven rod. This analysis is an effort to find a more efficient structural/acoustical model for power flow at medium and high frequency vibration where standard finite element methods become impractical.

The rod is one of the simplest cases of vibrational energy transmission because the equation of motion is a one dimensional second order differential equation with respect to both time and position. After the rod energy equations are developed, similar energy equations will be derived for a beam in chapter 4. Some complications will arise in the beam equations due to the fourth order nature of the equations of motion.

3.2 Rod Equations

The equation of motion for a rod, such as the one shown in figure (3.2.1), excited by a general forcing function is

$$E_c S \frac{\partial^2 U(x,t)}{\partial x^2} = \rho S \frac{\partial^2 U(x,t)}{\partial t^2} - f(x,t) \qquad (3.2.1)$$

where:

$U(x,t)$ is the longitudinal displacement in a rod.

$f(x,t)$ is the distributed forcing function per unit length.

ρS is the density per unit length.

$E_c S$ is the rod stiffness.

The spring end conditions in figure (3.2.1) represent general boundary conditions. For example an infinite spring rate σ_L represents a fixed end while a zero spring rate is a free end. The analysis will allow general impedance boundary conditions.

In this investigation the forcing function will be modeled as a harmonic point force. The harmonic nature of the driving force will simplify the analysis by allowing the time dependency in the governing equation of motion (3.2.1) to be removed. A harmonic point force, $f(x,t)$, may be mathematically represented as

$$f(x,t) = F\ \delta(x-x_o)e^{j\omega t} \tag{3.2.2}$$

where:

$\delta(x-x_o)$ is a dirac delta function. $\left\{ \begin{array}{c} \delta(x-x_o)=0 \text{ if } x \neq x_o \\ \text{and} \\ \int_{-\infty}^{\infty} \delta(x-x_o)dx = 1 \end{array} \right.$

F is the magnitude of forcing function.

ω is the excitation frequency (rads/sec).

A damping term, which models a hysteretic energy absorption mechanism in the rod, may be introduced into the rod formulation by using a complex modulus of elasticity. The complex modulus E_c is

$$E_c = E(1 + j\eta) \tag{3.2.3}$$

where

η is the hysteretic damping coefficient.

Since the force is harmonic, it follows that in steady state vibration, the displacement U(x,t) will also be harmonic in time. Using a separation of variables technique, U(x,t) may be written as

$$U(x,t) = u(x)e^{j\omega t} \tag{3.2.4}$$

Since damping has been introduced into the formulation, u(x) will be complex to account for phase differences between the force and the displacement. Combining equations (3.2.1) through (3.2.4) and canceling $e^{j\omega t}$ gives the governing equation

$$\frac{d^2u(x)}{dx^2} + \frac{\omega^2}{c^2}\,\frac{(1 - j\eta)}{(1 + \eta^2)}\,u(x) = \frac{-F}{E_cS}\,\delta(x-x_o) \tag{3.2.5}$$

where

$c^2 = \dfrac{E}{\rho}$ which is the square of the phase speed.

Equation (3.2.5) can be written more concisely if a complex wavenumber k is defined as

$$k^2 = \frac{\omega^2}{c^2} \frac{(1 - j\eta)}{(1 + \eta^2)} \tag{3.2.6}$$

Thus, the equation of motion is

$$\frac{d^2u(x)}{dx^2} + k^2u(x) = \frac{-F}{E_cS} \delta(x-x_o) \tag{3.2.7}$$

In many applications, the point force will be applied at the end of the rod. In such circumstances the force is most easily dealt with by applying it as a boundary condition. When the excitation is at a boundary, the equation of motion becomes homogeneous

$$\frac{d^2u(x)}{dx^2} + k^2u(x) = 0 \tag{3.2.8}$$

and has a simple solution of the form

$$u(x) = Ae^{-jkx} + Be^{jkx} \tag{3.2.9}$$

The constants A and B in equation (3.2.9) are complex and are determined by applying the boundary conditions.

The boundary conditions for a rod in longitudinal vibration are either a prescribed displacement or strain. The displacement condition at a point $x=x_o$ is

$$u(x_o) = u_o \tag{3.2.10}$$

where u_o is a known constant. A fixed end condition is modeled as $u_o = 0$. A known time harmonic velocity condition at an end is modeled as a constant not

equal to zero. As discussed by Soedel [29], the relationship between the magnitude of an axial point force in a rod and the resulting strain, ϵ, is

$$\epsilon_o = \frac{du}{dx}\Big|_{x=x_o} = \frac{F}{ES} \tag{3.2.11}$$

For the strain boundary condition only the real part of the complex modulus E_c is used. The real part of the modulus is assumed to be a valid approximation since in this analysis light structural damping, $\eta \ll 1$, will be considered. Though using only the real part of the complex modulus is not necessary, it will simplify the analysis. The important effects of the damping in the complex modulus are included in the complex wavenumber k, as defined in equation (3.2.6).

When a point force is applied at an interior point on a rod, it is necessary to divide the rod into two parts at the point of force application in order to find the analytical solution. Figure (3.2.2) shows a rod excited by a harmonic source at $x=x_o$. Figure (3.2.3) shows the rod split into two sections at $x=x_o$. Each rod section has its own displacement solution

$$u_1(x) = Ae^{-jkx} + Be^{jkx} \quad x_1 \leq x \leq x_o \tag{3.2.12}$$

and

$$u_2(x) = Ce^{-jkx} + De^{jkx} \quad x_o \leq x \leq x_2 \tag{3.2.13}$$

Note equations (3.2.12) and (3.2.13) contain four unknown constants. Therefore four boundary conditions must be applied in order to completely specify the problem. At $x=x_1$ and $x=x_2$ either a displacement or slope end condition must

be specified. At $x=x_o$ both a displacement and slope condition must be applied to supply the two remaining boundary conditions.

The first boundary condition at $x=x_o$ is continuity of displacement

$$u_1(x_o) = u_2(x_o) \tag{3.2.14}$$

The second condition at $x=x_o$ is a balance of forces. The internal longitudinal forces in both rods one and two must balance the applied force F. From equation (3.2.11) the force boundary condition is

$$(ES)_1 \left.\frac{du_1}{dx}\right|_{x=x_o} - (ES)_2 \left.\frac{du_2}{dx}\right|_{x=x_o} = F \tag{3.2.15}$$

Using the four boundary conditions, the constants A, B, C and D can be found. The complete solution for displacement in a rod section as a function of position and time is

$$U(x,t) = (Ae^{-jkx}+Be^{jkx})e^{j\omega t} \tag{3.2.16}$$

3.2.1 Power and Energy Equations for a Rod

As discussed in the introduction, one of goals of this analysis is to develop equations which relate the power flow and energy density in a rod. The solution given in equation (3.2.16) will be used to express the energy density and power flow in forms which are easily manipulated. As noted by Kinsler et al. [30] the time averaged power flow and energy density are usually of more interest then the instantaneous values. This analysis will concentrate on time averaged values.

In a rod where only axial forces are present, the power, q, defined locally as the force at a point times the velocity, is written in terms of the displacement as

$$q = -ES\frac{\partial U(x,t)}{\partial x}\ \frac{\partial U(x,t)}{\partial t} \tag{3.2.17}$$

where:

$-ES\frac{\partial U(x,t)}{\partial x}$ is the axial force.

$\frac{\partial U(x,t)}{\partial t}$ is the longitudinal velocity.

The time averaged product of the force and velocity is [31]

$$<(\text{force})(\text{velocity})> = \frac{1}{2}\,\text{Re}[(\text{force})(\text{velocity})^*] \tag{3.2.18}$$

where

$<\ >$ is a time averaged quantity.

Here the expression $(\text{velocity})^*$ is the complex conjugate of the velocity. Substituting equations (3.2.16) and (3.2.17) into equation (3.2.18), the time averaged power flow $<q>$ at a point can be expressed as

$$<q> = \frac{1}{2}\,\omega ES\{k_1[\,|A\,|^2e^{2k_2x} - |B\,|^2e^{-2k_2x}] - 2k_2[\text{Im}(AB^*)\cos 2k_1x - \text{Re}(AB^*)\sin 2k_1x]\} \tag{3.2.19}$$

where

$$k = k_1 + jk_2$$

The energy density is the sum of the potential (V) and kinetic (T) energy densities. For a rod, the potential and kinetic energy densities are

$$V = \frac{1}{2} ES \left(\frac{\partial U}{\partial x} \right)^2 \tag{3.2.20}$$

and

$$T = \frac{1}{2} \rho S \left(\frac{\partial U}{\partial t} \right)^2 \tag{3.2.21}$$

Following the steps used to derive the time averaged power flow, the time averaged potential and kinetic energies are

$$<V> = \frac{1}{4} ES |k|^2 \{ |A|^2 e^{2k_2 x} + |B|^2 e^{-2k_2 x} - 2[Re(AB^*)\cos 2k_1 x + Im(AB^*)\sin 2k_1 x] \} \tag{3.2.22}$$

and

$$<T> = \frac{1}{4} \rho S \omega^2 \{ |A|^2 e^{2k_2 x} + |B|^2 e^{-2k_2 x} + 2[Re(AB^*)\cos 2k_1 x + Im(AB^*)\sin 2k_1 x] \} \tag{3.2.23}$$

The total time averaged energy density at a point, <e>, is the sum of the kinetic and potential energy density. The total energy density is

$$\begin{aligned} <e> = \frac{1}{4} & \{ |A|^2 e^{2k_2 x} + |B|^2 e^{-2k_2 x} \} \{ ES |k|^2 + \rho S \omega^2 \} \\ & - \frac{1}{2} \{ Re(AB^*)\cos 2k_1 x + Im(AB^*)\sin 2k_1 x \} \} \{ ES |k|^2 - \rho S \omega^2 \} \end{aligned} \tag{3.2.24}$$

3.2.2 Simplifying the Power and Energy Expressions for a Rod

Equation (3.2.6) defines the square of the complex wavenumber. Assuming small damping in the rod

$$\eta \ll 1$$

the real and imaginary parts of the wavenumber are approximately

$$k_1 \approx \frac{\omega}{c} \tag{3.2.25}$$

and

$$k_2 \approx -\frac{\eta\omega}{2c} = -\frac{\eta}{2}k_1 \tag{3.2.26}$$

Thus, in this analysis it will be assumed that the imaginary part of the wavenumber is small compared to the real part. This assumption will be used to simplify the analysis and was found to be an excellent approximation for values of damping found in common structural materials such as steel.

Applying the assumption that $|k_1| \gg |k_2|$ to the expression for power flow, equation (3.2.19), it can be assumed that the second term involving the sine and cosine functions is significantly smaller than the first term and may be neglected. Thus, the power is approximately

$$\langle q \rangle \approx \frac{1}{2}\,\omega E S k_1 \{ |A|^2 e^{2k_2 x} - |B|^2 e^{-2k_2 x} \} \tag{3.2.27}$$

To illustrate the difference in the power flow expressions shown in equations (3.2.19) and (3.2.27), consider the harmonically excited rod in figure (3.2.4). The rod in figure (3.2.4) is driven by a harmonic point force at x_o and has a free end condition at x_1. Figure (3.2.5) shows the difference between the exact power flow, equation (3.2.19), and the approximate solution given in equation (3.2.27) when

the following rod parameters are used

$$\text{length of rod} = 5 \text{ m}$$

$$ES = 6 \times 10^7 \text{ N}$$

$$\rho S = 2.358 \text{ kg/m}$$

$$\rho = 7860 \text{ kg/m}^3$$

$$\eta = 0.01$$

$$\omega = 12677.79 \text{ rad/sec}$$

The magnitude of the excitation force has been adjusted so that the power flow into the rod at x_o is unity. Note in figure (3.2.5) that since there is a free end condition, no power can leave the rod at x_1. Equation (3.2.27) approximates the power flow as the sum of two exponential functions. The approximate solution passes through the middle of the exact solution. The component of power flow which is neglected is significantly smaller than the retained terms. In addition, the neglected terms are harmonic functions in space and the approximate solution represents the spatial average of the exact power flow. It will be shown in section 3.3 that the harmonic component of the exact solution for power flow is due to the type of damping used in this model. It is also important to note that with a single power source, (e.g. a single harmonic input), the magnitude of the power flowing through a point in the rod monotonically decreases as one moves away from the power source as expected due to conservation of energy.

Figure (3.2.6) is a plot of the exact, time averaged potential, kinetic and total energy densities from equations (3.2.22), (3.2.23) and (3.2.24), using the

same rod parameters as the power flow solutions used in figure (3.2.5). The potential and kinetic energies in figure (3.2.6) are spatial harmonic functions which are out of phase by 180 degrees. The reason for this phase shift is the form of the displacement solution, equation (3.2.16), and the nature of how potential and kinetic energies are stored. Equation (3.2.20) shows that the potential energy is proportional to the square of the first derivative of displacement with respect to x, while the kinetic energy is proportional to the square of the zeroeth derivative of displacement with respect to x. Though difficult to see in figure (3.2.6), a slight negative gradient does exist in the total energy density indicating the dissipation of power.

The light damping assumption allows a simplification of the energy density expression shown in equation (3.2.24). Using the light damping assumption, the square of the magnitude of the wavenumber is approximately

$$|k|^2 \approx \frac{\omega^2}{c^2}$$

Thus it can be shown that

$$ES|k|^2 \approx ES\frac{\omega^2}{c^2} = ES\frac{\omega^2\rho}{E} = \rho S\omega^2 \qquad (3.2.28)$$

Substituting equation (3.2.28) into (3.2.24) the time averaged total energy density may be written approximately as

$$\langle e \rangle \approx \frac{1}{2}\rho S\omega^2\{|A|^2 e^{2k_2 x} + |B|^2 e^{-2k_2 x}\} \qquad (3.2.29)$$

When the damping is light and the time averaged values are computed, the harmonic components of the potential and kinetic energy densities are essentially equal in magnitude but the negative of one another. The important result of such behavior is that when added together, the harmonic portions of the potential and kinetic energy densities cancel and the exact total energy density is well approximated by the simple expression given in equation (3.2.29). The importance of having no significant harmonic components in the total energy density will become more apparent when the energy density equations for the beam are developed.

3.2.3 Relationship Between Power and Energy Density in a Rod

The gradient of the approximate energy density is

$$\frac{d<e>}{dx} = \rho S \omega^2 k_2 \{ |A|^2 e^{2k_2 x} - |B|^2 e^{-2k_2 x} \} \tag{3.2.30}$$

Dividing the approximate expression for time averaged power, equation (3.2.27), by equation (3.2.30), and solving for <q>, a simple relationship between local power flow and the energy gradient for rods is found to be

$$<q> = -\frac{c^2}{\eta\omega} \frac{d<e>}{dx} \tag{3.2.31}$$

The assumption used in deriving equation (3.2.31) is that hysteretic damping is small $\eta \ll 1$, and thus, $|k_1| \gg |k_2|$.

3.2.4 Energy Balance in a Rod

Figure (3.2.7) shows an energy balance for a differential rod element. The time rate of change of energy within the control volume must be equal to the net power entering the volume minus the power dissipated within the volume. The resulting balance is

$$\frac{\partial e}{\partial t} = -\frac{\partial q}{\partial x} - \pi_{diss} \tag{3.2.32}$$

where:

e is the energy within the differential control volume.

q is the net power flow at a point.

π_{diss} is the power dissipated within the differential control volume.

Using the relationship between the power flow and energy found from the analytical rod solution, equation (3.2.31), the gradient of power flow in equation (3.2.32) can be expressed in terms of the second derivative of the energy density. Also, the time derivative of energy density in equation (3.2.32) is zero since power flow is being studied in a steady state condition. Thus, the time averaged, steady state form of equation (3.2.32) is

$$\frac{c^2}{\eta\omega}\frac{d^2<e>}{dx^2} - <\pi>_{diss} = 0 \tag{3.2.33}$$

3.2.5 Power Dissipation in a Rod

At steady state, equation (3.2.33) shows that the power dissipated at a point is proportional to the second derivative of energy density at that point. Calculating the second derivative of energy density, the power dissipated at a

point, from equation (3.2.33) is

$$<\pi>_{diss} = \frac{1}{2}\rho S\omega^2\eta\omega\left\{|A|^2e^{2k_2x} + |B|^2e^{-2k_2x}\right\} \qquad (3.2.34)$$

Dividing the expression for energy density as given by equation (3.2.29) by equation (3.2.34) and solving for dissipated power leads to the relationship

$$<\pi>_{diss} = \eta\omega <e> \qquad (3.2.35)$$

Thus the energy dissipated at a point is proportional to the energy density at that point, given the assumptions used to derive equations (3.2.29) and (3.2.33). The expression for power dissipation which Nefske and Sung [2] use in their power flow analysis is identical to equation (3.2.35). However, Nefske and Sung developed their power dissipation term from a Statistical Energy Analysis (SEA) assumption that the dissipated power is proportional to the total energy in a system.

3.2.6 Governing Equations for the Energy Density and Power Flow in a Rod

All the necessary equations needed to describe power flow and energy density in a rod have now been developed. Substituting the term for power dissipation, equation (3.2.35), into equation (3.2.33) and rearranging terms, the approximate governing equation of the energy distribution in a rod is

$$\frac{d^2<e>}{dx^2} - \psi^2<e> = 0 \tag{3.2.36}$$

where

$$\psi = \eta\frac{\omega}{c}$$

The assumption used in deriving equation (3.2.36) is that hysteretic damping is small $\eta \ll 1$, and thus, $|k_1| \gg |k_2|$.

The general solution to equation (3.2.36) is

$$<e> = C_1 e^{\psi x} + C_2 e^{-\psi x} \tag{3.2.37}$$

where the constants C_1 and C_2 are determined by applying the boundary conditions, either a specified energy density or power flux condition. The power flow is calculated by substituting equation (3.2.37) into equation (3.2.31) which results in the expression

$$<q> = -c\{C_1 e^{\psi x} - C_2 e^{-\psi x}\} \tag{3.2.38}$$

In this work the boundary conditions will all be power fluxes. This is similar to SEA where input power to a structure is a known parameter but energy levels generally are not.

3.3 Effect of Damping Model

Predicting the damped response of a structure can be approached on several different levels [32]. The most deterministic approach is to study damping on a

microscopic scale. A micromechanistic view attempts to predict the behavior by modeling the interactions between grains in the material and losses due to grain deformation. Though this is the most scientific approach it is usually limited to very special cases of geometry and loading, and is often too complex for efficient application to a mathematical model. More common approaches rely on a macroscopic study of damped behavior. The macroanalytical approach models damping by modifying equations of motion and material properties in an attempt to simulate the observed damped response of structures. However, since damping mechanisms are not completely understood on a macroscopic scale, modeling damping in this manner is not a deterministic process. Certain engineering assumptions are generally made to predict the damped response of a dynamic systems in a cost effective and reasonably accurate manner. Two examples of macroscopic damping schemes are the well known viscous and hysteretic damping models.

In this study, hysteretic damping was introduced into the rod and beam analysis through a complex modulus of elasticity. A hysteretic damping model was chosen over a viscous damping model because a constant hysteretic loss factor predicts results which are more consistent with experimental studies than a constant viscous loss factor [32].

The equations developed in section 3.2 describing power flow and energy in rods are functions of the type and degree of damping used. In spite of the apparent exact nature of the equations of motion, the uncertainty of how to

accurately model damping introduces a level of error into these relations. It is difficult to determine how closely the exact and simplified solutions for power and energy match what happens in real systems.

Figure (3.2.5) illustrates how the simplified solution for power flow in a rod, equation (3.2.27), differs from the apparent exact solution of equation (3.2.19). The simplified model decays exponentially away from the power source. The exact curve oscillates about this simplified model. The explanation of why these curves differ can be found by studying the power dissipation terms.

The power dissipation in the exact solution for a rod is more readily understood by using an equivalent viscous damping model. Consider the equation of motion for a rod, equation (3.2.1). A viscous damping term may be introduced into the forcing function, f(x,t), in equation (3.2.1) as

$$f(x,t) = F\delta(x-x_o)e^{j\omega t} - \eta_v \frac{\partial U(x,t)}{\partial t} \tag{3.3.1}$$

where

η_v is the viscous damping coefficient.

Substituting this force into equation (3.2.1) and removing the time dependence, the equation of motion is

$$\frac{d^2u}{dx^2} + \left(\frac{\omega^2}{c^2} - j\frac{\omega\eta_v}{ES}\right)u(x) = \frac{-F}{ES}\,\delta(x-x_o) \tag{3.3.2}$$

In equation (3.3.2), the modulus of elasticity is a real value since viscous damping is being modeled. Following the same procedures used in section 3.2,

the equation of motion can be simplified to

$$\frac{d^2u}{dx^2} + k_v{}^2u(x) = 0 \tag{3.3.3}$$

where the complex viscous wavenumber k_v is defined

$$k_v{}^2 = \left(\frac{\omega^2}{c^2} - j\frac{\omega\eta_v}{ES}\right) \tag{3.3.4}$$

Assuming again that the viscous damping is small, the components of k_v may be written approximately as

$$k_{v1} \approx \frac{\omega}{c} \tag{3.3.5}$$

$$k_{v2} \approx -\frac{\eta_v}{2\rho Sc} \tag{3.3.6}$$

Comparing the real and imaginary parts of the hysteretic wavenumber in a rod, equations (3.2.25), (3.2.26), to their counterparts for viscous damping given above, equivalent viscous damping implies that

$$k_1 = k_{v1} \tag{3.3.7}$$

$$k_2 = k_{v2} \tag{3.3.8}$$

For the equalities to be satisfied the equivalent viscous damping coefficient in terms of the hysteretic damping factor is

$$\eta_v = \rho S\omega\eta \tag{3.3.9}$$

It is important to note that for a constant hysteretic loss factor, η, the

equivalent viscous damping is a function of frequency. The result in equation (3.3.9) is derived by Soedel [29].

The local viscous damping force in equation (3.3.1) is

$$F_v = \eta_v \frac{\partial U(x,t)}{\partial t} \tag{3.3.10}$$

The power dissipated by the damping mechanism is the damping force times the local velocity

$$<\pi_{exact}>_{diss} = \frac{1}{2}Re\left[F_v\left(\frac{\partial U}{\partial t}\right)^*\right] = \frac{1}{2}\eta_v\left|\frac{\partial U}{\partial t}\right|^2 \tag{3.3.11}$$

From equation (3.2.21), the time averaged kinetic energy in a rod is

$$<T> = \frac{1}{4}\rho S\left|\frac{\partial U}{\partial t}\right|^2 \tag{3.3.12}$$

Thus, the dissipated power and kinetic energy are related as

$$<\pi_{exact}>_{diss} = \frac{2\eta_v}{\rho S}<T> \tag{3.3.13}$$

Using the equivalent damping factor in equation (3.3.9), this relationship may be rewritten as

$$<\pi_{exact}>_{diss} = 2\eta\omega<T> \tag{3.3.14}$$

Equation (3.3.14) indicates that the exact solution predicts that the power dissipated at a point is directly proportional to the local kinetic energy density. Equation (3.3.14) can be verified by plotting the potential and kinetic energy densities, shown in figure (3.2.6), with the exact power flow solution, shown in

figure (3.2.5). Such a plot is shown in figure (3.3.1). Note in figure (3.3.1) that at a maximum of kinetic energy the slope of the power flow is also maximum. From the discussion in section 3.2.4, it was shown that at steady state, the power dissipated at a point is equal to the negative of the slope of the power flow. Where the kinetic energy is zero the slope of the power flow is zero, indicating no power is dissipated. The harmonic component of the exact power flow is due to the spatial variation of the kinetic energy.

The simplified theory for power flow does not distinguish between potential and kinetic energies. It models the total energy density in the rod. Because the simplified model does not differentiate between energy types, it could not be expected to model power dissipation as proportional to the kinetic energy alone as the exact solution does. Equation (3.2.35) shows that in the simplified model the power dissipated at a point is proportional to the total energy density.

The average power dissipated over a wavelength using the exact formulation is

$$\bar{<\pi_{exact}>}_{diss}=\frac{1}{\lambda}\int_{x}^{x+\lambda}<\pi_{exact}>d\sigma = \frac{1}{2\lambda}(\eta\omega)\rho S\omega^2\left\{\frac{1}{2k_2}\left[|A|^2e^{2k_2\sigma}-|B|^2e^{-2k_2\sigma}\right]\right.$$
$$\left.+\frac{1}{k_1}\left[Re(AB^*)sink_1\sigma-Im(AB^*)cosk_1\sigma\right]\right\}\Bigg|_{x}^{x+\lambda} \qquad (3.3.15)$$

where λ is a wavelength of vibration and is defined for light damping as

$$\lambda = \frac{2\pi}{k} \approx \frac{2\pi}{k_1}$$

The harmonic terms in equation (3.3.15) go to zero when evaluated between x

and x+λ. Thus, the exact average power dissipated over a wavelength is

$$<\bar{\pi}_{exact}>_{diss} = \frac{1}{4k_2\lambda}(\eta\omega)\rho S\omega^2\{|A|^2e^{2k_2\sigma} - |B|^2e^{-2k_2\sigma}\}\Big|_x^{x+\lambda} \qquad (3.3.16)$$

A similar calculation for power dissipation using the simplified model gives

$$<\bar{\pi}>_{diss} = \frac{1}{4k_2\lambda}(\eta\omega)\rho S\omega^2\{|A|^2e^{2k_2\sigma} - |B|^2e^{-2k_2\sigma}\}\Big|_x^{x+\lambda} \qquad (3.3.17)$$

The average power dissipated over a wavelength, or an integer number of wavelengths, by the simplified and exact solutions is identical in spite of the fact that the spatial profiles of the two power flow solutions are different. It is important to note that the power dissipated by the exact and simplified solutions are identical only when integrated over an integer number of wavelengths. This is because in equation (3.3.15), the harmonic portions of the exact solution go to zero only when integrated over an integer number of wavelengths. In essence, the simplified model averages the power absorption over a wavelength.

A similar comparison of the exact and simplified theories for a beam, to be discussed in chapter 4, would produce results analogous to those for a rod. For the exact solution of a beam, power is dissipated in proportion to the local kinetic energy levels while the simplified theory models the dissipation of power in proportion to the average total energy density.

Due to the uncertain nature of damping models, it is difficult to say if the exact or simplified solution is a more accurate representation of the power

dissipation. Experimental data on the detailed spatial variation of power flow in rods or beams are not widely published in literature. For purposes of medium to high frequency analyses of energy in structures, the simplified solution models the actual power absorption mechanism in rods and beams well enough to predict accurate average energy and power flow values.

3.4 Summary

Equation (3.2.31) shows that for the assumption that hysteretic damping is small $\eta \ll 1$:

1) $|k_1| \gg |k_2|$.

2) $<q>$ is approximated by equation (3.2.27).

3) $<e>$ is approximated by equation (3.2.29).

Using these assumptions it was found that the power flow in a rod is proportional to the gradient of energy density. Furthermore, the control volume analysis shown in figure (3.2.7) along with the relationship between power dissipation and energy density allows the development of a Poisson's equation (3.2.36) which models the power flow and energy distribution in a rod. Thus, the thermal conduction analogy, which was discussed in the introduction, for studying the power flow and energy density in a rod is a valid model for conditions of small hysteretic damping.

With respect to damping models, equation (3.3.14) showed that in the exact solution, hysteretic damping results in power dissipation in proportion to the local kinetic energy. The simplified theory models power dissipation in proportion to the total energy density. Thus, the difference of power flow between the exact and simplified power flow solutions can be attributed to the different ways in which each models power dissipation. However, at medium to high frequencies, these differences are small and the simplified model is a good engineering model of power flow in rods.

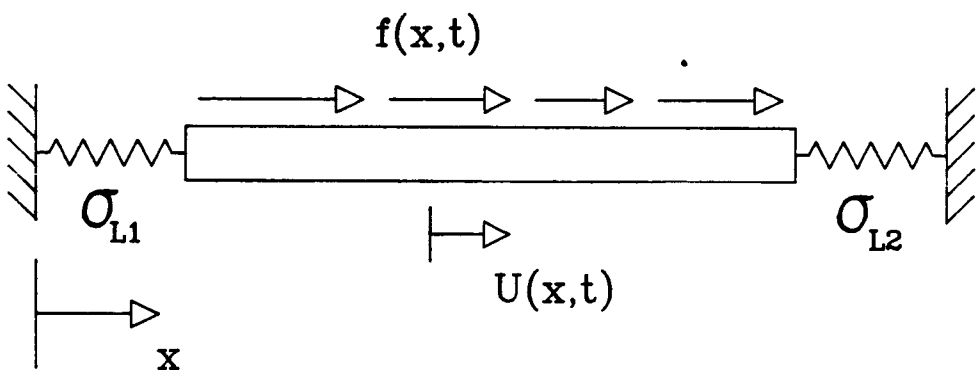

Figure 3.2.1 - Longitudinally Vibrating Rod Excited by a Distributed Forcing Function with General Spring Boundary Conditions

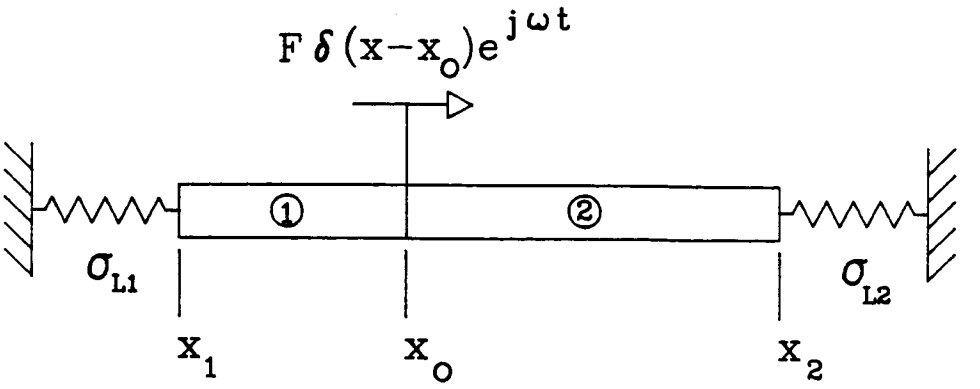

Figure 3.2.2 - Longitudinally Vibrating Rod Excited by a Harmonic Point Force at x_o with General Spring Boundary Conditions

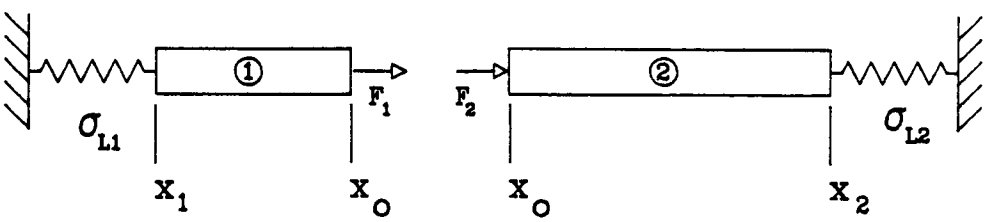

Figure 3.2.3 - Longitudinally Vibrating Rod from Figure (3.2.2) Split into Two Components to Allow the Harmonic Point Force to be Applied as a Boundary Condition

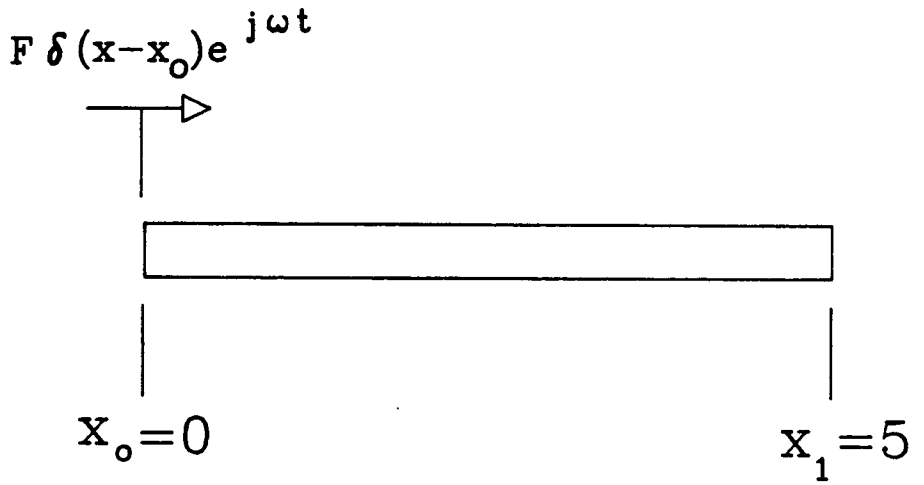

Figure 3.2.4 - Longitudinally Vibrating Rod Excited by a Harmonic Point Force at x_o with a Free End Condition at x_1

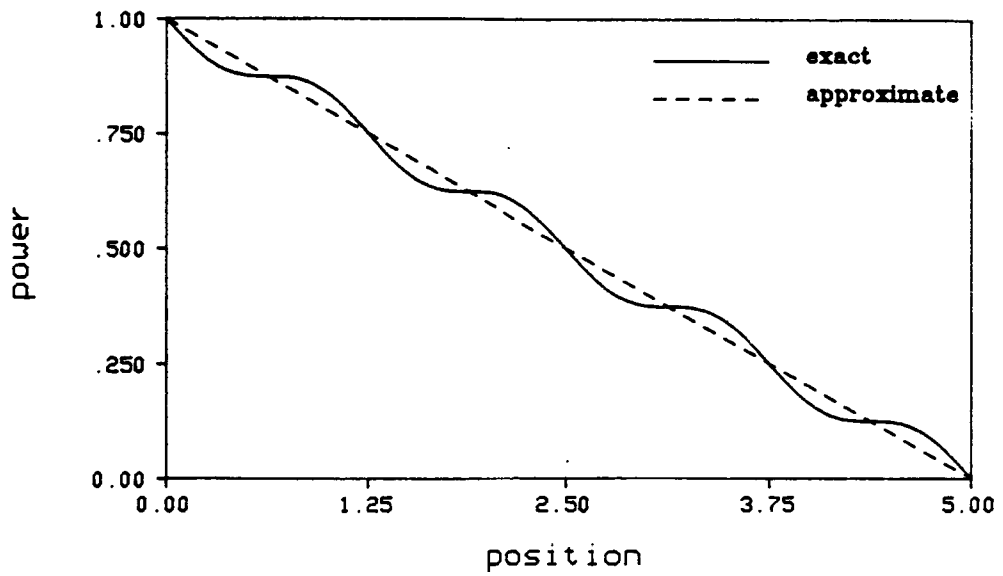

Figure 3.2.5 - Comparison of the Power Flow Solutions for the Longitudinally Vibrating Rod Shown in Figure (3.2.4) Using an Exact Solution, Shown in Equation (3.2.19), and the Approximate Solution, Shown in Equation (3.2.27)

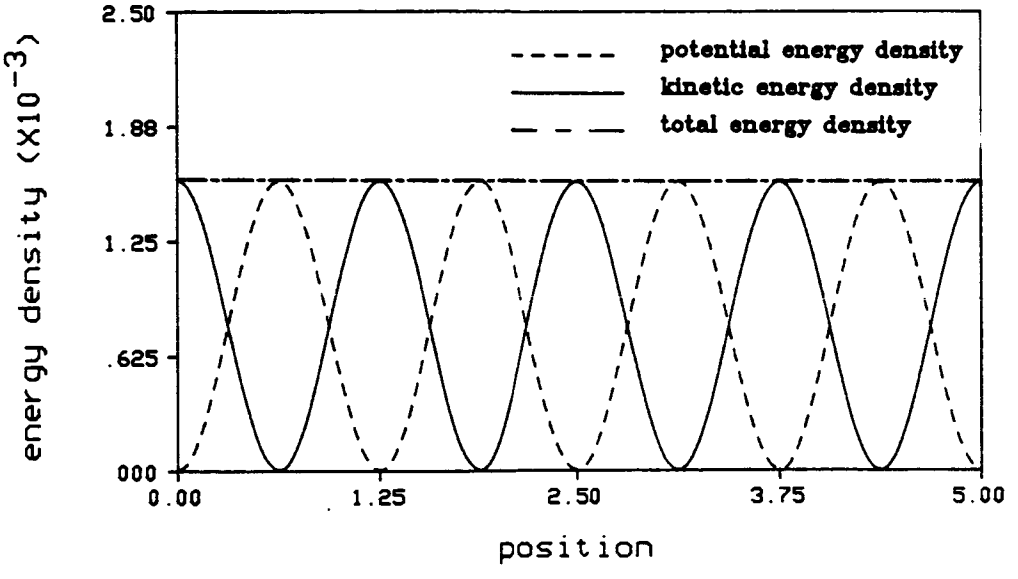

Figure 3.2.6 - Exact Potential, Kinetic and Total Energy Density Solutions for the Longitudinally Vibrating Rod Shown in Figure (3.2.4) Using the Solutions Shown in Equations (3.2.22), (3.2.23) and (3.2.24)

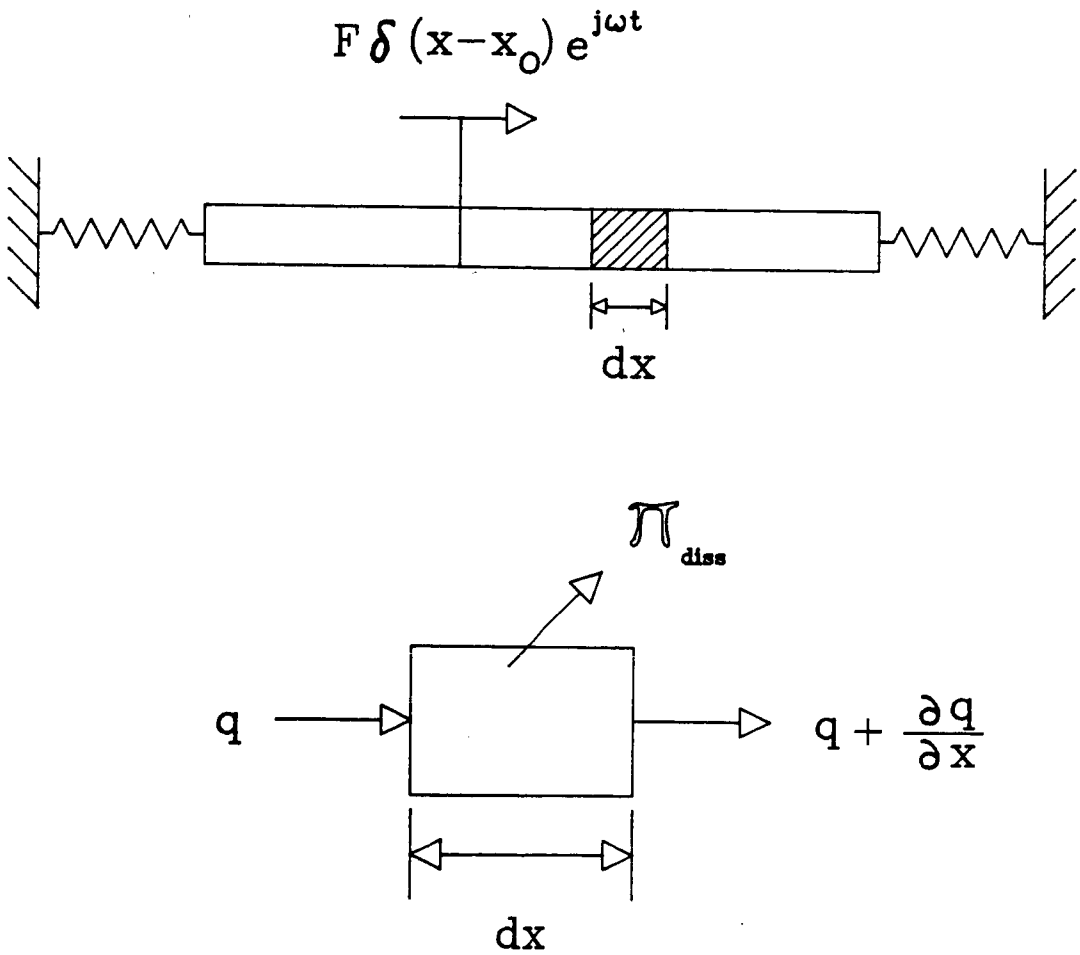

Figure 3.2.7 - Energy Balance on a Differential Element in a Longitudinally Vibrating Rod Excited by a Harmonic Point Force

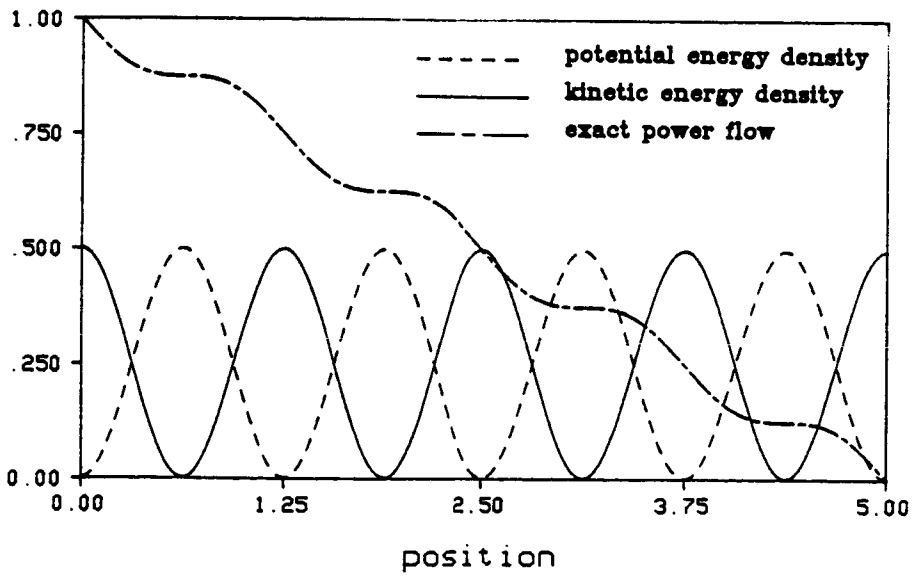

Figure 3.3.1 - Exact Solutions for the Power Flow and Potential and Kinetic Energy Densities in a Longitudinally Vibrating Rod

CHAPTER 4 - THEORETICAL DEVELOPMENT FOR BEAMS

4.1 Introduction

In this chapter, the governing equations used to model power flow through a beam will be developed. As for the rod analysis, the power flow and energy density equations will be developed from the classical solutions of motion of a harmonically excited beam.

4.2 Beam Equations

The equation of motion for a uniform Bernoulli-Euler beam, figure (4.2.1), excited by a general forcing function is

$$E_c I \frac{\partial^4 U(x,t)}{\partial x^4} + \rho S \frac{\partial^2 U(x,t)}{\partial t^2} = f(x,t) \qquad (4.2.1)$$

where:

U(x,t) is the tranverse displacement of beam.

$E_c I$ is the flexural rigidity of beam.

ρS is the density per unit length.

f(x,t) is the distributed forcing function per unit length.

The spring end conditions shown in figure (4.2.1) represent general boundary conditions. The torsional spring rates σ_T control the relationships between the moments and angular displacements at the ends. The transverse spring rates σ_L control the relationships between the shear forces and linear displacements at

the ends.

For this investigation the beam excitation will be modeled as a harmonic point force. The excitation will be a transverse force acting perpendicular to the neutral axis and is defined mathematically as

$$f(x,t) = F\delta(x-x_o)e^{j\omega t} \tag{4.2.2}$$

Damping in the beam will be introduced using a hysteretic model which results in a complex modulus of elasticity E_c, as shown in equation (3.2.3).

Following a procedure similar to that used for the rod analysis, only steady state harmonic conditions will be investigated. Thus, the time dependence of the beam equation of motion will be removed by a separation of variables technique. Substituting equations (3.2.4) and (4.2.2) into (4.2.1) and removing the time dependence gives

$$\frac{d^4u(x)}{dx^4} - \omega^2 \frac{\rho S}{EI} \frac{(1-j\eta)}{(1+\eta^2)} u(x) = \frac{F}{E_c I}\delta(x-x_o) \tag{4.2.3}$$

Equation (4.2.3) may be further simplified by defining a complex wavenumber k for a beam such that

$$k^4 = \omega^2 \frac{\rho S}{EI} \frac{(1-j\eta)}{(1+\eta^2)} \tag{4.2.4}$$

which results in an equation of motion

$$\frac{d^4u(x)}{dx^4} - k^4u(x) = \frac{F}{E_c I}\delta(x-x_o) \tag{4.2.5}$$

When forces are applied at the boundary, equation (4.2.5) is homogeneous

$$\frac{d^4u(x)}{dx^4} - k^4u(x) = 0 \tag{4.2.6}$$

and has a solution of the form

$$u(x) = Ae^{-jkx} + Be^{jkx} + Ce^{-kx} + De^{kx} \tag{4.2.7}$$

In general, the constants A, B, C and D are complex numbers which are determined by applying the boundary conditions.

The four unknown constants in the beam displacement solution require specification of two boundary conditions at each end of the beam to pose the problem correctly. For a transversely vibrating beam, the appropriate boundary conditions are displacement, slope, moment and shear force. The displacement condition for a beam at $x=x_o$ is

$$u(x_o) = u_o \tag{4.2.8}$$

A specified slope is

$$\frac{du}{dx}\Big|_{x=x_o} = \theta_o \tag{4.2.9}$$

where u_o and θ_o are known constants, and are often zero. From elementary beam theory, the second and third derivatives of u(x) are related to the internal moment (M) and shear force (F) respectively as

$$\frac{d^2u}{dx^2} = \frac{M}{EI} \tag{4.2.10}$$

and

$$\frac{d^3u}{dx^3} = \frac{F}{EI} \tag{4.2.11}$$

The sign conventions for positive moment and shear are shown in figure (4.2.2). For the moment and shear boundary conditions only the real part of the complex modulus E_c is used. The real part of the modulus of elasticity is again assumed to be a valid approximation of the modulus for light damping. The important damping effects are included in the complex wavenumber k. Only certain combinations of the boundary conditions can be used. At each end of the beam the two boundary conditions must be given as [29]

$$u(x_o) = u_o \quad \text{or} \quad \frac{d^3u}{dx^3}\Big|_{x=x_o} = \frac{F}{EI} \tag{4.2.12}$$

and

$$\frac{du}{dx}\Big|_{x=x_o} = \theta_o \quad \text{or} \quad \frac{d^2u}{dx^2}\Big|_{x=x_o} = \frac{M}{EI} \tag{4.2.13}$$

For a point force applied along the beam, analytical solutions are found by dividing the beam into two sections. Figure (4.2.3) shows a beam driven by a transverse harmonic point force. As with the rod, the solution procedure requires the beam to be divided into two sections at the location of the driving force, as shown in figure (4.2.4). Each of the two beam sections now have its own displacement solution

$$u_1(x) = (Ae^{-jkx} + Be^{jkx} + Ce^{-kx} + De^{kx}) \qquad (4.2.14)$$
$$x_1 \leq x \leq x_o$$

and

$$u_2(x) = (Ee^{-jkx} + Fe^{jkx} + Ge^{-kx} + He^{kx}) \qquad (4.2.15)$$
$$x_o \leq x \leq x_2$$

At $x = x_1$ and $x = x_2$, one boundary condition from both equations (4.2.12) and (4.2.13) must be specified. At the point where the two beam sections are joined, $x = x_o$, four boundary conditions must be enforced. Three of the four conditions are the continuity of displacement, slope and moment relationships

$$u_1(x_o) = u_2(x_o) \qquad (4.2.16)$$

$$\frac{du_1}{dx}\Big|_{x=x_o} = \frac{du_2}{dx}\Big|_{x=x_o} \qquad (4.2.17)$$

$$(EI)_1\frac{d^2u_1}{dx^2}\Big|_{x=x_o} = (EI)_2\frac{d^2u_2}{dx^2}\Big|_{x=x_o} \qquad (4.2.18)$$

The fourth condition at $x=x_o$ is a balance of forces. The internal shear forces in both beams at the coupling location must balance the applied shear force F such that

$$(EI)_1\frac{d^3u_1}{dx^3}\Big|_{x=x_o} - (EI)_2\frac{d^3u_2}{dx^3}\Big|_{x=x_o} = F \qquad (4.2.19)$$

Using the four continuity relationships and two boundary conditions at each end

of the beam, the problem in figure (4.2.3) is completely defined and the eight constants in equations (4.2.14) and (4.2.15) can be found. The complete solution for a beam section as a function of both position and time has the form

$$U(x,t) = (Ae^{-jkx} + Be^{jkx} + Ce^{-kx} + De^{kx})e^{j\omega t} \tag{4.2.20}$$

4.2.1 Power and Energy Equations for a Beam

Power in a transversely vibrating beam is transmitted by two separate mechanisms. This is in contrast to a rod vibrating longitudinally in which all the power is transported by the internal axial force, equation (3.2.17). Power flow in a beam is transmitted by shear and moment mechanisms. The time averaged power associated with the shear force $<q>_s$ is

$$<q>_s = \frac{1}{2}\mathrm{Re}\left\{\left(EI\frac{\partial^3 U}{\partial x^3}\right)\left(\frac{\partial U}{\partial t}\right)^*\right\} \tag{4.2.21}$$

where:

$EI\dfrac{\partial^3 U}{\partial x^3}$ is the shear force.

$\dfrac{\partial U}{\partial t}$ is the transverse velocity.

The time averaged power carried by the moment $<q>_m$ is

$$<q>_m = \frac{1}{2}\mathrm{Re}\left\{\left(EI\frac{\partial^2 U}{\partial x^2}\right)\left(-\frac{\partial^2 U}{\partial x \partial t}\right)^*\right\} \tag{4.2.22}$$

where:

$EI\frac{\partial^2 U}{\partial x^2}$ is the moment.

$-\frac{\partial^2 U}{\partial x \partial t}$ is the angular velocity.

Substituting the displacement solution U(x,t) into equations (4.2.21) and (4.2.22) the expressions for shear and moment power may be written as

$$<q>_s = -\frac{1}{2}EI\omega Re\{jk^3[jAe^{-jkx} - jBe^{jkx} - Ce^{-kx} + De^{kx}] \\ [Ae^{-jkx} + Be^{jkx} + Ce^{-kx} + De^{kx}]^*\} \qquad (4.2.23)$$

and

$$<q>_m = \frac{1}{2}EI\omega |k|^2 Re\{jk[Ae^{-jkx} + Be^{jkx} - Ce^{-kx} - De^{kx}] \\ [jAe^{-jkx} - jBe^{jkx} + Ce^{-kx} - De^{kx}]^*\} \qquad (4.2.24)$$

The total energy density in a transversely vibrating beam is the sum of its potential energy density (V)

$$V = \frac{1}{2}EI\left(\frac{\partial^2 U}{\partial x^2}\right)^2 \qquad (4.2.25)$$

and kinetic energy density (T)

$$T = \frac{1}{2}\rho S\left(\frac{\partial U}{\partial t}\right)^2 \qquad (4.2.26)$$

Substituting the displacement solution equation (4.2.20) into equations (4.2.25) and (4.2.26) and calculating time averaged values of potential and kinetic energy

results in the relationships

$$<V> = \frac{1}{4}EI\,|k^2\,|^2 Re\{[Ae^{-jkx} + Be^{jkx} - Ce^{-kx} - De^{kx}]$$
$$[Ae^{-jkx} + Be^{jkx} - Ce^{-kx} - De^{kx}]^*\} \qquad (4.2.27)$$

and

$$<T> = \frac{1}{4}\rho S\omega^2 Re\{[Ae^{-jkx} + Be^{jkx} + Ce^{-kx} + De^{kx}]$$
$$[Ae^{-jkx} + Be^{jkx} + Ce^{-kx} + De^{kx}]^*\} \qquad (4.2.28)$$

4.2.2 Nearfield and Farfield Terms

The complex wavenumber for a beam is defined in equation (4.2.4). Assuming damping in the beam is small

$$\eta \ll 1$$

the real part of k^4 is much larger than the imaginary part. Using this assumption, the real and imaginary part of the wavenumber k can be shown to be approximately

$$k_1 \approx \left(\omega^2 \frac{\rho S}{EI}\right)^{\frac{1}{4}} = \frac{\omega}{c_b} \qquad (4.2.29)$$

and

$$k_2 \approx -\frac{\eta}{4}\left(\omega^2 \frac{\rho S}{EI}\right)^{\frac{1}{4}} = -\frac{\eta}{4}\,k_1 \qquad (4.2.30)$$

where

$$c_b = \left(\omega^2 \frac{EI}{\rho S}\right)^{\frac{1}{4}} \text{ wave velocity in a beam.}$$

These expressions are excellent approximations for small damping.

The displacement solution for a longitudinally vibrating rod, equation (3.2.16), is the sum of two traveling wave solutions. The partial solution of the form $e^{j(\omega t-kx)}$ is commonly referred to as a "right traveling wave", while the partial solution $e^{j(\omega t+kx)}$ is a "left traveling wave". Actually since k is a complex number the term $e^{j(\omega t-kx)}$ may be rewritten in the form

$$e^{j(\omega t-kx)} = e^{j(\omega t-k_1 x)}\, e^{k_2 x} \tag{4.2.31}$$

Equation (4.2.31) represents a right traveling wave whose magnitude is decaying exponentially (k_2 is a negative quantity).

The displacement for the beam, equation (4.2.20), is a four term solution. Four terms are necessary since the governing differential equation for the beam is fourth order with respect to x. The first two terms in equation (4.2.20) are identical in form to the displacement solution for the rod, and consequently they represent exponentially decaying traveling wave solutions. Since k_2 is small, the rate of decay is small and this portion of the displacement has come to be known as the farfield solution. The last two terms in equation (4.2.20), the exponential functions, are commonly referred to as the nearfield solution since the effect of these terms is significant only near a boundary.

The terminology "nearfield solution" implies that with respect to the total displacement solution the nearfield terms are generally only important "near" some type of discontinuity. In this formulation a discontinuity includes all the

classical end conditions where the beam terminates, e.g. clamped end, free end, pinned end, mass loaded end, etc. In addition discontinuities can occur where two different beams are coupled and at the location of a driving force.

The nearfield terms in equation (4.2.20) complicate the displacement solution for a beam. If it were true that the farfield terms were always much larger than the nearfield terms the beam analysis could be simplified by neglecting the nearfield terms. However, in separate studies on the measurement of structure-borne wave intensity, Pavic [34] and Noiseux [35] found that, at a discontinuity, the magnitude of the nearfield terms can be of the same order as the farfield terms. In their text on structure-borne sound, Cremer et al. [8] discussed the role of the nearfield solution in transverse beam vibration. Cremer et al. explained that the nearfield is necessary in order that the displacement solution, equation (4.2.14), can satisfy the equilibrium conditions at a discontinuity. The farther away a point in a beam is from a discontinuity, the less significant is the contribution of the nearfield to the total solution u(x). Goyder and White [25] discussed the importance of the nearfield in a study of power flow in infinite structures. Goyder and White derived the displacement solution for an infinite beam driven by a harmonic point force, as shown in figure (4.2.5). Using a spatial Fourier transformation and contour integral Goyder and White derived the displacement solution for $x \geq 0$ in terms of a farfield and nearfield term

$$u(x) = Ae^{-jkx} + Ce^{-kx} = Ae^{-jk_1x}\, e^{k_2x} + Ce^{-k_1x}\, e^{-jk_2x} \qquad (4.2.32)$$

where the constants A and C were shown to be

$$A = \frac{jF}{4EIk^3}$$

and

$$C = \frac{-F}{4EIk^3}$$

Note the magnitude of A and C are the same. Thus, the magnitude of displacement in the vicinity of the drive point, x=0, will be equally dependent on both the nearfield and farfield effects. However, both terms in equation (4.2.32) decay exponentially as x increases. The farfield term decays as e^{k_2x} while the nearfield term decays as e^{-k_1x}. Since $|k_1| \gg |k_2|$ the nearfield term will decay much more quickly than the farfield term. As an example, consider the case of an infinite beam made of steel. The hysteretic damping coefficient for steel is commonly assumed to be of the order $\eta = 0.001$ [32]. Making use of the relationship between the wavenumber and wavelength

$$k_1 \approx k = \frac{2\pi}{\lambda} \qquad (4.2.33)$$

where

λ is the wavelength of vibration.

the exponential decay terms in equation (4.2.32) can be written as

$$e^{-k_1 x} = e^{-2\pi \frac{x}{\lambda}} \tag{4.2.34}$$

and

$$e^{k_2 x} = e^{-\frac{\eta}{4} k_1 x} = e^{-\frac{\eta\pi}{2\lambda} x} \tag{4.2.35}$$

It was pointed out earlier that at the drive point the magnitude of the nearfield and farfield terms in equation (4.2.32) were the same. Using the expressions in equations (4.2.34) and (4.2.35) it is found that one wavelength from the drive point in a steel beam, $x = \lambda$, the magnitude of the nearfield term is less than two percent of the farfield term. At $x = 2\lambda$ the ratio of the two is less than 0.0004 percent. Figure (4.2.6) shows a plot of the ratio of the magnitude of the nearfield term in equation (4.2.32) to the magnitude of the farfield term, for $x \geq 0$, as a function of position in wavelengths for a infinite steel beam. Goyder and White concluded that for large values of kx the nearfield term in equation (4.2.32) could be neglected. Figure (4.2.6) and equations (4.2.34) and (4.2.35) support this conclusion.

For small damping, the displacement solution for the infinite beam, equation (4.2.32), is essentially the sum of a right traveling wave solution plus an exponentially decaying function. The two term solution is sufficient for an infinite beam since there is no discontinuity in the beam to reflect the wave and create a left traveling wave. The displacement solution for a finite beam, equation (4.2.14), consists essentially of a right and left traveling wave solution plus two exponential functions. Both a right and left traveling wave solution

are required in a finite beam to account for reflections which occur when a propagating wave encounters a discontinuity. The finite beam also requires two nearfield solutions to allow the boundary conditions at each end of the beam to be satisfied.

The displacement solution for beam section 2, shown in figure (4.2.4), is $u_2(x)$. For light damping, the magnitude of the traveling wave solution, $Ae^{-jkx} + Be^{jkx}$ is essentially constant over the length of the section since the decay terms are small. The nearfield solution Ce^{-kx} is associated with the left boundary, $x=x_o$, on beam section 2 while the nearfield solution De^{kx} is associated with the right boundary at $x = x_2$. Except for the case when the beam section length is much less than the wavelength of vibration, it can be shown that the nearfield solution associated with one boundary is negligible at the other boundary. For example, consider the case shown in figure (4.2.4) where the wavelength of vibration is equal to twice the length of beam section 2. At $x=x_o$ the magnitude of the partial nearfield solution associated with that boundary, Ce^{-kx}, can be of the same order as the magnitude of the traveling wave portion of the total displacement solution. However, at the other boundary, $x = x_2$, the magnitude of Ce^{-kx_2} is about four percent of its value at $x=x_o$, and therefore can be neglected near $x = x_2$. At the same time, at $x = x_2$ the magnitude of the partial nearfield solution associated with the right boundary, De^{kx_2}, can be of the same order of magnitude as the traveling wave solution but is negligible near $x=x_o$. The concept of nearfield solutions being associated with a particular

boundary, allows approximations of the total displacement solution near a discontinuity. It can be argued that if the length of beam section 2 in figure (4.2.4) is greater than one half the wavelength of vibration, in the vicinity of the left boundary, $x=x_o$, the total displacement solution $u_2(x)$ can be written approximately as

$$u_{2L}(x) = Ae^{-jkx} + Be^{jkx} + Ce^{-kx} \tag{4.2.36}$$

Equation (4.2.36) is based on the assumption that the nearfield solution De^{kx} is negligible near $x=x_o$. By the same reasoning the displacement solution near the right boundary, $x = x_2$, can be written approximately as

$$u_{2R}(x) = Ae^{-jkx} + Be^{jkx} + De^{kx} \tag{4.2.37}$$

As the driving frequency of the forcing function increases, the approximations in equations (4.2.36) and (4.2.37) become better. As the driving frequency increases, the wavenumber, which is proportional to the square root of frequency, also increases. As the wavenumber increases the wavelength of vibration decreases and the effective region of the nearfield solution gets smaller.

When the driving frequency is high enough, such that the length of beam section 2 for the case in figure (4.2.4) is ten wavelengths long ($x_2 = 10\lambda$) and $x_o=0$, the partial nearfield solution Ce^{-kx} is significant only in the region $0 \leq x \leq .05x_2$ while De^{kx} is significant only in the region $.95x_2 \leq x \leq x_2$. At this frequency, the nearfield solutions are significant on only one tenth of the total beam section 2. This means that on the region

$.05x_2 \leq x \leq .95x_2$ the displacement solution for section 2 can be written approximately by the traveling wave solution

$$u_{2FF}(x) = Ae^{-jkx} + Be^{jkx} \tag{4.2.38}$$

The validity of equation (4.2.38) is based on the assumption that the partial nearfield solutions are negligible over most of the beam.

As a final example of the relative importance of the nearfield and farfield terms to the total displacement solution, consider the case of the harmonically excited beam shown in figure (4.2.3) with no end constraints, i.e. a free-free beam, with the following beam parameters.

$$x_1 = -0.5 \text{ m}$$

$$x_o = 0$$

$$x_2 = 0.5 \text{ m}$$

$$EI = 500 \text{ Nm}^2$$

$$\rho S = 2.358 \text{ kg/m}$$

$$\rho = 7860 \text{ kg/m}^3$$

$$\eta = 0.001$$

A free end condition can be accomplished by setting the spring rates of the system shown in figure (4.2.3) to zero. Figure (4.2.7) is a plot of the ratio of the magnitude of the nearfield solution to the magnitude of the farfield solution

$$\frac{|Ce^{-kx}| + |De^{kx}|}{|Ae^{-jkx}| + |Be^{jkx}|} \tag{4.2.39}$$

for beam section 2 in figure (4.2.4), as a function of position. The four curves in figure (4.2.7) correspond to the four cases where the wavelength of vibration equals $2x_2$, x_2, $.5x_2$, and $.25x_2$. When $\lambda=2x_2=1$ and $\lambda=x_2=0.5$ figure (4.2.7) suggests that the effects of the nearfield terms are important over the entire beam section length. Thus approximating the displacement using only the farfield terms, equation (4.2.38), is not valid anywhere on the beam. For the case when $\lambda=.5x_2=0.25$, equation (4.2.38) is a good approximation over the middle section of the beam but not near the boundaries. When $\lambda=.25x_2=0.125$ however, figure (4.2.7) indicates that the farfield displacement solution is valid over the region $.05 \leq x \leq .45$, or approximately eighty percent of the beam length. As the wavelength of vibration gets smaller, the farfield displacement solution becomes valid over more of the beam.

The arguments and figures in section 4.3.3 demonstrate how to determine which conditions and ranges the displacement solution for a transversely vibrating beam is well modeled by the farfield solution. Neglecting the nearfield displacements in power flow analysis is fairly common in the literature. Nefske and Sung [2], Goyder and White [25], Pavic [34], and Noiseux [35], at some point in their analyses assumed the nearfield effects were negligible.

4.2.3 Energy Density in a Beam

The expressions for the time averaged potential and kinetic energies for a beam in terms of wave amplitudes are

$$\begin{aligned}<V> = \frac{1}{4}EI\,|k^2\,|^2\{\,&|A\,|^2e^{2k_2x}+|B\,|^2e^{-2k_2x}+|C\,|^2e^{-2k_1x}+|D\,|^2e^{2k_1x}\\ &-2e^{-z_2x}[Re(AC^*)cosz_2x+Im(AC^*)sinz_2x]-2e^{z_1x}[Re(AD^*)cosz_1x+Im(AD^*)sinz_1x]\\ &-2e^{-z_1x}[Re(CB^*)cosz_1x+Im(CB^*)sinz_1x]-2e^{z_2x}[Re(DB^*)cosz_2x+Im(DB^*)sin(z_2x)]\\ &+2[Re(AB^*)cos2k_1x+Im(AB^*)sin2k_1x]+2[Re(CD^*)cos2k_2x+Im(CD^*)sin2k_2x]\}\end{aligned} \tag{4.2.40}$$

and

$$\begin{aligned}<T> = \frac{1}{4}\rho S\omega^2\{\,&|A\,|^2e^{2k_2x}+|B\,|^2e^{-2k_2x}+|C\,|^2e^{-2k_1x}+|D\,|^2e^{2k_1x}\\ &+2e^{-z_2x}[Re(AC^*)cosz_2x+Im(AC^*)sinz_2x]+2e^{z_1x}[Re(AD^*)cosz_1x+Im(AD^*)sinz_1x]\\ &+2e^{-z_1x}[Re(CB^*)cosz_1x+Im(CB^*)sinz_1x]+2e^{z_2x}[Re(DB^*)cosz_2x+Im(DB^*)sinz_2x]\\ &+2[Re(AB^*)cos2k_1x+Im(AB^*)sin2k_1x]+2[Re(CD^*)cos2k_2x+Im(CD^*)sin2k_2x]\}\end{aligned} \tag{4.2.41}$$

where

$$z_1 = k_1 + k_2 = k_1(1 - \frac{\eta}{4})$$

and

$$z_2 = k_1 - k_2 = k_1(1 + \frac{\eta}{4})$$

To illustrate the distribution of the energy density components in a transversely vibrating beam, consider the harmonically excited beam in figure (4.2.8). The beam in figure (4.2.8) is excited by a transverse point force at x_o and is simply supported at both ends. Figure (4.2.9) is a plot of the exact potential, kinetic

and total energy densities when the following beam parameters are used.

$$x_1 = 0$$

$$x_o = 0.25 \text{ m}$$

$$x_2 = 0.5 \text{ m}$$

$$EI = 500 \text{ Nm}^2$$

$$\rho S = 2.358 \text{ kg/m}$$

$$\rho = 7860 \text{ kg/m}^3$$

$$\eta = 0.001$$

$$\omega = 36791.95 \text{ rad/sec}$$

The potential and kinetic energy densities in figure (4.2.9) are calculated from equations (4.2.40) and (4.2.41). The total energy density is the sum of the potential and kinetic energy densities. Over most of the beam length the potential and kinetic energies are in phase with each other and of the same magnitude. The only place where the potential and kinetic energies are out of phase or of different magnitude is near the point force. Such behavior near the point force is the result of the nearfield effects. Figure (4.2.9) shows that the total energy density in a beam is a spatial harmonic function. This is in contrast to the distribution of energy density in a rod where the total energy density has no significant harmonic components.

Using the assumption of light damping, some simplifications may be made to the exact energy density solution. When $\eta \ll 1$ the magnitude of $|k^2|^2$ may be written approximately as

$$|k^2|^2 \approx \omega^2 \frac{\rho S}{EI} \tag{4.2.42}$$

Thus, the following relationship may be written

$$EI\,|k^2|^2 \approx EI\omega^2 \frac{\rho S}{EI} = \rho S \omega^2 \tag{4.2.43}$$

The total time averaged energy density at a point is calculated by adding equations (4.2.40) and (4.2.41). Substituting equation (4.2.43) into the potential energy expression, equation (4.2.40), and adding the potential energy to the kinetic energy, equation (4.2.41), the approximate total time averaged energy density $<e>$ is

$$<e> = \frac{1}{2}\rho S\omega^2\{\,|A|^2 e^{2k_2 x} + |B|^2 e^{-2k_2 x} + |C|^2 e^{-2k_1 x} + |D|^2 e^{2k_1 x}$$
$$+2[\mathrm{Re}(AB^*)\cos 2k_1 x + \mathrm{Im}(AB^*)\sin 2k_1 x] + 2[\mathrm{Re}(CD^*)\cos 2k_2 x + \mathrm{Im}(CD^*)\sin 2k_2 x]\} \tag{4.2.44}$$

The assumptions used in deriving equation (4.2.44) are that hysteretic damping is small $\eta \ll 1$, thus, $|k^2|^2 \approx \omega^2 \frac{\rho S}{EI}$ and $E_c \approx E$.

There are several differences between the approximate total energy density function for a rod, equation (3.2.29), and the approximate total energy density for a beam, equation (4.2.44). There are two nearfield terms in equation (4.2.44) which will only be important near the boundaries. For the beam, a harmonic farfield function

$$2[\mathrm{Re}(AB^*)\cos 2k_1 x + \mathrm{Im}(AB^*)\sin 2k_1 x] \tag{4.2.45}$$

exists. It has been shown that when damping is light the harmonic portions of

the potential and kinetic energies in a rod were out of phase with one another and therefore add to zero when the potential and kinetic expressions were summed. Investigation of the expressions for potential and kinetic energies for a beam, equations (4.2.40) and (4.2.41), shows that both the potential and kinetic energies have harmonic terms which are in phase with each other. Thus, when the potential and kinetic energies are added, the harmonic function in equation (4.2.45) is not canceled as it is in a rod.

The spatially harmonic portions of the time averaged potential and kinetic energies are in phase with one another due to the potential energy storage mechanism in a beam. Equation (4.2.25) shows that the potential energy in a beam is proportional to the square of the second derivative of displacement with respect to x. In a rod the potential energy is proportional to the square of the first derivative of displacement with respect to x. In both cases the kinetic energy is proportional to the displacement with respect to x. In a beam therefore, the maximum time averaged values for both the farfield potential and kinetic energies occur at the same location in the beam. For a rod these maximum values were out of phase with each other.

4.2.4 Simplifying the Power and Energy Expressions for a Beam

In general, none of the terms in equation (4.2.44) are negligible. However, in many applications the exact spatial profile of energy may not be required. As an example consider the farfield of a small acoustic noise source. It has been shown by Kinsler et al. [30] that in the acoustic farfield the distinguishing

characteristics of a simple noise source is its source strength. The source strength is defined as the surface integral of the normal velocity over the source. Thus, the details of the velocity distribution on the source are not important. Two sound sources with different velocity distributions but equal source strengths would be indistinguishable in the acoustic farfield. In SEA, which is used as a noise prediction technique, the average values of energy are converted into expressions for averaged displacement or velocity in a system. These average values can be used to estimate the acoustic radiation of a structure.

One may apply this idea of space average values to the power and energy equations for a beam. Expanding the expressions for the time averaged shear and moment power, equations (4.2.23) and (4.2.24), gives

$$\begin{aligned}<q>_s = -\frac{1}{2}EI\omega Re\{jk^3[j\,|A|^2e^{2k_2x}+jAB^*e^{-2jk_1x}+jAC^*e^{-(1+j)z_2x}+jAD^*e^{(1-j)z_1x}\\ -jBA^*e^{2jk_1x}-j\,|B|^2e^{-2k_2x}-jBC^*e^{-(1-j)z_1x}-jBD^*e^{(1+j)z_2x}\\ -CA^*e^{-(1-j)z_2}-CB^*e^{-(1+j)z_1x}-|C|^2e^{-2k_1x}-CD^*e^{-2jk_2x}\\ +DA^*e^{(1+j)z_1x}+DB^*e^{(1-j)z_2x}+DC^*e^{2jk_2x}+|D|^2e^{2k_1x}]\}\end{aligned} \tag{4.2.46}$$

and

$$\begin{aligned}<q>_m = -\frac{1}{2}EI\omega Re\{jk\,|k|^2[j\,|A|^2e^{2k_2x}-jAB^*e^{-2jk_1x}-AC^*e^{-(1+j)z_2x}+AD^*e^{(1-j)z_1x}\\ +jBA^*e^{2jk_1x}-j\,|B|^2e^{-2k_2x}-BC^*e^{-(1-j)z_1x}+BD^*e^{(1+j)z_2x}\\ -jCA^*e^{-(1-j)z_2}+jCB^*e^{-(1+j)z_1x}+|C|^2e^{-2k_1x}-CD^*e^{-2jk_2x}\\ -jDA^*e^{(1+j)z_1x}+jDB^*e^{(1-j)z_2x}+DC^*e^{2jk_2x}-|D|^2e^{2k_1x}]\}\end{aligned} \tag{4.2.47}$$

When the sum of the shear and moment power expressions in equations (4.2.46) and (4.2.47), is spaced averaged by

$$\langle \bar{q} \rangle = \frac{1}{\lambda} \int_{x}^{x+\lambda} \langle q \rangle d\sigma$$

the average power $\langle \bar{q} \rangle$ in a beam is found to be

$$\langle \bar{q} \rangle =$$

$$\frac{EI\omega}{4\pi}\{4\pi(k_1^3-k_1k_2^2)[\,|A|^2e^{2k_2x}-|B|^2e^{-2k_2x}]+(k_1^2k_2-k_2^3)[\,|D|^2e^{2k_1x+4\pi}-|C|^2e^{-2k_1x}]$$

$$+2\frac{k_1^4-k_1^2k_2^2}{k_2}[\mathrm{Re}(CD^*)[\cos 2k_2x-\cos 2k_2(x+\lambda)]+\mathrm{Im}(CD^*)[\sin 2k_2x-\sin 2k_2(x+\lambda)]]$$

$$+2k_1^2k_2e^{-k_1x}[\mathrm{Re}(AC^*)\sin k_1x-\mathrm{Im}(AC^*)\cos k_1x+\mathrm{Re}(CB^*)\sin k_1x-\mathrm{Im}(CB^*)\cos k_1x]$$

$$+2k_1^2k_2e^{(2\pi+k_1x)}[\mathrm{Re}(AD^*)\sin k_1x-\mathrm{Im}(AD^*)\cos k_1x+\mathrm{Re}(DB^*)\sin k_1x-\mathrm{Im}(DB^*)\cos k_1x]\} \tag{4.2.48}$$

In integrating the sums of equations (4.2.46) and (4.2.47) to derive equation (4.2.48) the following approximations, based on light damping, were used

$$z_1 \approx z_2 \approx k_1 \tag{4.2.49}$$

$$\lambda = \frac{2\pi}{k} \approx \frac{2\pi}{k_1} \tag{4.2.50}$$

$$e^{4\pi} - 1 \approx e^{4\pi} \tag{4.2.51}$$

$$e^{-4\pi} - 1 \approx -1 \tag{4.2.52}$$

$$e^{4\pi\frac{k_2}{k_1}} - 1 \approx 4\pi\frac{k_2}{k_1} \tag{4.2.53}$$

$$e^{-4\pi\frac{k_2}{k_1}} - 1 \approx -4\pi\frac{k_2}{k_1} \tag{4.2.54}$$

Similarly, the space averaged gradient of the total energy density is found by integrating the derivative of equation (4.2.44) as

$$\frac{d\bar{<e>}}{dx} = \frac{1}{\lambda}\int_{x}^{x+\lambda} \frac{d<e>}{d\sigma} d\sigma$$

which results in the expression

$$\frac{d\bar{<e>}}{dx} = \frac{EI}{4\pi}\{4\pi k_1^4 k_2[\,|A|^2 e^{2k_2x} - |B|^2 e^{-2k_2x}] - |C|^2 e^{-2k_1x} + |D|^2 e^{(4\pi+2k_1x)}$$
$$+\mathrm{Re}(CD^*)[\cos 2k_2(x+\lambda) - \cos 2k_{2x}] + \mathrm{Im}(CD^*)[\sin 2k_2(x+\lambda) - \sin 2k_{2x}]\} \tag{4.2.55}$$

The presence of the nearfield terms in the displacement solution for a beam complicates the power flow and energy density expressions to the point where no simple relationship exists between the average power flow, equation (4.2.48), and the average gradient of the energy density, equation (4.2.55). In section 3.2.3 an expression relating the power flow in a rod to the gradient of energy density was developed. This relationship allowed the development of equation (3.2.36) which models the energy density in a rod. In working with the space averaged power and energy equations for a beam it was found that a similar equation relating power flow and the gradient of the energy density could be developed only if the nearfield effects could be neglected. In section 4.2.2 it was shown that at a sufficiently high frequency, the displacement solution for a beam, equation (4.2.14), is well approximated over most of the beam's length by the farfield solution, equation (4.2.38). If the analysis is restricted to frequencies where the

farfield displacement solution is a good approximation, then the equations describing the average power flow and energy density gradient simplify to

$$\langle \bar{q} \rangle_{ff} = EI\omega\{k_1^3[\,|A|^2 e^{2k_2 x} - |B|^2 e^{-2k_2 x}]\} \tag{4.2.56}$$

where $\langle \bar{q} \rangle_{ff}$ is the average farfield power flow and

$$\frac{d\langle \bar{e} \rangle_{ff}}{dx} = EI\{k_1^4 k_2[\,|A|^2 e^{2k_2 x} - |B|^2 e^{-2k_2 x}]\} \tag{4.2.57}$$

where $\langle \bar{e} \rangle_{ff}$ is the average farfield energy density. The assumptions used in calculating equations (4.2.56) and (4.2.57) are the same as used in calculating the spaced averaged power flow plus the following assumption based on light damping

$$k_1^3 - k_1 k_2^2 = k_1^3\left(1 - \frac{\eta^2}{16}\right) \approx k_1^3 \tag{4.2.58}$$

Dividing equation (4.2.56) by (4.2.57) and solving for $\langle \bar{q} \rangle_{ff}$ yields the relationship

$$\langle \bar{q} \rangle_{ff} = \frac{-4c_b^2}{\eta\omega} \frac{d\langle \bar{e} \rangle_{ff}}{dx} \tag{4.2.59}$$

Thus, the average farfield power flow in a beam is proportional to the gradient of the average farfield energy density.

The relationship between power flow and energy density in a beam developed by Nefske and Sung [2] is, in the present notation

$$<q>_{ff} = \frac{-4c_b^2}{\eta\omega} \frac{d<e>_{ff}}{dx} \tag{4.2.60}$$

Note that equations (4.2.59) and (4.2.60) are almost identical. The only difference between the two equations is that equation (4.2.59) relates spaced averaged power and energy density while equation (4.2.60) relates local values of power and energy density. In their work, Nefske and Sung apparently ignore the spatial variation of energy density which exists in a transversely vibrating beam. The gradient of the energy density in a beam varies between positive and negative values, as shown in figure (4.2.9). Thus, in writing an expression for which the power flow is proportional to the local gradient in energy density, as shown in equation (4.2.60), it would be found that the power flow would change signs (directions) in a region where no additional power is added. This would be a violation of the conservation of energy.

4.2.5 Energy Balance in a Beam

Figure (4.2.10) shows an energy balance done on a differential beam element. Using average values of energy density and power flow, a control volume analysis of power flow in a beam element in figure (4.2.10) leads to a energy balance

$$\frac{\partial \bar{<e>}}{\partial t} = -\frac{\partial \bar{<q>}}{\partial x} - \bar{<\pi>}_{diss} \tag{4.2.61}$$

where

$\bar{<\pi>}_{diss}$ is the time and averaged dissipated power.

For time and space averaged farfield values of power flow and energy density one may use the relationship given in equation (4.2.59) to replace $\langle \bar{q} \rangle$ by a term proportional to the first derivative of $\langle \bar{e} \rangle_{ff}$ with respect to x. The time derivative of energy is equal to zero for steady state conditions, and thus equation (4.2.61) may be written

$$\frac{4c_b^2}{\eta\omega}\frac{d^2\langle \bar{e} \rangle_{ff}}{dx^2} - \bar{\pi}_{diss} = 0 \qquad (4.2.62)$$

4.2.6 Power Dissipation in a Beam

At steady state, equation (4.2.62) shows the average power dissipated is proportional to the second derivative of the average energy density. Calculating the second derivative of energy density, the average dissipated power is

$$\bar{\pi}_{diss} = \frac{\rho S\omega^2}{2}\omega\eta\{|A|^2 e^{2k_2 x} - |B|^2 e^{-2k_2 x}\} \qquad (4.2.63)$$

The average energy density over a wavelength is

$$\langle \bar{e} \rangle_{ff} = \frac{\rho S\omega^2}{2}\{|A|^2 e^{2k_2 x} - |B|^2 e^{-2k_2 x}\} \qquad (4.2.64)$$

Dividing equation (4.2.63) by (4.2.64) and solving for $\bar{\pi}_{diss}$ gives the result that

$$\bar{\pi}_{diss} = \eta\omega \langle \bar{e} \rangle_{ff} \qquad (4.2.65)$$

Thus the space averaged power dissipated in a beam is proportional to the average energy density. Equation (4.2.65) is identical in form to (3.2.35) which

relates local power disspation to the local energy density in a rod.

4.2.7 Governing Equations for the Energy Density and Power Flow in a Beam

Substituting equation (4.2.65) into (4.2.62) and rearranging terms gives the approximate governing equation for the farfield space averaged energy density in a beam

$$\frac{d^2\bar{<e>}_{ff}}{dx^2} - \phi^2\bar{<e>}_{ff} = 0 \tag{4.2.66}$$

where

$$\phi = \frac{\eta\omega}{2c_b}$$

The assumptions used in developing equation (4.2.66) are the same as those used in section 4.2.4 to develop equation (4.2.48) along with the assumption that the displacement in the beam is well modeled by the traveling wave solution in equation (4.2.38).

The general solution to equation (4.2.66) is

$$\bar{<e>}_{ff} = C_1 e^{\phi x} + C_2 e^{-\phi x} \tag{4.2.67}$$

where the constants C_1 and C_2 are determined by applying the boundary conditions, either a specified energy density or power flux condition. The power flow is calculated by finding the derivative of $\bar{<e>}_{ff}$ as discussed in equation (4.2.59)

$$<\bar{q}>_{ff} = -2c_b(C_1 e^{\phi x} - C_2 e^{-\phi x}) \qquad (4.2.68)$$

4.3 Summary

In developing the power and energy density equations, it was found that two complications arose in the beam analysis in chapter 4 which did not occur in the rod analysis in chapter 3. The first complication in the beam analysis was the existence of a nearfield in the displacement solution, as shown in equation (4.2.20). The second complication was the harmonic, spatial variation of energy density in a beam, as shown in figure (4.2.9).

In section 4.2.2 the conditions for which the nearfield terms in the beam displacement solution could be neglected were determined. Thus, under certain conditions the displacement solution can be approximated by the farfield terms. It was also shown that the spatial variation in the farfield energy density could be removed by integrating the farfield energy density over a wavelength of vibration to achieve a local space average.

Equation (4.2.59) shows that under the assumptions that hysteretic damping is small $\eta \ll 1$:

1) $|k_1| \gg |k_2|$.

2) the displacement solution in a beam is well modeled by the farfield solution as shown in equation (4.2.38).

3) $\langle \bar{q} \rangle_{ff}$ is approximated by equation (4.2.56).

4) $\frac{d\langle \bar{e} \rangle_{ff}}{dx}$ is approximated by equation (4.2.57).

Using these assumptions, it was found that the space averaged power flow in a beam is proportional to the space averaged gradient of energy density. Furthermore, the control volume analysis shown in figure (4.2.10) along with the relationship between space averaged power dissipation and space averaged energy density allows the development of equation (4.2.66) which models the energy distribution in a beam.

In their study of power flow in beams, Nefske and Sung ignored the harmonic, spatial variation in energy density which exists in a vibrating beam. Thus, in deriving a relationship between the power flow and the gradient of energy density in a beam, equation (4.2.60), Nefske and Sung used local values of power and energy density instead of space averaged values.

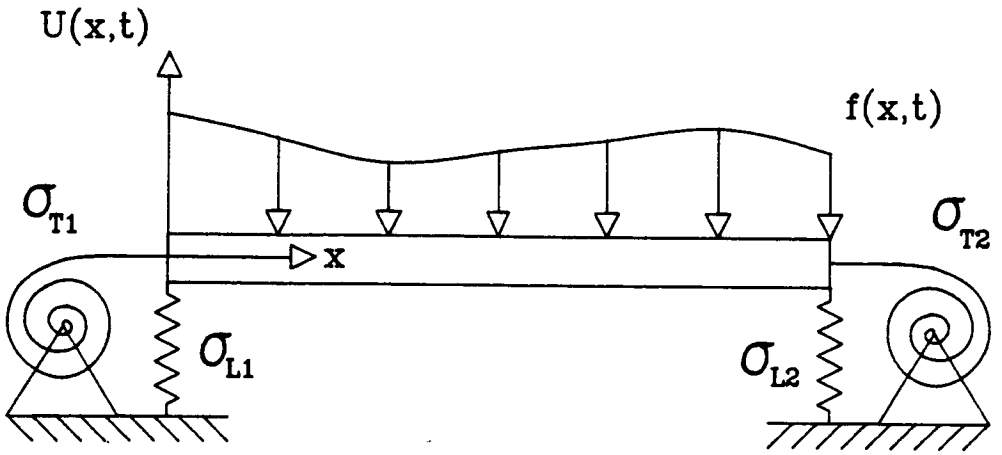

Figure 4.2.1 - Transversely Vibrating Beam Excited by a Distributed Forcing Function with General Spring Boundary Conditions

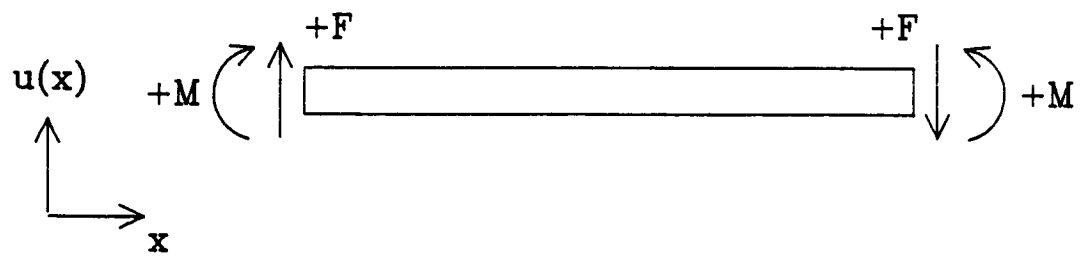

Figure 4.2.2 - Sign Conventions for Positive Moment and Shear Force in a Transversely Deflected Beam

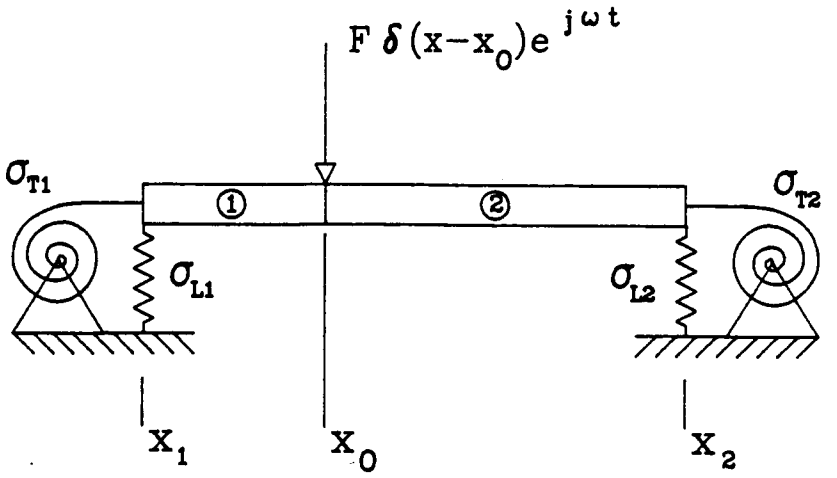

Figure 4.2.3 - Transversely Vibrating Beam Excited by a Harmonic Point Force at x_o with General Spring Boundary Conditions

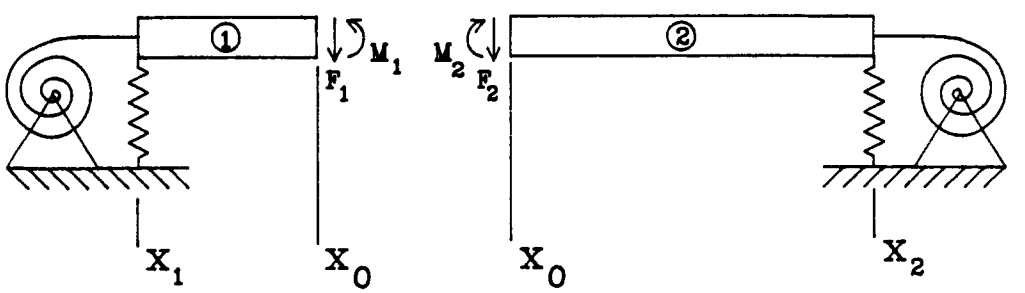

Figure 4.2.4 - Transversely Vibrating Beam from Figure (4.2.3) Split into Two Components to Allow the Harmonic Point Force to be Applied as a Boundary Condition

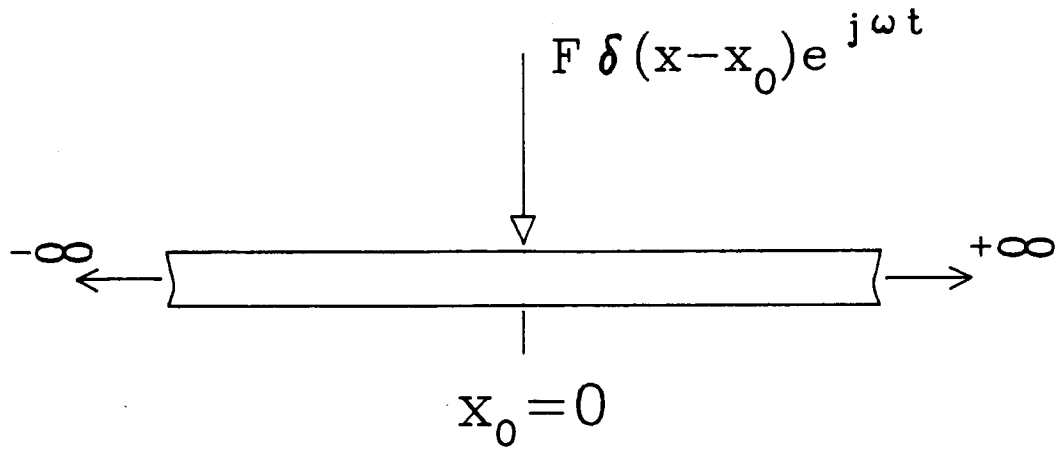

Figure 4.2.5 - Infinite, Transversely Vibrating Beam Excited by a Harmonic Point Force at x_o

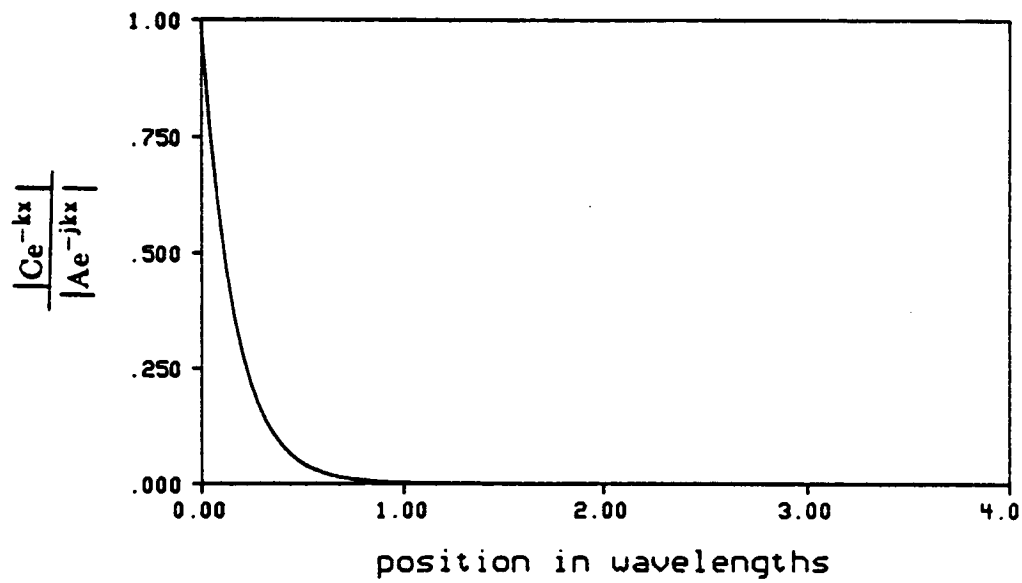

Figure 4.2.6 - Ratio of the Magnitude of the Nearfield Term to the Farfield Term in Equation (4.2.32) for $x \geq 0$ as a Function of Position in Wavelengths

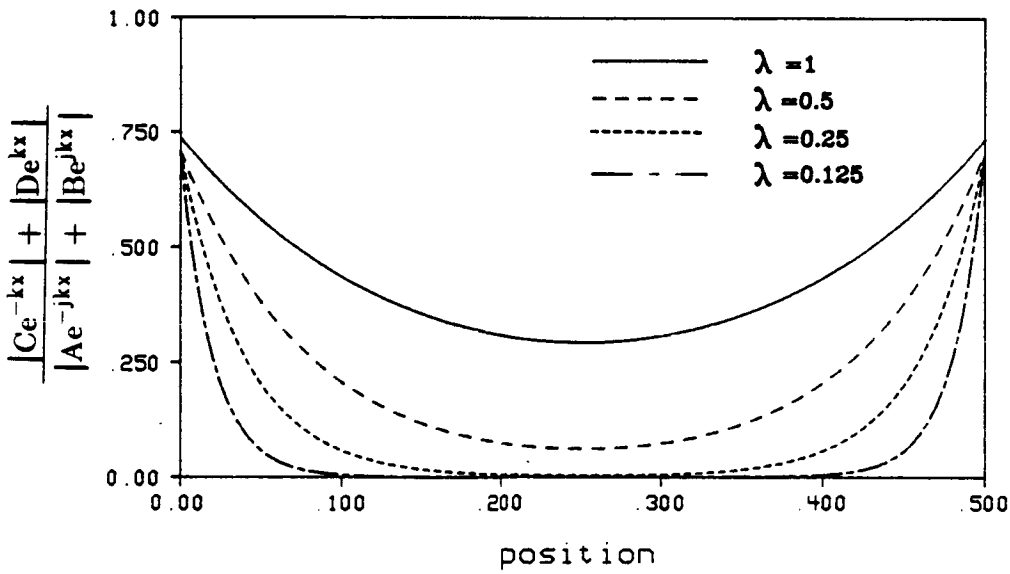

Figure 4.2.7 - Ratio of the Sum of the Magnitudes of the Nearfield Terms to the Sum of the Magnitudes of the Farfield Terms as Shown in Equation (4.2.39) for Beam Section 2 in Figure (4.2.3) with Free-Free Boundary Conditions as a Function of Position

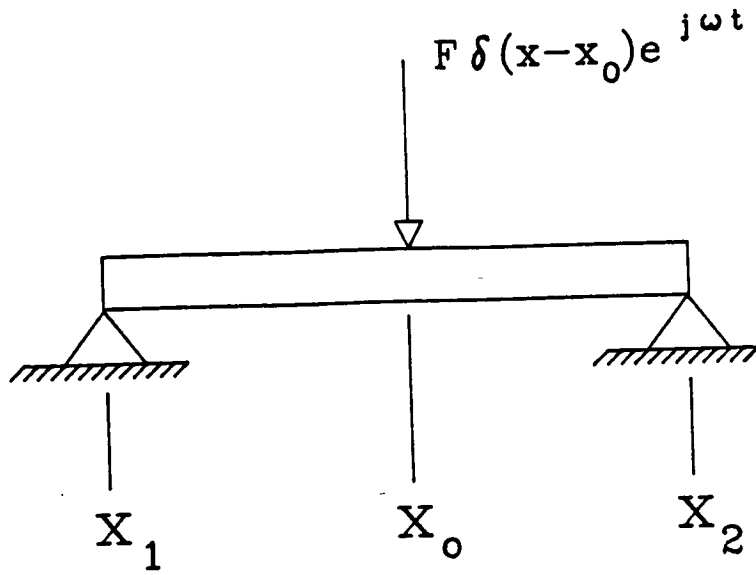

Figure 4.2.8 - Simply Supported, Transversely Vibrating Beam Excited by a Harmonic Point Force at x_o

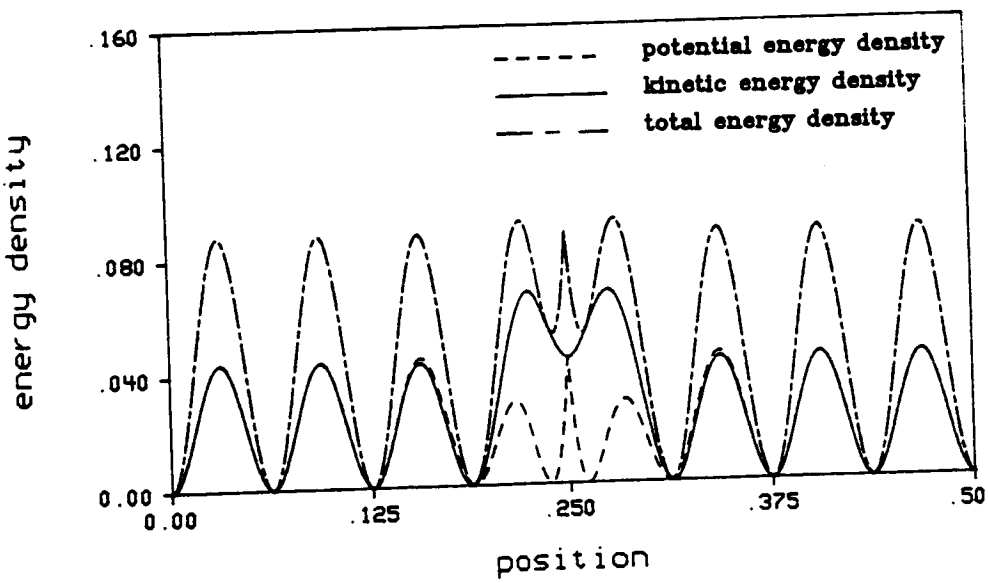

Figure 4.2.9 - Exact Potential, Kinetic and Total Energy Densities in the Transversely Vibrating Beam Shown in Figure (4.2.8)

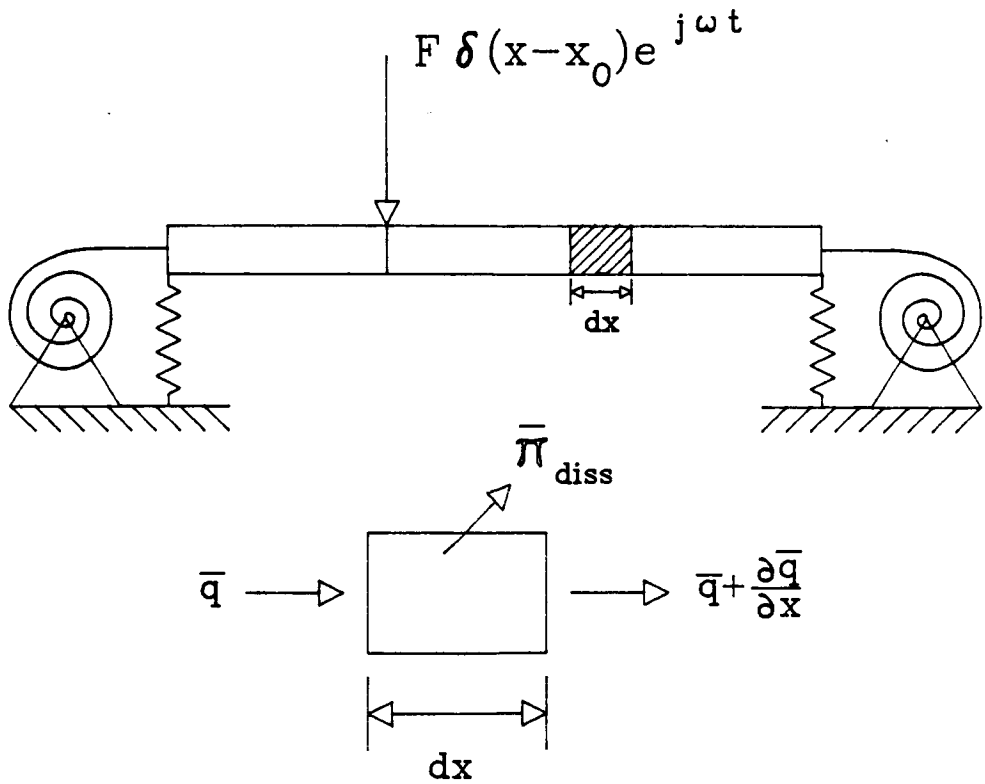

Figure 4.2.10 - Energy Balance on a Differential Element in a Transversely Vibrating Beam Excited by a Harmonic Point Force

CHAPTER 5 - COUPLING ENERGY SOLUTIONS

5.1 Introduction

The objective of power flow analysis is to provide a means by which the propagation of vibrational power through a structural/acoustic system can be studied. The governing equations which model power flow and energy density in individual rods and beams were developed in chapters 3 and 4. However, to analyze the power flow in a built up structure a method of coupling the solutions for individual rod and beam elements must be developed. A complete coupling scheme will provide the necessary boundary conditions so that the unknown constants in the energy solutions for rods and beams, equations (3.2.37) and (4.2.67) can be solved. However, even in simple configurations, coupling rods and beams for this energy formulation without using an exact solution, can be a formidable task. One of the major difficulties in calculating the coupling parameters of a complex system is accurately describing the resonant behavior of a built up structure and its components.

5.2 Energy Density Jump Conditions

Figure (5.2.1) shows the simple case of two rods joined rigidly at the ends, undergoing longitudinal vibration. The input and output power fluxes in figure (5.2.1) are assumed to be known. From equation (3.2.37) the energy density solutions for rod 1 and rod 2 are

$$<e>_1 = C_1 e^{\psi_1 x} + C_2 e^{-\psi_1 x} \tag{5.2.1}$$

and

$$<e>_2 = C_3 e^{\psi_2 x} + C_4 e^{-\psi_2 x} \tag{5.2.2}$$

where

$$\psi_1 = \eta_1 \frac{\omega}{c_1}$$

and

$$\psi_2 = \eta_2 \frac{\omega}{c_2}$$

The four unknown constants in equations (5.2.1) and (5.2.2) require four boundary conditions to completely define the problem.

To illustrate one method of coupling the energy solutions for two rigidly connected rods, the analogous heat transfer problem will be discussed. The analogous heat transfer problem for the two coupled rods is a simple 1-D thermal conduction through two connected fins with a convective heat loss, q_{conv}, as shown in figure (5.2.2). In one dimensional thermal conduction, the relationship between the heat flux and the temperature is [36]

$$q_t(x) = -\kappa \frac{dT}{dx} \tag{5.2.3}$$

where:

$T(x)$ is the rod temperature.

$q_t(x)$ is the thermal heat flux in the x direction.

κ is the thermal conductivity of the material.

The general temperature solution to the conduction/convection problem in figure (5.2.2) is

$$\theta_1(x) = D_1 e^{m_1 x} + D_2 e^{-m_1 x} \tag{5.2.4}$$

and

$$\theta_2(x) = D_3 e^{m_2 x} + D_3 e^{-m_2 x} \tag{5.2.5}$$

where:

$$\theta(x) = T(x) - T_\infty$$

T_∞ is the ambient temperature.

The values of m_1 and m_2 are functions of the convection coefficient, material conductivity and fin geometry. Note the similarities between equations (5.2.1), (5.2.2), (5.2.4) and (5.2.5).

As with equations (5.2.1) and (5.2.2) the solutions for the temperature distributions require specification of four boundary conditions to solve for the four unknown constants in equations (5.2.4) and (5.2.5). Two of the boundary conditions in figure (5.2.2) are specified heat fluxes at the ends, $q_{in,t}$ and $q_{out,t}$. At the fin interface, $x = x_o$, the assumption used in heat transfer is that there exists a continuity of both temperature

$$\theta_1(x_o) = \theta_2(x_o) \tag{5.2.6}$$

and heat flow

$$q_{12,t} = q_{1t}(x_o) = q_{2t}(x_o) \tag{5.2.7}$$

The continuity of heat flow in equation (5.2.7) implies the coupling of the fins in figure (5.2.2) is conservative. Thus, any heat (energy) leaving one fin at the interface $x=x_o$ must enter the other fin. The boundary conditions in equations (5.2.6) and (5.2.7) along with the heat fluxes at the ends and a given value for T_∞ complete the specification of the heat transfer problem shown in figure (5.2.2) and allow the constants D_1 through D_4 in equations (5.2.4) and (5.2.5) to be evaluated.

In the rod vibration problem, figure (5.2.1), a conservative coupling between rods 1 and 2 may also be assumed. Thus the power flow out of rod 1 in the x direction at $x = x_o$ must be equal to the power flow into rod 2 in the x direction at $x = x_o$

$$q_{12} = \langle q \rangle_1 \Big|_{x=x_o} = \langle q \rangle_2 \Big|_{x=x_o} \tag{5.2.8}$$

Equation (5.2.8) provides the third boundary condition needed to couple the vibrating rod system. The fourth condition needed to solve for the unknown constants in equations (5.2.1) and (5.2.2) is more elusive.

In the case of the conducting fins, figure (5.2.2), a continuity of the primary variable, temperature, at the coupling location was used as the fourth boundary condition. However, in the structure to structure coupling shown in figure (5.2.1), the primary variable, energy density, is not continuous at $x = x_o$. A "jump" condition in energy density occurs at the rod-rod interface. The actual jump in energy levels at $x = x_o$ depends on the material properties and cross

sectional area of the two rods. The energy jump also depends on the amount of kinetic and potential energy density at the coupling location.

In the case of two rigidly coupled rods, a continuity of both velocity

$$\frac{\partial U_1}{\partial t}\Big|_{x=x_o} = \frac{\partial U_2}{\partial t}\Big|_{x=x_o} \tag{5.2.9}$$

and axial force, which can be expressed as

$$(ES)_1 \frac{\partial U_1}{\partial x}\Big|_{x=x_o} = (ES)_2 \frac{\partial U_2}{\partial x}\Big|_{x=x_o} \tag{5.2.10}$$

must be maintained at the interface. Using the continuity conditions in equations (5.2.9) and (5.2.10), relationships between the potential $<V>$ and kinetic $<T>$ energy densities for rods 1 and 2 at the coupling location can be developed. Using the definition of kinetic energy density given in equation (3.2.21) and the velocity condition in equation (5.2.9) it can be shown that the relationship between the kinetic energy density of rod 1 and rod 2 at $x = x_o$ is

$$<T>_1\Big|_{x=x_o} = \frac{(\rho S)_1}{(\rho S)_2} <T>_2\Big|_{x=x_o} \tag{5.2.11}$$

Similarly, using the definition of potential energy density in a rod, equation (3.2.20), and the continuity of force in equation (5.2.10), a relationship between the potential energy densities at the coupling location can be shown to be

$$<V>_1\Big|_{x=x_o} = \frac{(ES)_2}{(ES)_1} <V>_2\Big|_{x=x_o} \tag{5.2.12}$$

Adding equations (5.2.11) and (5.2.12) the total energy density of rod 1 at $x = x_o$ is

$$\langle e \rangle_1 \Big|_{x=x_o} = \frac{(\rho S)_1}{(\rho S)_2} \langle T \rangle_2 \Big|_{x=x_o} + \frac{(ES)_2}{(ES)_1} \langle V \rangle_2 \Big|_{x=x_o} \tag{5.2.13}$$

Equation (5.2.13) can be put in a more useful form by writing the kinetic energy density of rod 2 at $x = x_o$ as

$$\langle T \rangle_2 \Big|_{x=x_o} = a \langle e \rangle_2 \Big|_{x=x_o} \tag{5.2.14}$$

and the potential energy density of rod 2 as

$$\langle V \rangle_2 \Big|_{x=x_o} = b \langle e \rangle_2 \Big|_{x=x_o} \tag{5.2.15}$$

where

$$0 \leq a \leq 1$$

$$b = 1 - a$$

Substituting equations (5.2.14) and (5.2.15) into equation (5.2.13) gives the relationship between the total energy densities of rod 1 and 2 at the rod-rod interface as

$$\langle e \rangle_1 \Big|_{x=x_o} = \left\{ a \frac{(\rho S)_1}{(\rho S)_2} + b \frac{(ES)_2}{(ES)_1} \right\} \langle e \rangle_2 \Big|_{x=x_o} \tag{5.2.16}$$

Equation (5.2.16) is the jump condition in energy density which exists at the interface. The variable "a" in equation (5.2.14) is the ratio of kinetic energy density to the total energy density in rod 2 at $x = x_o$. "b" is the ratio of potential energy density to the total energy in rod 2 at $x = x_o$.

Figures (5.2.3)-(5.2.5) are plots of the energy densities in the two coupled rods, shown in figure (5.2.1), driven by a harmonic point force at $x = x_1$. Rod 2 has a free end condition at $x=x_2$ (i.e. $\sigma_L=0$). In figures (5.2.3)-(5.2.5), the parameters for the two coupled rods are

$$\text{length of rod 1} = 5 \text{ m}$$

$$\text{length of rod 2} = 5 \text{ m}$$

$$(ES)_1 = 6 \times 10^7 \text{ N}$$

$$(ES)_2 = 3 \times 10^7 \text{ N}$$

$$(\rho S)_1 = 2.358 \text{ kg/m}$$

$$(\rho S)_2 = 1.179 \text{ kg/m}$$

$$\eta_1 = \eta_2 = 0.01$$

Thus for the plots in figures (5.2.3)-(5.2.5) the ratios in equation (5.2.16) are

$$\frac{(\rho S)_1}{(\rho S)_2} = \frac{2.358}{1.179} = 2$$

and

$$\frac{(ES)_2}{(ES)_1} = \frac{3 \times 10^7}{6 \times 10^7} = \frac{1}{2}$$

The first plot, figure (5.2.3), illustrates a case where the driving frequency of the input is ω= 11093.1 rad/sec. At this frequency, the potential energy density is zero at the interface, x=5. Thus, b=0 and the energy density is all kinetic energy density, a=1. In this case where a=1 and b=0 equation (5.2.16) indicates that the jump condition at $x = x_o$ is

$$\langle e\rangle_1 \Big|_{x=x_o} = \frac{(\rho S)_1}{(\rho S)_2} \langle e\rangle_2 \Big|_{x=x_o} = 2\langle e\rangle_2 \Big|_{x=x_o} \tag{5.2.17}$$

At $x = x_o$ the energy density in rod 1 is twice that in rod 2. This behavior is illustrated in figure (5.2.3). The second plot, figure (5.2.4), demonstrates another case where the driving frequency is ω= 12677.8 rad/sec. At this frequency, the kinetic energy density is zero, a=0, at the interface and the total energy density is all potential energy density, b=1. With a=0 and b=1 equation (5.2.16) predicts that

$$\langle e\rangle_1 \Big|_{x=x_o} = \frac{(ES)_2}{(ES)_1} \langle e\rangle_2 \Big|_{x=x_o} = \frac{1}{2}\langle e\rangle_2 \Big|_{x=x_o} \tag{5.2.18}$$

In this case equation (5.2.18) shows that the energy density in rod 1 at $x = x_o$ is one half the total energy density in rod 2. Again the result in equation (5.2.18) is illustrated in figure (5.2.4).

The last example, shown in figure (5.2.5), is a case where the driving frequency is ω= 11885.44 rad/sec and at the interface, half the energy density in rod 2 is kinetic energy density, a=$\frac{1}{2}$, and half is potential energy density, b=$\frac{1}{2}$. The jump condition from equation (5.2.16) is

$$\langle e\rangle_1 \Big|_{x=x_o} = \frac{1}{2}\left\{\frac{(\rho S)_1}{(\rho S)_2} + \frac{(ES)_2}{(ES)_1}\right\}\langle e\rangle_2 \Big|_{x=x_o} = 1.25\langle e\rangle_2 \Big|_{x=x_o} \tag{5.2.19}$$

which is illustrated in figure (5.2.5).

If the value of either a or b in equation (5.2.16) were known, the jump condition between $<e>_1$ and $<e>_2$ at $x = x_o$ could be calculated. It would follow that the problem shown in figure (5.2.1) would be completely defined and the constants in equations (5.2.1) and (5.2.2) could be evaluated. Unfortunately, calculating the percentage of potential and kinetic energy density at a coupling location would require a complete classical analysis of the system in figure (5.2.1). If a classical analysis is available, there is no need for the simplified theory in chapter 3.

Equation (5.2.16) is still a useful relationship in that even without knowing the exact values of a and b, it can be used to set bounds on the ratio of the local energy densities $\frac{<e>_1}{<e>_2}$ at the coupling location. The maximum ratio of $<e>_1$ to $<e>_2$ at x_o is

$$\left\{ \frac{<e>_1}{<e>_2} \Big|_{x=x_o} \right\}_{max} = \max\left\{ \frac{(\rho S)_1}{(\rho S)_2} , \frac{(ES)_2}{(ES)_1} \right\} \tag{5.2.20}$$

where the operator $\max\left\{ \frac{(\rho S)_1}{(\rho S)_2} , \frac{(ES)_2}{(ES)_1} \right\}$ gives the largest of the two values in the brackets. The minimum ratio of $<e>_1$ to $<e>_2$ is

$$\left\{ \frac{<e>_1}{<e>_2} \Big|_{x=x_o} \right\}_{min} = \min\left\{ \frac{(\rho S)_1}{(\rho S)_2} , \frac{(ES)_2}{(ES)_1} \right\} \tag{5.2.21}$$

where the operator $\min\left\{ \frac{(\rho S)_1}{(\rho S)_2} , \frac{(ES)_2}{(ES)_1} \right\}$ gives the smallest of the two values in the brackets.

For a given set of known power flux end conditions and at a specific frequency, the ratios in equations (5.2.20) and (5.2.21) can be used to set upper and lower bounds on the energy density levels and power flow in the coupled rod system in figure (5.2.1). For example, consider the system in figure (5.2.1) with the same rod parameters used for the test cases shown in figures (5.2.3)-(5.2.5). For this example, it will be assumed that the power flow into rod 1 in the x direction at $x=x_1$ is $q_{in}=1$ and the power flowing out of rod 2 in the x direction at $x=x_2$ is $q_{out}=0$. A conservative coupling between rods 1 and 2 will be assumed which allows equation (5.2.8) to be used as the third boundary condition. Thus, three of the four necessary boundary conditions are

$$\langle q\rangle_1 \Big|_{x=x_1} = 1$$

$$\langle q\rangle_2 \Big|_{x=x_2} = 0$$

$$\langle q\rangle_1 \Big|_{x=x_o} = \langle q\rangle_2 \Big|_{x=x_o}$$

From equation (5.2.20) and the given system parameters, the maximum value of the ratio between $\langle e\rangle_1$ and $\langle e\rangle_2$ at x_o is

$$\left\{\frac{\langle e\rangle_1}{\langle e\rangle_2}\Big|_{x=x_o}\right\}_{max} = \frac{(\rho S)_1}{(\rho S)_2} = 2 \qquad (5.2.22)$$

The minimum ratio from equation (5.2.21) is

$$\left\{\frac{\langle e\rangle_1}{\langle e\rangle_2}\Big|_{x=x_o}\right\}_{min} = \frac{(ES)_2}{(ES)_1} = \frac{1}{2} \qquad (5.2.23)$$

Equations (5.2.22) and (5.2.23) can be used to provide the fourth boundary

condition needed to solve for the unknown constants in equations (5.2.1) and (5.2.2). For one solution, the fourth boundary condition, from equation (5.2.22), is

$$\langle e \rangle_1 \Big|_{x=x_o} = 2\langle e \rangle_2 \Big|_{x=x_o} \tag{5.2.24}$$

For the second solution, the fourth boundary conditions from equation (5.2.23) is

$$\langle e \rangle_1 \Big|_{x=x_o} = \frac{1}{2}\langle e \rangle_2 \Big|_{x=x_o} \tag{5.2.25}$$

Figures (5.2.6) and (5.2.7) show the upper and lower bounds on the power flow and energy density at a driving frequency of ω= 11885.44 rad/sec as calculated from the boundary conditions in equations (5.2.24) and (5.2.25). At the same frequency, with the same power flux end conditions and a rigid, conservative coupling of rods 1 and 2, any combination of a and b in equation (5.2.16) would result in a power flow solution and energy density levels which would fall within the bounds illustrated in figures (5.2.6) and (5.2.7).

Figures (5.2.6) and (5.2.7) demonstrate that while equation (5.2.16) cannot provide exact information about the power flow and energy density levels, it can provide useful information about the dynamic response of the coupled rod system. A similar analysis of the local energy densities of two rigidly coupled beams would produce results analogous to those found in equations (5.2.11), (5.2.12) and (5.2.16). However, the coupling junction of two dissimilar beams is

a discontinuity. Thus, the nearfield terms in the beam displacement solution cannot be neglected when local coupling methods are studied since the nearfield terms can be of the same magnitude as the farfield terms at a discontinuity. Modifications must be made to the farfield energy density solutions developed in chapter 4 to include the nearfield effects at a coupling junction.

5.3 Coupled Rods

Figure (5.3.1) shows two rods vibrating longitudinally, coupled by a linear spring of spring rate σ_{L1}. From equation (3.2.36) the energy solutions for rods 1 and 2 are

$$<e>_1 = C_1 e^{\psi_1 x} + C_2 e^{-\psi_1 x} \tag{5.3.1}$$

$$<e>_2 = C_3 e^{\psi_2 x} + C_4 e^{-\psi_2 x} \tag{5.3.2}$$

where

$$\psi_1 = \eta_1 \frac{\omega}{c_1}$$

and

$$\psi_2 = \eta_2 \frac{\omega}{c_2}$$

The coupling schemes to be introduced in this section will provide the necessary boundary conditions to solve for the unknown constants in equations (5.3.1) and (5.3.2) by calculating the power flow, q_{12}, between rods 1 and 2. By assuming a conservative coupling, the power flowing out of rod 1 at $x = x_o$ is equal to the power flowing into rod 2 at $x = x_o$. The coupled structure in figure (5.3.1) can

be split into two components, as shown in figure (5.3.2), where a power flux is specified on both ends for each component. Knowing the power flux on both ends of each rod will allow the constants in equations (5.3.1) and (5.3.2) to be solved.

5.3.1 Coupling Rods Using Receptance

The receptance method is an exact solution by which the vibrational response of a built up structure can be analyzed by studying the dynamic characteristics of its individual component parts. Using receptances to calculate the power transferred between coupled systems has been suggested by both Pinnington and White [16] and Cuschieri [37] in their work with power flow solutions. A good introduction to the receptance method is found in Soedel's book on the vibration of plates and shells [29]. As defined by Soedel, the receptance of a structure is " the ratio of a steady state deflection response at a certain point to a harmonic force or moment input at the same or different point." Actually, in a power flow analysis it is more convenient to use mobility functions (α_{ij}) which are the ratio of a steady state velocity response at a certain point to a harmonic force input at the same or different point

$$\alpha_{ij} = \frac{\text{velocity response at location i}}{\text{harmonic input at location j}} \tag{5.3.3}$$

Though mobility functions are used in this analysis the coupling technique is still referred to as the receptance method.

Consider the coupled rod system in figure (5.3.3). The receptance method allows the coupled system in figure (5.3.3) to be analyzed by studying the vibrational characteristics of the two components shown in figure (5.3.4). In this analysis α_{ij} will represent a mobility function of rod 1, β_{ij} will represent a mobility function of rod 2. The mobility of rod 1 in figure (5.3.4) is

$$\alpha_{ij} = \frac{V_{ai}e^{j\omega t}}{F_{aj}e^{j\omega t}} = \frac{V_{ai}}{F_{aj}} \tag{5.3.4}$$

where:

$V_{ai}e^{j\omega t}$ is the velocity of rod 1 at point ai.

$F_{aj}e^{j\omega t}$ is the point force acting on rod 1 at point aj.

For example, α_{12} is the ratio of the velocity of rod 1 at x=a1 due to a harmonic point force acting at x=a2. For a given set of boundary conditions the mobility of rod 1 is easily calculated using a classical solution. In figure (5.3.4) rod 1 is excited by two forces. The input force $F_{a1}e^{j\omega t}$ acts on rod 1 at x=a1 while a reaction force, $F_{a2}e^{j\omega t}$ due to the coupling with the spring-rod system 2, acts on rod 1 at x=a2. Using the definition of mobilities, equation (5.3.4), the velocities at x=a1 and x=a2 are

$$V_{a1}e^{j\omega t} = (\alpha_{11}F_{a1} + \alpha_{12}F_{a2})e^{j\omega t} \tag{5.3.5}$$

and

$$V_{a2}e^{j\omega t} = (\alpha_{21}F_{a1} + \alpha_{22}F_{a2})e^{j\omega t} \tag{5.3.6}$$

For the spring-rod system 2 in figure (5.3.4) Soedel [29] has shown that the displacement at x_o, $x_{b0}e^{j\omega t}$ of the spring due to a harmonic force input $F_{b0}e^{j\omega t}$ is

$$x_{b0}e^{j\omega t} = \frac{1}{\sigma_{L1}}(1 + \sigma_{L1}\bar{\beta}_{22})F_{b0}e^{j\omega t} \tag{5.3.7}$$

where

$\bar{\beta}_{22}$ is the receptance of rod 2 at the spring attachment point.

Converting equation (5.3.7) to use a mobility function instead of receptance function gives

$$V_{b0}e^{j\omega t} = \frac{1}{\sigma_{L1}}(j\omega + \sigma_{L1}\beta_{22})F_{b0}e^{j\omega t} \tag{5.3.8}$$

where

β_{22} is the mobility of rod 2 at the spring attachment point.

From equation (5.3.8) the mobility of the spring-rod system in figure (5.3.4) is

$$\beta_{00} = \frac{V_{b0}e^{j\omega t}}{F_{b0}e^{j\omega t}} = \frac{1}{\sigma_{L1}}(j\omega + \sigma_{L1}\beta_{22}) \tag{5.3.9}$$

Using equation (5.3.9), the velocity of the spring at b0 due to a harmonic input is

$$V_{b0}e^{j\omega t} = \beta_{00}F_{b0}e^{j\omega t} \tag{5.3.10}$$

In figure (5.3.4) where rod 1 is attached to the spring, there is a continuity of velocity

$$V_{a2}e^{j\omega t} = V_{b0}e^{j\omega t} \tag{5.3.11}$$

and a balance of forces

$$F_{a2}e^{j\omega t} = -F_{b0}e^{j\omega t} \tag{5.3.12}$$

Using the continuity of velocity, equation (5.3.11), equations (5.3.6) and (5.3.10) can be equated

$$(\alpha_{21}F_{a1} + \alpha_{22}F_{a2})e^{j\omega t} = \beta_{00}F_{b0}e^{j\omega t} \tag{5.3.13}$$

Substituting the force balance in equation (5.3.12) into equation (5.3.13) and solving for the reaction force in the spring gives

$$F_{b0}e^{j\omega t} = \left(\frac{\alpha_{21}}{\alpha_{22} + \beta_{00}}\right)F_{a1}e^{j\omega t} \tag{5.3.14}$$

Equation (5.3.14) shows the reaction force between rod 1 and the spring-rod system 2 due to a harmonic force input to rod 1 at point a1. The power input to rod 1 from the force $F_{a1}e^{j\omega t}$ is

$$q_{in} = \frac{1}{2}\mathrm{Re}\{F_{a1}V_{a1}^{*}\} = \frac{1}{2}\mathrm{Re}\{F_{a1}[\alpha_{11}F_{a1} + \alpha_{12}F_{a2}]^{*}\} \tag{5.3.15}$$

Substituting equations (5.3.12) and (5.3.14) into equation (5.3.15), q_{in} can be written as

$$q_{in} = \frac{1}{2}|F_{a1}|^2\mathrm{Re}\left\{\alpha_{11} - \frac{\alpha_{12}\,\alpha_{21}}{\alpha_{11} + \beta_{00}}\right\} \tag{5.3.16}$$

The power flowing between system 1 and 2 in figure (5.3.4) is

$$q_{12} = \frac{1}{2}\mathrm{Re}\{F_{b0}V_{b0}^{*}\} = \frac{1}{2}|F_{b0}|^2\mathrm{Re}\{\beta_{00}^{*}\} \tag{5.3.17}$$

From equation (5.3.14), the magnitude of $|F_{b0}|^2$ is

$$|F_{b0}|^2 = \left|\frac{\alpha_{21}}{\alpha_{22}+\beta_{00}}\right|^2 |F_{a1}|^2 \tag{5.3.18}$$

Substituting equation (5.3.18) into the expression for q_{12} the relationship between the power input to rod 1 and the power transferred between systems 1 and 2 is

$$q_{12} = \left|\frac{\alpha_{21}}{\alpha_{22}+\beta_{00}}\right|^2 \frac{\mathrm{Re}(\beta_{00})}{\mathrm{Re}\left[\alpha_{11}-\dfrac{\alpha_{12}\,\alpha_{21}}{\alpha_{22}+\beta_{00}}\right]} q_{in} \tag{5.3.19}$$

In the coupled rod system shown in figure (5.3.1) the power flowing into rod 1, q_{in}, and the power flowing out of rod 2, q_{out}, are assumed to be known and thus represent two boundary conditions. A conservative coupling provides the third boundary condition. Equation (5.3.19) is the fourth boundary condition needed to fully specify the coupled rod problem and allow the unknown constants in equations (5.3.1) and (5.3.2) to be solved.

5.3.2 Introduction to Statistical Energy Analysis

Another technique which can be used to couple the energy density solutions for rods and beams is the wave transmission approach. In most applications, the wave transmission approach is used to couple subsystems in a SEA model. Therefore, to understand how the wave transmission approach can be used to couple the simplified energy density solutions, it is necessary to understand how

it is used in Statistical Energy Analysis.

As discussed in chapter 2, Statistical Energy Analysis (SEA) is an analytical technique which is used to model the flow of power and distribution of vibrational energy in acoustical, structural and acoustical/structural systems. One of the original investigators of SEA, Lyon [38], wrote that "SEA is based on the concept that constructed systems form a statistical population, and the problem of design is to estimate statistics of the dynamical response of that population." In other words, the goal of Statistical Energy Analysis is to predict the average values of a system response when the excitation is a randomly distributed, broadband frequency source.

A general SEA model is shown in figure (5.3.5). The model in figure (5.3.5) consists of two coupled subsystems each with its own power input, $q_{in,1}$ and $q_{in,2}$. In SEA, the power input is generally assumed to be a broadband frequency source which is spatially distributed in a random manner over the subsystem. Each subsystem is assumed to dissipate a certain amount of power, $\pi_{1,diss}$ and $\pi_{2,diss}$. There is also power flowing between the two systems. q_{12} indicates the net power flowing from system 1 to system 2 while q_{21} is the net power flow from system 2 to system 1.

The power inputs in a SEA model are assumed to be known values. The input power to a system is either measured experimentally or predicted using an analytical technique. The power dissipated in a subsystem is modeled as being proportional to the total energy in the subsystem

$$\pi_{i,diss} = \omega \eta_{di} E_{i,tot} \tag{5.3.20}$$

where:

$\pi_{i,diss}$ is the power dissipated in the ith subsystem.

ω is the center frequency of the broadband input.

η_{di} is the loss factor associated with the ith subsystem.

$E_{i,tot}$ is the total energy in the ith subsystem.

Note the similarities between how power dissipation is modeled in SEA and how power is dissipated in the simplified models of equations (3.2.35) and (4.2.65). The major difference between the SEA model of power dissipation and that of the simplified models is that power dissipation in SEA is a global parameter based on the total energy in a subsystem. The simplified models for a rod and beam model power dissipation in a local sense. The local power dissipated in the simplified models is proportional to the local values of energy density.

One of the basic assumptions of SEA is that for randomly excited coupled subsystems, the power flow between subsystems i and j is proportional to the difference in the average modal energies, $\frac{E_{i,tot}}{N_i}$ and $\frac{E_{j,tot}}{N_j}$ and flows from the subsystem of higher modal energy to the subsystem of lower modal energy. Here N_i is the approximate number of modes excited in the frequency band. The power flow between subsystems in SEA is written as

$$q_{ij} = \omega \eta_{ij} n_i \left\{ \frac{E_{i,tot}}{n_i} - \frac{E_{j,tot}}{n_j} \right\} \tag{5.3.21}$$

where:

q_{ij} is the power flow from subsystem i to j.

η_{ij} is the coupling loss factor.

n_i is the modal density of the ith subsystem at ω.

The modal density of a continuous structure is the approximate number of natural frequencies, per hertz or per radians/second, found in a given frequency bandwidth.

Equation (5.3.21) is based on the following assumptions:

1) Each mode of vibration is equally excited, i.e. equally energetic.

2) Coupling is mode to mode.

3) Coupling is based on global energy levels, not local energy densities.

4) Each mode is assumed to have a natural frequency which is uniformly probable over a frequency bandwidth.

Performing a control volume analysis of subsystems 1 and 2 in figure (5.3.5) gives the power balances

$$q_{1,in} = \pi_{1,diss} + q_{12} \tag{5.3.22}$$

and

$$q_{2,in} = \pi_{2,diss} + q_{21} \tag{5.3.23}$$

It can also be shown through a power balance that

$$q_{12} = -q_{21} \tag{5.3.24}$$

thus

$$q_{2,in} = \pi_{2,diss} - q_{12} \tag{5.3.25}$$

Substituting the power dissipation expression, equation (5.3.20), and the power flow term, equation (5.3.21), into the energy balances in equations (5.3.22) and (5.3.25) results in a set of simultaneous equations which model the flow of power in the system depicted in figure (5.3.5)

$$\begin{Bmatrix} \omega\eta_{d1} + \omega\eta_{12} & -\omega\eta_{12}\dfrac{n_1}{n_2} \\ -\omega\eta_{12} & \omega\eta_{d2} + \omega\eta_{12}\dfrac{n_1}{n_2} \end{Bmatrix} \begin{Bmatrix} E_{1,tot} \\ E_{2,tot} \end{Bmatrix} = \begin{Bmatrix} q_{1,in} \\ q_{2,in} \end{Bmatrix} \tag{5.3.26}$$

The modal densities n_i in equation (5.3.26) can be calculated analytically for many structural members. Lyon has calculated and tabulated the modal densities for a number of common structures [7].

One of the most important parameters in SEA, and one of the most difficult to evaluate, is the coupling loss factor η_{ij}. Due to their importance, a large portion of the work done in SEA has been devoted to calculating the coupling loss factors for various systems. Many times however, the systems being studied are too complicated to easily calculate analytical loss factors. When analytical solutions are not available it is sometimes necessary to experimentally measure the values of η_{ij}. Various investigations of coupling loss factors were reviewed in chapter 2.

When all the terms in equation (5.3.26) are known, the total energies in subsystems 1 and 2 can be calculated by solving the matrix equation (5.3.26). Using conversion factors in Lyon's book [7], the total energies in subsystems 1 and 2 can then be used to calculate more useful dynamic responses such as average values of displacement, velocity, stress etc. The total energies can also be substituted into equation (5.3.21) to calculate the power flow between subsystem 1 and 2.

In this brief introduction, some of the important aspects of SEA have been discussed. In the following sections, two examples of coupled subsystems will be examined for which analytical coupling loss factors have been developed. These coupled subsystems will illustrate how SEA coupling parameters can be applied to the power flow solutions in chapters 3 and 4. It is important when using the coupling parameters from a SEA model that the user remain aware of the assumptions made in deriving the SEA coupling loss factors discussed here and in chapter 2. These assumptions include limiting the analysis to broadband frequency inputs and neglecting the resonant behavior of finite structures.

5.3.3 Coupling Rods Using a Wave Transmission Approach

Consider again the coupled rod system in figure (5.3.2). The general SEA model in figure (5.3.5) will be used to analyze the coupled rods. Rod 1 in figure (5.3.2) will be represented by subsystem 1 in the SEA model while rod 2 will be represented by subsystem 2. Note that the spring in figure (5.3.2) is not included in either subsystem 1 or 2 in the SEA model. The spring connecting

the rods will come into the Statistical Energy Analysis model through the coupling loss factor, η_{12}.

The matrix equation (5.3.26) now models the energy distribution in the coupled rod system in figure (5.3.2). The energy value $E_{1,tot}$ in equation (5.3.26) is the total energy in rod 1 and $E_{2,tot}$ is the total energy in rod 2. Since in figure (5.3.2) there is no external source acting on rod 2, the power input $q_{2,in}$ in equation (5.3.26) is zero. Due to the similarities in the SEA power dissipation expression, as shown in equation (5.3.20), and the simplified power dissipation expression for a rod, shown in equation (3.2.35), the power dissipation factors, η_{d1} and η_{d2}, in equation (5.3.26) will be approximated as the hysteretic damping coefficients used for rods 1 and 2. The modal densities for longitudinally vibrating rods, n_1 and n_2, are [7]

$$n_i = \frac{L_i}{c_i \pi} \tag{5.3.27}$$

where:

n_i is the modal density in rod i.

L_i is the length of rod i.

c_i is the phase speed in rod i.

The only remaining unknown in equation (5.3.26) is the coupling loss factor η_{12}. In a study of coupling loss factors, Remington and Manning [17] developed an expression for η_{12} which controls the flow of vibrational power in a SEA model of two coupled rods. Remington and Manning based their coupling

equation on the "wave transmission approach" which, as discussed in chapter 2, allows the coupling of continuous structures by approximating the input impedance of finite structures by that of infinite structures. The infinite impedance of rod 1 is [8]

$$Z_{1\infty} = (\rho S)_1 c_1 \tag{5.3.28}$$

while the infinite impedance of rod 2 is

$$Z_{2\infty} = (\rho S)_2 c_2 \tag{5.3.29}$$

where

$(\rho S)_i$ is the density per unit length of rod i.

Remington and Manning also showed the impedance of a spring attached to the infinite rod 2 is

$$Z_{2S\infty} = Z_{2\infty}\left\{\frac{j\frac{\sigma_{L1}}{\omega}}{j\frac{\sigma_{L1}}{\omega} - Z_{2\infty}}\right\} \tag{5.3.30}$$

Using infinite impedances, Remington and Manning calculated the coupling loss factors for the system in figure (5.3.4) to be

$$\omega\eta_{12} = \frac{1}{(\rho S)_1 L_1}\left|\frac{1}{\alpha_\infty + \beta_{S\infty}}\right|^2 \mathrm{Re}\{\beta_\infty\}\left\{\frac{1}{1 - \frac{1}{4}\frac{(\rho S)_1}{(\rho S)_2}\left|\frac{\alpha_\infty}{\alpha_\infty + \beta_{S\infty}}\right|^2}\right\} \tag{5.3.31}$$

where

$$\alpha_{\infty} = \frac{1}{Z_{1\infty}}$$

$$\beta_{\infty} = \frac{1}{Z_{2\infty}}$$

$$\beta_{S\infty} = \frac{1}{Z_{2S\infty}}$$

The coupling loss factor in equation (5.3.31) was found, by Remington and Manning, to compare well with an exact solution when the exact solution was averaged over frequency.

All the terms in the square matrix of equation (5.3.26) can now be calculated and the total energies $E_{1,tot}$ and $E_{2,tot}$ can be solved. The values of $E_{1,tot}$ and $E_{2,tot}$ may then be substituted into equation (5.3.21) and the power flow between rods 1 and 2 evaluated.

5.3.4 Comparing Coupling Solutions for a Rod

To compare the receptance method and the wave transmission approach, the power flow between the two rods in figure (5.3.1) has been calculated using the coupling solutions presented in sections 5.3.1 and 5.3.3. Figure (5.3.6) shows the power flow q_{12}, calculated from using the receptance method and wave transmission approach, equations (5.3.19) and (5.3.31), as a function of frequency with a unit power input, q_{in}=1. For the example in figure (5.3.6) the system parameters are

length of rod 1 = 5 m

length of rod 2 = 5 m

$$(ES)_1 = (ES)_2 = 6 \times 10^7 \text{ N}$$

$$(\rho S)_1 = (\rho S)_2 = 2.358 \text{ kg/m}$$

$$\sigma_{L1} = 3 \times 10^7 \text{ N/m}$$

$$\eta_1 = \eta_2 = 0.01$$

Figure (5.3.6) illustrates the expected inability of the wave transmission coupling solution to model the resonant behavior of the coupled rod system. The wave transmission approach could not therefore be used to accurately predict the power flow for a single frequency input. However the wave model appears to be a good approximate frequency average of the exact solution and could be used for a broadband frequency source. The receptance solution is an exact solution and is able to model the resonant behavior of the coupled rod system and therefore can be used for either a single frequency or broadband power input.

5.4 Coupled Beams

Figure (5.4.1) shows two simply supported beams vibrating transversely, coupled by a torsional spring of spring rate σ_T. The power input to beam 1 from the transverse harmonic point source, q_{in}, is assumed to be known. From equation (4.2.67) the farfield energy solutions for beams 1 and 2 are

$$\langle \bar{e} \rangle_{1ff} = C_1 e^{\phi_1 x} + C_2 e^{-\phi_1 x} \tag{5.4.1}$$

$$\langle \bar{e} \rangle_{2ff} = C_3 e^{\phi_2 x} + C_4 e^{-\phi_2 x} \tag{5.4.2}$$

where

$$\phi_1 = \frac{\eta_1 \omega}{2c_{b1}}$$

and

$$\phi_2 = \frac{\eta_2 \omega}{2c_{b2}}$$

As with the coupled rod examples in section 5.3 the coupling schemes to be introduced in this section will provide the necessary boundary conditions to solve for the unknown constants in equations (5.4.1) and (5.4.2) by calculating the power flow, q_{12}, between beams 1 and 2 in figure (5.4.1). A conservative coupling between beams 1 and 2 is assumed.

5.4.1 Coupling Beams Using Receptance

Power flow between the beams in figure (5.4.1) is transmitted purely by the moment and angular velocity at the coupling location. The simple supports of the two beams prevent any transverse velocity at the ends. Thus the power flow associated with the shear force, as defined in equation (4.2.21), is zero at the supports. Since the two beams in figure (5.4.1) are coupled only by a moment, the procedure of calculating the power flow between beams 1 and 2 with receptances will be very similar to the process used for the coupled rods in section 5.3.1.

Using the receptance method, the coupled system in figure (5.4.1) can be split into its two components as shown in figure (5.4.2). The mobility of beam 1 in figure (5.4.2) is

$$\alpha_{ij} = \frac{V_{ai}e^{j\omega t}}{F_{aj}e^{j\omega t}} = \frac{V_{ai}}{F_{aj}} \tag{5.4.3}$$

where:

$V_{ai}e^{j\omega t}$ is the linear or angular velocity of beam 1 at point ai.

$F_{aj}e^{j\omega t}$ is the point force or moment acting on beam 1 at point aj.

Note in equation (5.4.3) that $V_{ai}e^{j\omega t}$ can represent either a linear or angular velocity while $F_{aj}e^{j\omega t}$ can be either a transverse force or moment. The mobility for beam 1 is calculated using a classical beam displacement solution. In figure (5.4.2) beam 1 is acted upon by two forces. The transverse point force $F_{a1}e^{j\omega t}$ acts on beam 1 at x=a1 while a reaction moment, $F_{a2}e^{j\omega t}$, due to the coupling with the spring-beam system 2, acts on beam 1 at x=a2. Using the mobility functions as defined in equation (5.3.3) the transverse velocity at x=a1 is

$$V_{a1}e^{j\omega t} = (\alpha_{11}F_{a1} + \alpha_{12}F_{a2})e^{j\omega t} \tag{5.4.4}$$

and the angular velocity at x=a2 is

$$V_{a2}e^{j\omega t} = (\alpha_{21}F_{a1} + \alpha_{22}F_{a2})e^{j\omega t} \tag{5.4.5}$$

In a procedure analogous to that used to calculate the mobility of the spring-rod system 2, the mobility of the spring-beam system 2 in figure (5.4.2) is

$$\beta_{00} = \frac{V_{b0}e^{j\omega t}}{F_{b0}e^{j\omega t}} = \frac{1}{\sigma_T}(j\omega + \sigma_T\beta_{22}) \tag{5.4.6}$$

where:

$V_{b0}e^{j\omega t}$ is the angular velocity of the torsional spring at point b0.

$F_{b0}e^{j\omega t}$ is the harmonic moment applied the torsional spring at point b0.

β_{22} is the mobility of beam 2 at the spring attachment point.

From equation (5.4.6), the angular velocity of the torsional spring at b0 is

$$V_{b0}e^{j\omega t} = \beta_{00}F_{b0}e^{j\omega t} \tag{5.4.7}$$

In figure (5.4.2), where beam 1 is attached to the spring, there is a continuity of angular velocity

$$V_{a2}e^{j\omega t} = V_{b0}e^{j\omega t} \tag{5.4.8}$$

and a balance of moments

$$F_{a2}e^{j\omega t} = -F_{b0}e^{j\omega t} \tag{5.4.9}$$

From this point the derivation is exactly the same as the one used in section 5.3.1. Using the continuity of angular velocity, equation (5.4.8), and the moment balance in equation (5.4.9), the power flow between beams 1 and 2 in figure (5.4.1) is

$$q_{12} = \left| \frac{\alpha_{21}}{\alpha_{22} + \beta_{00}} \right|^2 \frac{\mathrm{Re}(\beta_{00})}{\mathrm{Re}\left[\alpha_{11} - \dfrac{\alpha_{12}\,\alpha_{21}}{\alpha_{22} + \beta_{00}} \right]} q_{in} \tag{5.4.10}$$

In the coupled beam system shown in figure (5.4.1) the power flowing into beam 1, q_{in}, and the power flowing out of beam 2, q_{out}, are assumed to be known and thus represent two boundary conditions. A conservative coupling provides the third boundary condition. Equation (5.4.10) is the fourth boundary condition needed to fully specify the coupled beam problem and allow the unknown constants in equations (5.4.1) and (5.4.2) to be solved.

5.4.2 Coupling Beams Using a Wave Transmission Approach

The power flow between beam 1 and beam 2 in figure (5.4.1) can also be calculated using a wave transmission approach. The general SEA diagram in figure (5.3.5) will be used to model the energy distribution in the coupled beam system. Beam 1 in figure (5.4.2) will be represented by subsystem 1 in the SEA model and beam 2 will be represented by subsystem 2.

The matrix equation (5.3.25) now models the energy in the coupled beam system in figure (5.4.1). The energy values $E_{1,tot}$ and $E_{2,tot}$ in equation (5.3.25) are the total energies in beam 1 and 2. Since beam 2 has no external power source, $q_{2,in}$ is zero. Due to the similarities in the SEA power dissipation expression, as shown in equation (5.3.20), and the simplified power dissipation expression for a beam, shown in equation (4.2.65), the power dissipation factors, η_{d1} and η_{d2}, in equation (5.3.26) will be approximated as the hysteretic damping coefficients used for beams 1 and 2. The modal density for a beam is [7]

$$n_i = \frac{L_i}{2\pi c_{bi}} \tag{5.4.11}$$

where:

n_i is the modal density in beam i.

L_i is the length of beam i.

c_{bi} is the wave speed in beam i.

In a review of coupling loss factors, Crandall and Lotz [20] discussed some work done by Scharton and Lyon [15] on developing a coupling loss factor η_{12} for the system in figure (5.4.1) using a wave transmission approach. Crandall

and Lotz found that Scharton's and Lyon's work leads to a coupling loss factor of

$$\omega\eta_{12} = \frac{2\pi\sigma_T{}^2 n_2}{\{(\rho S)_1 L_1{}^2 (EI)_1\}^{1/2}\{(\rho S)_2 L_1{}^2 (EI)_2\}^{1/2}} \qquad (5.4.12)$$

Using the result in equation (5.4.12), the matrix equation (5.3.25) can be solved and the energy levels in beam 1 and beam 2 calculated. The energies $E_{1,tot}$ and $E_{2,tot}$ can then be substituted into equation (5.3.20) and the power flow between beam 1 and beam 2 in figure (5.4.1) can be evaluated and the energy densities in beams 1 and 2 can be found.

5.4.3 Comparing Coupling Solutions for a Beam

The plot in figure (5.4.3) shows the power flow, q_{12}, as a function of frequency for the coupled beam system in figure (5.4.1) using the coupling solutions in sections 5.4.1 and 5.4.2. The system parameters used in figure (5.4.3) are

$$\text{length of beam 1} = 0.5 \text{ m}$$

$$\text{length of beam 2} = 0.5 \text{ m}$$

$$(EI)_1 = (EI)_2 = 500 \text{ Nm}^2$$

$$(\rho S)_1 = (\rho S)_2 = 2.358 \text{ kg/m}$$

$$\sigma_{T1} = 1 \times 10^5 \text{ (Nm)/rad}$$

$$\eta_1 = \eta_2 = 0.001$$

Figure (5.4.3) shows the inability of the wave transmission coupling solution in section 5.4.2 to model the resonant behavior of the connected beam system. For

a broadband frequency excitation the wave transmission coupling in figure (5.4.3) might provide an acceptable approximation for power flow. The exact solution from the receptance method can be used for single frequency or broadband inputs.

5.5 Summary

In this chapter the coupling of the energy solutions for the rods and beams developed in chapters 3 and 4, was discussed. It was found that a discontinuous jump in energy density occurs at a coupling location. This jump condition was found to be related to the amounts of potential and kinetic energy density at the coupling location. During the development of the simplified theory in chapters 3 and 4 it was hoped that the energy equations would lead to an efficient and accurate method of coupling solutions for both single frequency and broadband inputs. The key to the development of such a method is a relationship between the local energy densities at the junction. However, a simple relationship between the local energy density has not yet been developed. It is recommended that effort continue toward this objective using the energy relationships developed in section 5.2. Nevertheless, it was shown in section 5.2 that even though equation (5.2.16) cannot provide exact information about the power flow and energy density in a coupled rod system, it can provide upper and lower bounds of both power flow and energy density for a given set of power flux boundary conditions. This information could be useful in designing complicated built-up structures.

The coupling methods presented in sections 5.3 and 5.4 are approximations similar to common power flow analysis methods. The methods provide the needed boundary conditions to couple the energy solutions by estimating the power flow between coupled elements. The first coupling scheme discussed in sections 5.3 and 5.4 was the receptance method. The receptance method is a powerful tool which allows complex structures to be analyzed by studying the resonant responses of its component parts. It is an exact solution and thus can be used to accurately couple structures driven by both single frequency and broadband inputs. It is not clear yet how a systematic procedure of combining receptances for a general structure can be developed. Each built up structure must be individually analyzed. For a complex structure, deriving the receptance equations is currently a prohibitively difficult process but it is possible that numerical methods might be used to compute the required information accurately and efficiently. Once a system has been analyzed by the receptance method the simplified theory can be used to show the energy distribution and power flow throughout built-up structures.

The second method discussed for coupling structures was based on the wave transmission approach used in Statistical Energy Analysis. The wave transmission approach couples structures by approximating the input impedance of a finite structure by the input impedance of an infinite structure. The input impedance of an infinite structure has been shown to be a good frequency average of impedance. However, since impedance varies significantly from its

average value at a specific frequency, the wave transmission approach cannot accurately couple structures excited by a single frequency excitation, but it can be used to couple structures excited by a broadband frequency source.

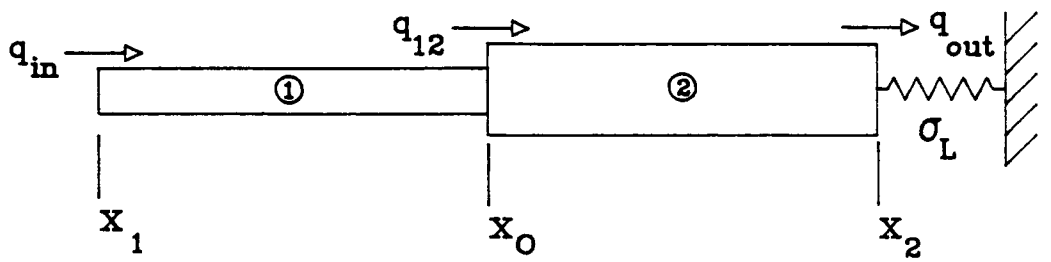

Figure 5.2.1. Rigidly Coupled, Longitudinally Vibrating Rods with Known Power Flux Boundary Conditions, q_{in} and q_{out}, at x_1 and x_2

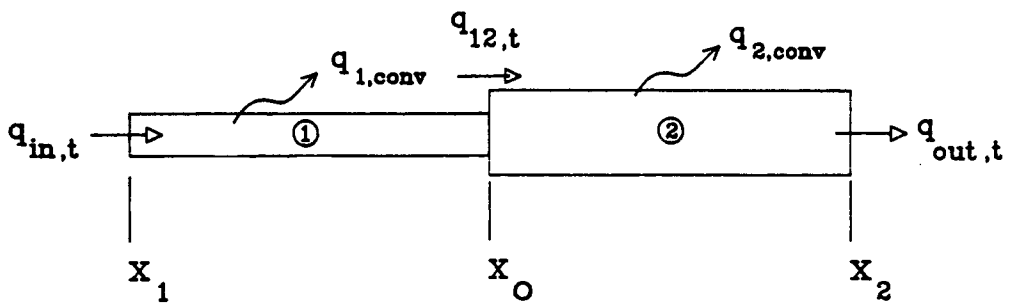

Figure 5.2.2. 1-D Heat Conduction Through Two Dissimilar Fins with a Convective Heat Loss, q_{conv}, and Known Thermal Power Flux Boundary Conditions, $q_{in,t}$ and $q_{out,t}$ at x_1 and x_2

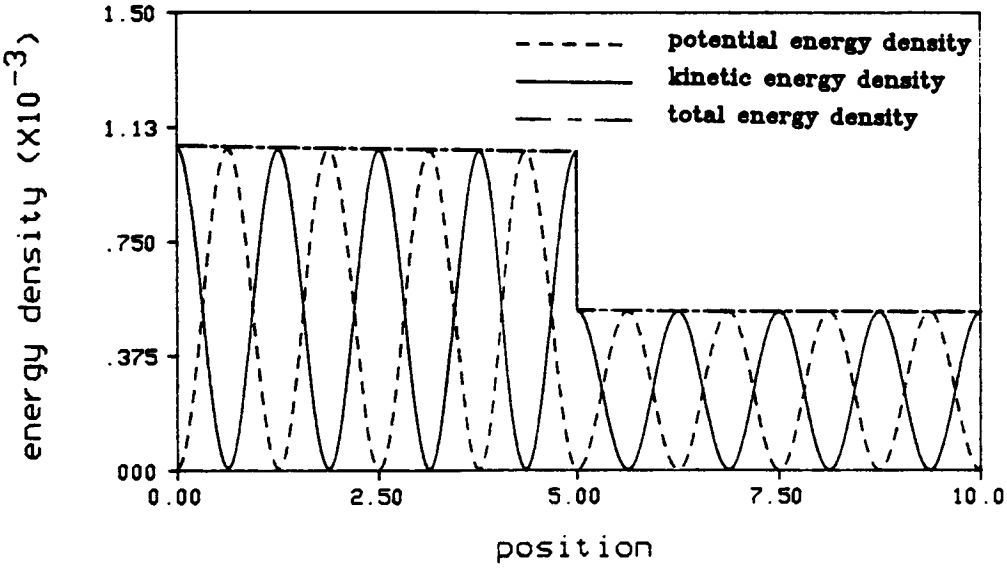

Figure 5.2.3. Total, Potential and Kinetic Energy Densities in Two Rigidly Coupled, Longitudinally Vibrating Rods, as Shown in Figure (5.2.1), with Zero Potential Energy Density at the Coupling Interface, x_o

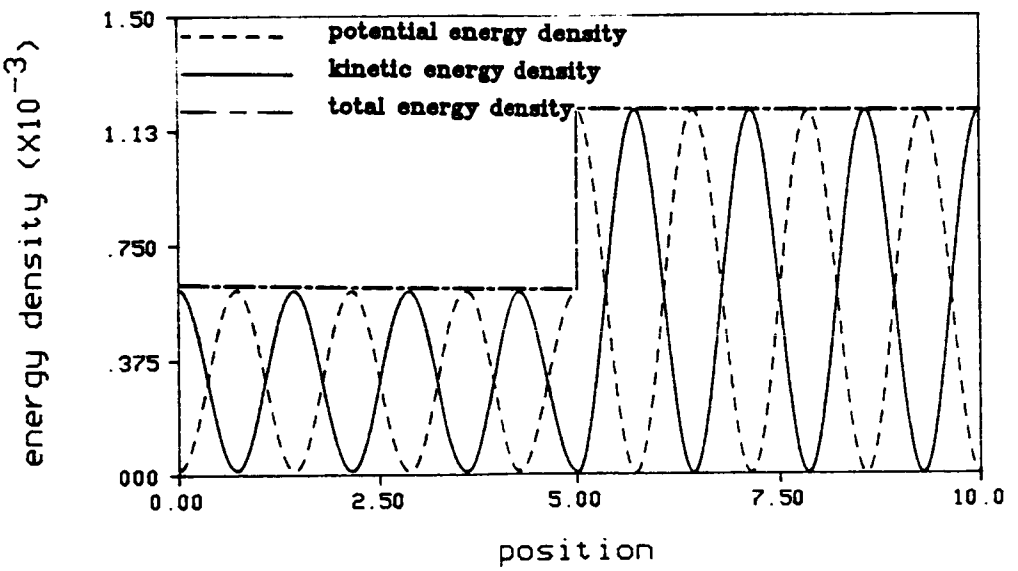

Figure 5.2.4. Total, Potential and Kinetic Energy Densities in Two Rigidly Coupled, Longitudinally Vibrating Rods, as Shown in Figure (5.2.1), with Zero Kinetic Energy Density at the Coupling Interface, x_o

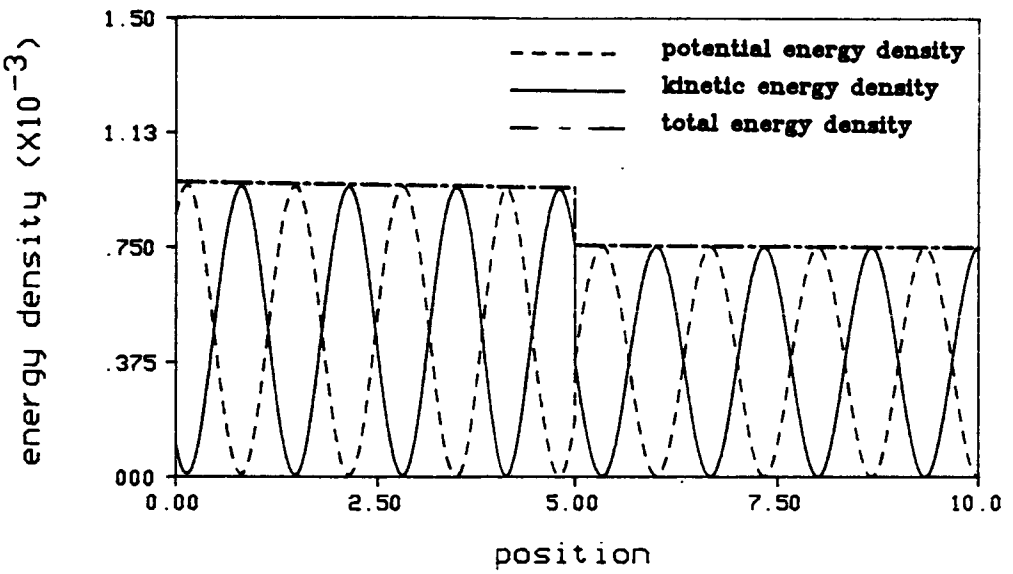

Figure 5.2.5. Total, Potential and Kinetic Energy Densities in Two Rigidly Coupled, Longitudinally Vibrating Rods, as Shown in Figure (5.2.1), with Equal Amounts of Potential and Kinetic Energy Density in Rod 2 at the Coupling Interface, x_o

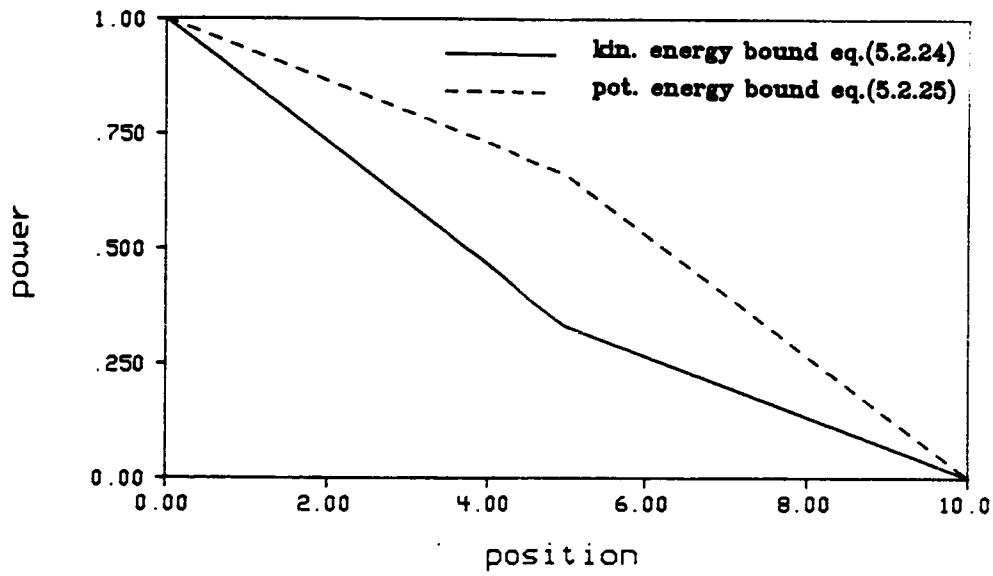

Figure 5.2.6. Upper and Lower Bounds on the Power Flow Through Two Rigidly Coupled, Longitudinally Vibrating Rods, as Shown in Figure (5.2.1), with q_{in}=1 and q_{out}=0

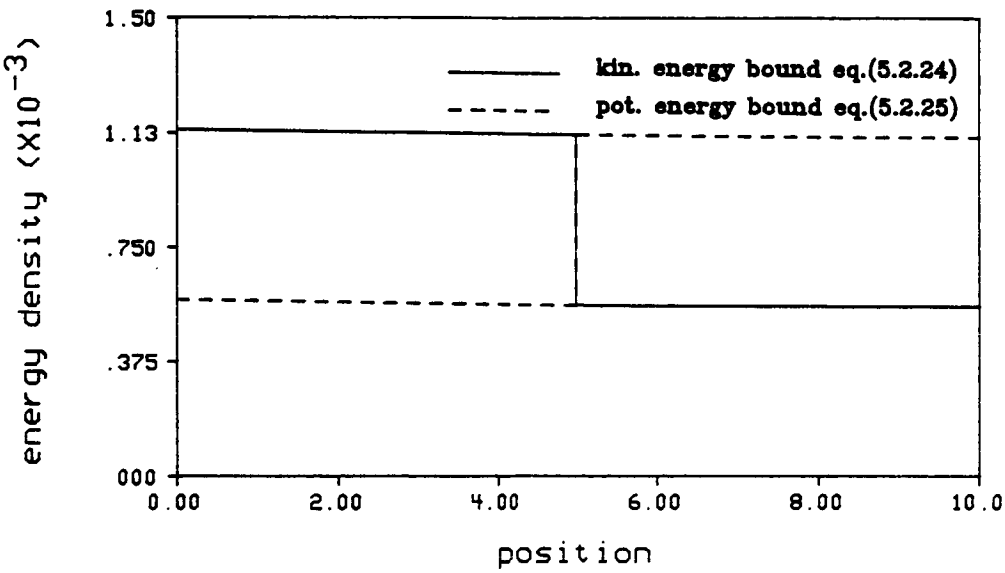

Figure 5.2.7. Upper and Lower Bounds on the Energy Density in Two Rigidly Coupled, Longitudinally Vibrating Rods, as Shown in Figure (5.2.1), with q_{in}=1 and q_{out}=0

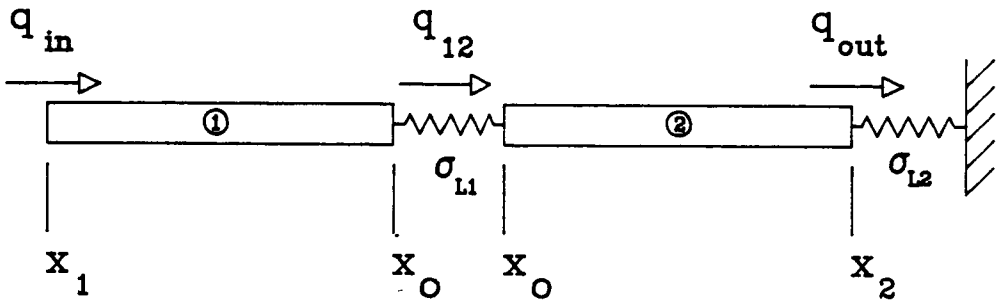

Figure 5.3.1. Spring Coupled, Longitudinally Vibrating Rods with Known Power Flux Boundary Conditions, q_{in} and q_{out}, at x_1 and x_2

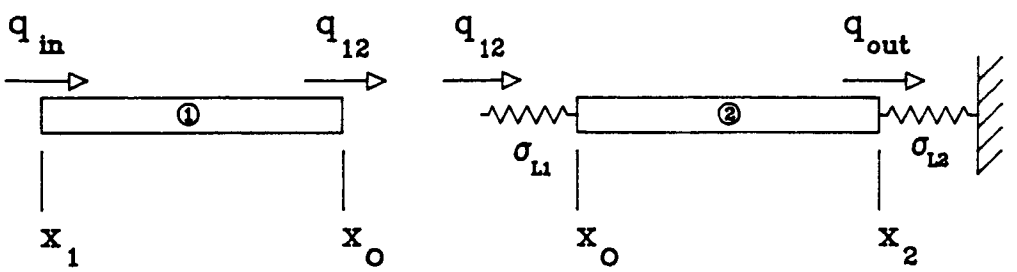

Figure 5.3.2. Spring Coupled, Longitudinally Vibrating Rods from Figure (5.3.1) Split into Two Components

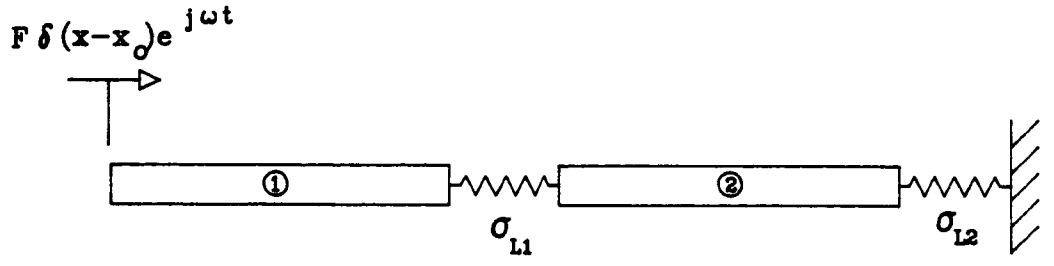

Figure 5.3.3. Spring Coupled, Longitudinally Vibrating Rods Excited by a Harmonic Point Force

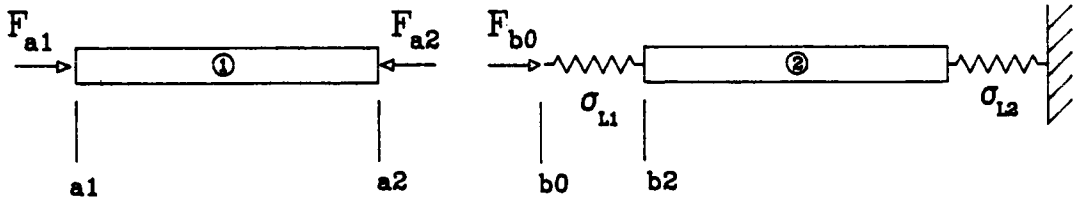

Figure 5.3.4. Spring Coupled, Longitudinally Vibrating Rods from Figure (5.3.3) Split into Two Components for Receptance Analysis

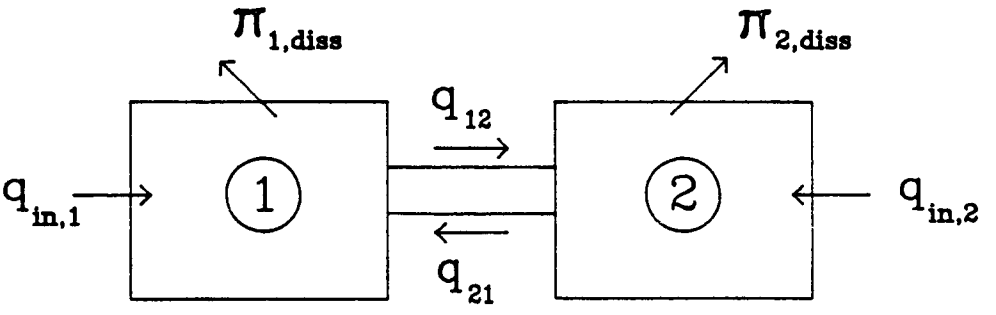

Figure 5.3.5. General SEA Model of Two Coupled Dynamic Systems

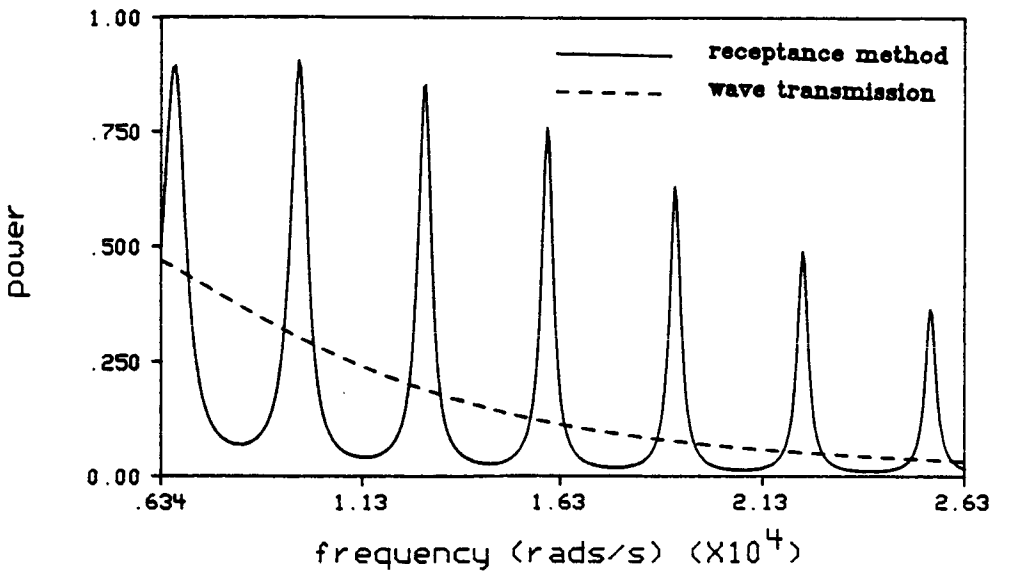

Figure 5.3.6. Comparison of the Calculated Power Flow Between the Coupled Rods Shown in Figure (5.3.3) Using Solutions from the Receptance Method, as shown in Equation (5.3.19), and the Wave Transmission Approach, as Shown in Equation (5.3.31), as a Function of Frequency

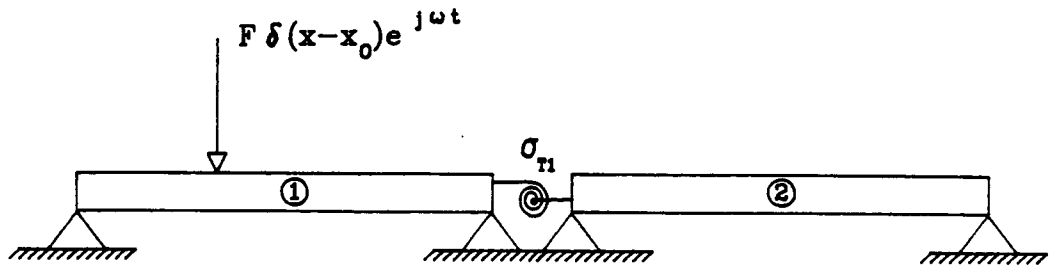

Figure 5.4.1. Spring Coupled, Transversely Vibrating Beams Excited by a Harmonic Point Force

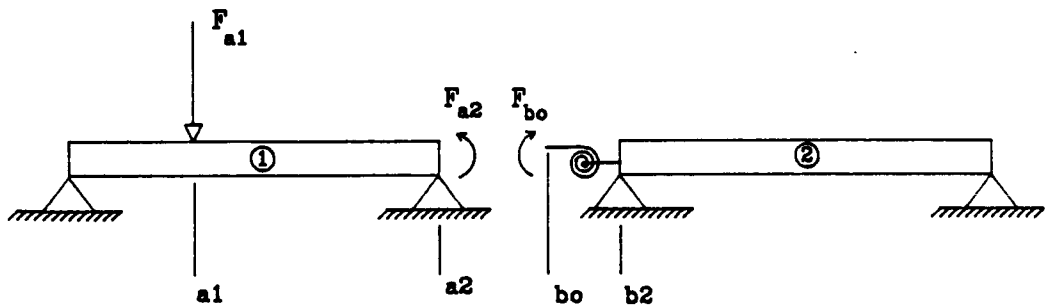

Figure 5.4.2. Spring Coupled, Transversely Vibrating Beams from Figure (5.4.1) Split into Two Components for a Receptance Analysis

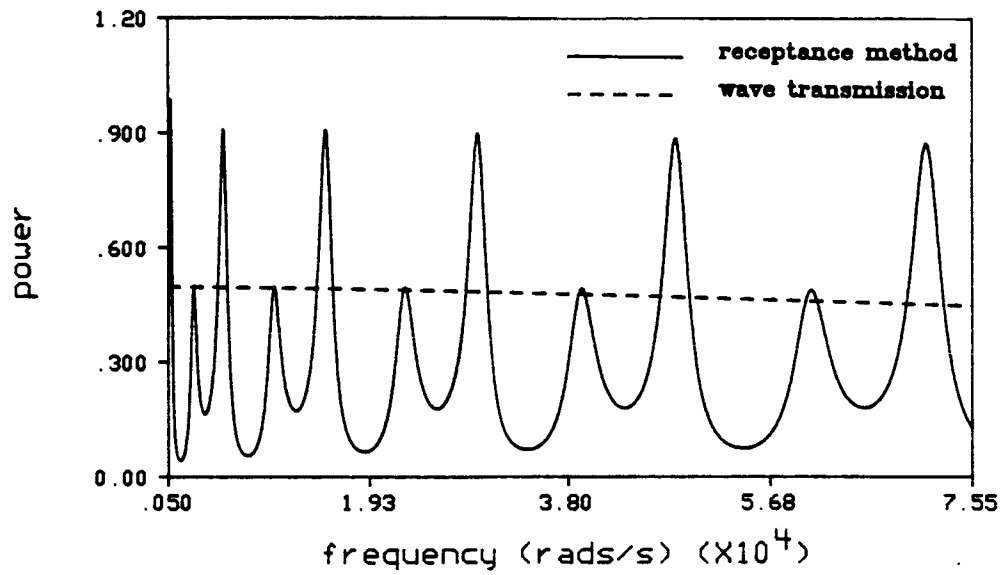

Figure 5.4.3. Comparison of the Calculated Power Flow Between the Coupled Beams Shown in Figure (5.4.1) Using Solutions from the Receptance Method, as Shown in Equation (5.4.10), and the Wave Transmission Approach, as Shown in Equation (5.4.12), as a Function of Frequency

CHAPTER 6 - POWER FLOW EXAMPLES

6.1 Introduction

In this chapter, the simplified solutions for power flow and energy density developed in chapters 3 and 4 will be compared to exact solutions. This comparison will illustrate some of the differences in how the simplified and exact theories model the power flow and energy density in coupled rods and beams. It will also serve as an indication on the quality of the assumptions made in developing the simplified theories.

For all the examples in this chapter, the coupled systems will be excited by a harmonic point force as discussed in chapters 3 and 4. The magnitude of the excitation force $|F|$ will be adjusted for each example so that the total power input to the systems is unity. The receptance method will be used to couple the simplified energy density solutions.

6.2 Coupled Rods

Figure (6.2.1) shows two rods coupled by a linear spring of spring rate σ_L. Rod 1 is excited by a harmonic point source at the end x_1=0. Rod 2 has a free end condition at x_2=10 m. The coupled rod parameters for this example are

$$\text{length of rod 1} = 5 \text{ m}$$

$$\text{length of rod 2} = 5 \text{ m}$$

$$(ES)_1 = (ES)_2 = 6 \times 10^7 \text{ N}$$

$$E_1 = E_2 = 200 \times 10^9 \text{ N/m}^2$$

$$(\rho S)_1 = (\rho S)_2 = 2.358 \text{ kg/m}$$

$$\rho_1 = \rho_2 = 7860 \text{ kg/m}^3$$

$$\sigma_L = 3 \times 10^7 \text{ N/m}$$

$$\eta_1 = \eta_2 = 0.01$$

The exact power flow solution for a rod used in this section is shown in equation (3.2.19). The exact energy density solution is shown in equation (3.2.24). The simplified energy density and power flow solutions are shown in equations (3.2.37) and (3.2.38) respectively.

Figures (6.2.2) and (6.2.3) show the power flow and energy density in the coupled rod system, as shown in figure (6.2.1), with a excitation frequency of ω=6338.9 rad/sec. At this frequency the wavelength of vibration is equal to the length of each rod, $\lambda = 5$ m. Note in figure (6.2.2) how the exact power flow solution oscillates about the simplified solution. Identical energy density levels are predicted from both the simplified and exact theories, as shown in figure (6.2.3). The power flow and energy density levels for ω=12677.79 rad/sec are shown in figures (6.2.4) and (6.2.5). At this excitation frequency, the wavelength

of vibration is one half the length of the rods, λ=2.5 m. Again the simplified and exact theories predict identical energy density levels as shown in figure (6.2.5). Figures (6.2.6) and (6.2.7) plot the power flow and energy density with ω=25355.58 rad/sec, λ=1.25 m while figures (6.2.8) and (6.2.9) plot the power flow and energy density with ω=38033.37 rad/sec, λ=0.8333 m. Note that in all the cases shown, as the excitation frequency gets higher, the simplified power flow solution gets closer to the exact solution. This indicates that the harmonic terms in the exact power flow expression which are neglected in the simplified solution become less important at higher frequencies.

Although the energy density levels predicted by the exact and simplified solutions in the four previous examples were identical, differences can occur. Figure (6.2.10) and (6.2.11) illustrate the power flow and energy density for a excitation frequency of ω=7131.26 rad/sec, λ=4.444 m. Note in figure (6.2.10) that the simplified power solution does not pass directly through the center of the exact solution. Subsequently, the energy density predictions of the two solutions are not the same, though the error is relatively small. The explanation for the difference in the energy density levels can be found in section 3.3 which discussed the damping model used in the rod analysis.

It was pointed out in section 3.3 that the average power dissipated by the exact and simplified solutions were identical only when integrated over an integer number of wavelengths. Equations (3.3.15) and (3.3.17) demonstrated this fact. In a given rod, the total power dissipated by the simplified solution,

π_{simp}, can be calculated by integrating $<\pi>_{diss} = \eta\omega<e>$ over the length (L) of the rod

$$\pi_{simp} = \eta\omega\int_L <e>dx = \eta\omega\left\{\int_L <T>dx + \int_L <V>dx\right\} \qquad (6.2.1)$$

The total power dissipated by the exact solution, π_{exact}, can be calculated by integrating $<\pi_{exact}>_{diss} = 2\eta\omega<T>$ over the length of the rod

$$\pi_{exact} = 2\eta\omega\int_L <T>dx \qquad (6.2.2)$$

Subtracting equation (6.2.1) from equation (6.2.2), a relationship between the total power dissipated by the exact and simplified solutions is shown to be

$$\pi_{exact} - \pi_{simp} = \eta\omega\left\{\int_L <T>dx - \int_L <V>dx\right\} \qquad (6.2.3)$$

When there are an integer number of wavelengths in the rod, the total potential and kinetic energies are equal. When the rod length is not an integer number of wavelengths, the total potential and kinetic energy in the rod are not equal. Equation (6.2.3) clearly shows that when there are an integer number of wavelengths in the rod, the total power dissipated by the exact and simplified solutions are exactly the same. When the rod length is not an integer number of wavelengths, equation (6.2.3) gives the difference in the total power dissipated by the exact and simplified solutions.

In the four cases shown in figures (6.2.2)-(6.2.9), the excitation frequencies were such that were an integer number of wavelengths of vibration per rod

length. Therefore the power dissipated by the exact and simplified solutions over each rod was the same and the energy density predictions were identical. However, with ω=7131.26 rad/sec there are not an integer number of wavelengths vibration per rod length. Therefore the exact and simplified power dissipation over a rod length is not identical, which accounts for the discrepancies in the energy density level predictions in figure (6.2.11).

The excitation frequencies used in the power flow and energy density examples, shown in figures (6.2.2)-(6.2.9), are what would be considered the low to mid-frequency range for the coupled rod system shown in figure (6.2.1). At the highest excitation frequency of ω=38033.37 rad/sec, the simplified solution is in almost perfect agreement with the exact solution and will improve as the frequency increases. However, when ω=38933.37 rad/sec, the wavelength of vibration is one sixth of the rod length and is in the frequency range where the finite element method would begin to require a large number of elements to maintain its accuracy. These examples show that the simplified solution for a rod can be used to make accurate predictions at frequencies where the FEM starts to be inefficient and thus bridge the gap between FEM and SEA.

6.3 Coupled Beams

Figure (6.3.1) illustrates two simply supported beams, coupled by a torsional spring of spring rate σ_T. Beam 1 is excited by a transverse, harmonic point force at x=0.25 m. The coupled beam parameters for this example are

$$\text{length of beam 1} = 0.5 \text{ m}$$

$$\text{length of beam 2} = 0.5 \text{ m}$$

$$(EI)_1 = (EI)_2 = 500 \text{ Nm}^2$$

$$E_1 = E_2 = 200 \times 10^9 \text{ N/m}^2$$

$$(\rho S)_1 = (\rho S)_2 = 2.358 \text{ kg/m}$$

$$\rho_1 = \rho_2 = 7860 \text{ kg/m}^3$$

$$\sigma_T = 300 \text{ (Nm)/rad}$$

$$\eta_1 = \eta_2 = 0.001$$

The exact power flow solution for a beam is the sum of the shear $<q>_s$ and moment $<q>_m$ power flow components as shown in equations (4.2.23) and (4.2.24). The exact energy density solution is the sum of the potential and kinetic energy densities as shown in equations (4.2.27) and (4.2.28). The simplified energy density and power flow solutions for a beam, shown in equations (4.2.67) and (4.2.68), represent spatial averaged, farfield approximations of the exact solutions. The simplified solution is based on the assumption that the total displacement solution for a beam is well approximated by the farfield terms as shown in equation (4.2.38). In section 4.2.2 it was shown that approximating the displacement solution in a beam by the farfield terms becomes a better assumption as the frequency increases. It is expected therefore, that the simplified solution for the energy density and power flow in a beam will become a better average approximation as the excitation frequency increases.

Figures (6.3.2) and (6.3.3) show the power flow and energy density in the coupled beam system in figure (6.3.1) with a excitation frequency of 2300 rad/sec. At this frequency the wavelength of vibration is equal to the length of each beam, λ =0.5 m. As discussed in section 4.2.2, since the wavelength of vibration is equal to the length of the beams, the total displacement solution for a beam is not well approximated by the farfield terms. Thus, as illustrated in figure (6.3.3) the simplified energy density solution is not a good average approximation of the exact solution. The power flow and energy density levels with ω=9197.8 rad/sec are shown in figures (6.3.4) and (6.3.5). At this frequency the wavelength of vibration is one half the length of the two beams, λ=0.25 m. At this higher frequency, the simplified energy density prediction in figure (6.3.5) shows improvement over the prediction at ω=2300 rad/sec. Figures (6.3.6) and (6.3.7) plot the power and energy density for ω=20695.5 rad/sec, λ=0.167 m, while figures (6.3.8) and (6.3.9) plot the power flow and energy density for ω=36792.0 rad/sec, λ=0.125 m. The power flow and energy density in the final coupled beam example are shown in figures (6.3.10) and (6.3.11). In these last two figures the frequency is ω=82781.88 rad/sec, which gives a wavelength of vibration of λ=0.08333 m. From figures (6.3.2)-(6.3.11) it is clear that the simplified theory for beams becomes more accurate as the excitation frequency increases. At ω=82781.88 rad/sec, the simplified energy density, as shown in figure (6.3.11), is a good average approximation of the exact energy density solution. The results in figures (6.3.2)-(6.3.11) are typical for the power flow and energy density predictions in beams.

In the coupled beam system in figure (6.3.1), there are 4 discontinuities. The simple supports at x_1 and x_2 and the coupling at x_o are all discontinuities. The fourth discontinuity in figure (6.3.1) is at the forcing location, x=0.25 m. In general, each discontinuity will have a nearfield effect associated with it. In section 4.2.2, it was shown that for a free-free beam the farfield displacement approximation in a beam becomes a good assumption when the distance between discontinuities in the beam is of the order of four or more wavelengths of vibration. The results in figures (6.3.2)-(6.3.11) support this conclusion.

The simplified energy density solutions for a beam can be applied to a beam with any type of boundary condition. Figure (6.3.12) illustrates two beams coupled by a torsional spring of spring rate σ_T. Beam 1 has a clamped boundary condition at x_1=0 and is simply supported at x_o=0.5 m. Beam 2 is simply supported at x_o=0.5 m and is clamped at x_2=1 m. The beam parameters for this example are the same as those used for the example in figure (6.3.1) except that the coupling spring rate has been increased to $\sigma_T=1 \times 10^5$ (Nm)/rad.

Figures (6.3.13)-(6.3.22) show the power flow and energy density in the coupled beam system shown in figure (6.3.12) at the same excitation frequencies which were used for the coupled beam system in figure (6.3.1). These frequencies are ω=2300 rad/sec, ω=9187.8 rad/sec, ω=20695.5 rad/sec, and 82871.88 rad/sec. The power flow and energy density predictions in figures (6.3.13)-(6.3.22) further support the conclusion that the simplified solution for a

beam becomes a better approximation as the excitation frequency increases.

The excitation frequencies used in the power flow and energy density examples, shown in figures (6.3.2)-(6.3.11) and figures (6.3.13)-(6.3.22), are what would be considered the low to mid-frequency range for the coupled beam systems shown in figures (6.3.1) and (6.3.12). At the highest excitation frequency of ω=82781.88 rad/sec, the simplified solution does an excellent job in predicting the average values of energy density and power flow and will improve as the frequency increases. However, when ω=82781.88 rad/sec, the wavelength of vibration is one sixth of the beam length and is in the region where the finite element method would begin to require a large number of elements to maintain its accuracy. These examples show that the simplified solution for the beam can be used to make accurate predictions of the average energy density levels at frequencies where the FEM starts to be inefficient and thus bridge the gap between FEM and SEA.

6.4 Summary

For the coupled rod system in section 6.2, it was found that the simplified solutions for energy density and power flow compared well with the exact solutions. As the excitation frequency increased, the power flow solution was better approximated by the simplified solution. It was also shown that the differences in energy density predictions for a rod were found to be a result of how the exact and simplified solutions modeled the power dissipation in a rod. Equation (6.2.3) shows that the difference in the total power dissipated by the

simplified and exact solutions in a rod is proportional to the difference in the total kinetic and potential energy in the rod.

The predictions of the power flow and energy density levels in the coupled beam system in figure (6.3.1) were discussed in section 6.3. As expected from the discussions in chapter 4, the simplified energy density and power flow solutions became better average approximations as the excitation frequency increased.

In both the coupled rod and coupled beam examples, the excitation frequencies were in the low to mid-frequency ranges. From the accuracy of the simplified solutions at the higher frequencies, it was concluded that the simplified energy density solutions for both the rod and beam can be used to bridge the mid-frequency gap where the FEM becomes too expensive and SEA is unreliable.

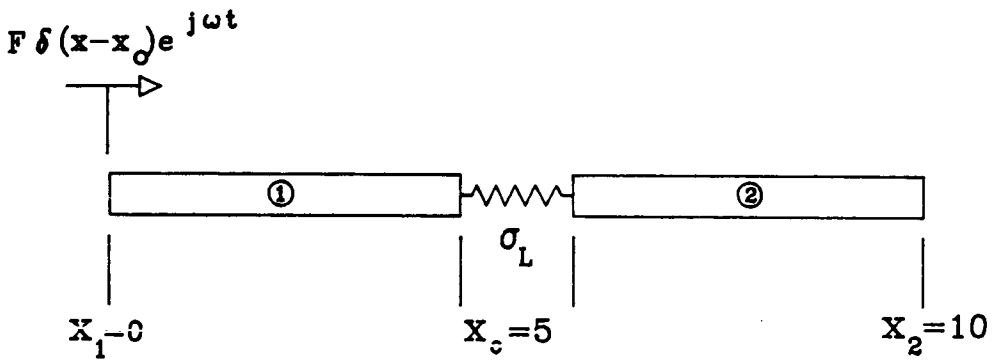

Figure 6.2.1 - Spring Coupled, Longitudinally Vibrating Rods Excited by a Harmonic Point Force at $x_1=0$ with a Free End Condition at $x_2=10$

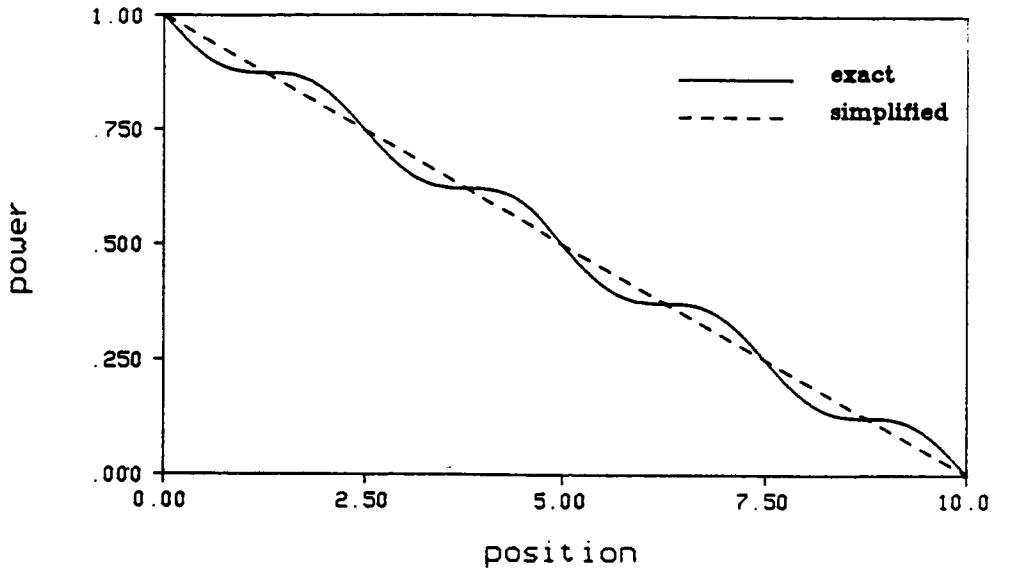

Figure 6.2.2 - Comparison of the Exact and Simplified Power Flow Solutions for the Coupled Rod System Shown in Figure (6.2.1) with ω=6338.9 rad/sec

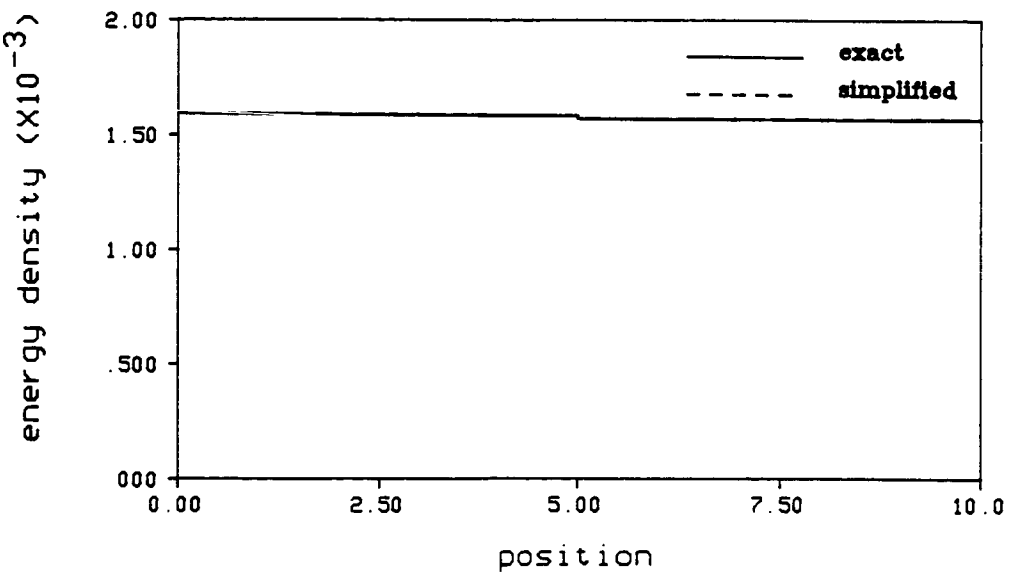

Figure 6.2.3 - Comparison of the Exact and Simplified Energy Density Solutions for the Coupled Rod System Shown in Figure (6.2.1) with ω =6338.9 rad/sec

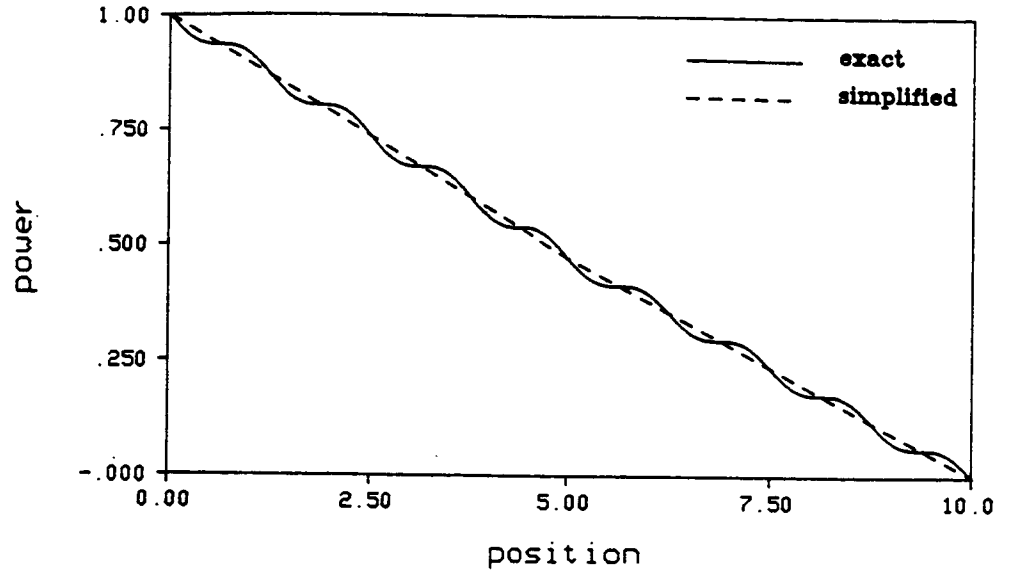

Figure 6.2.4 - Comparison of the Exact and Simplified Power Flow Solutions for the Coupled Rod System Shown in Figure (6.2.1) with ω=12677.79 rad/sec

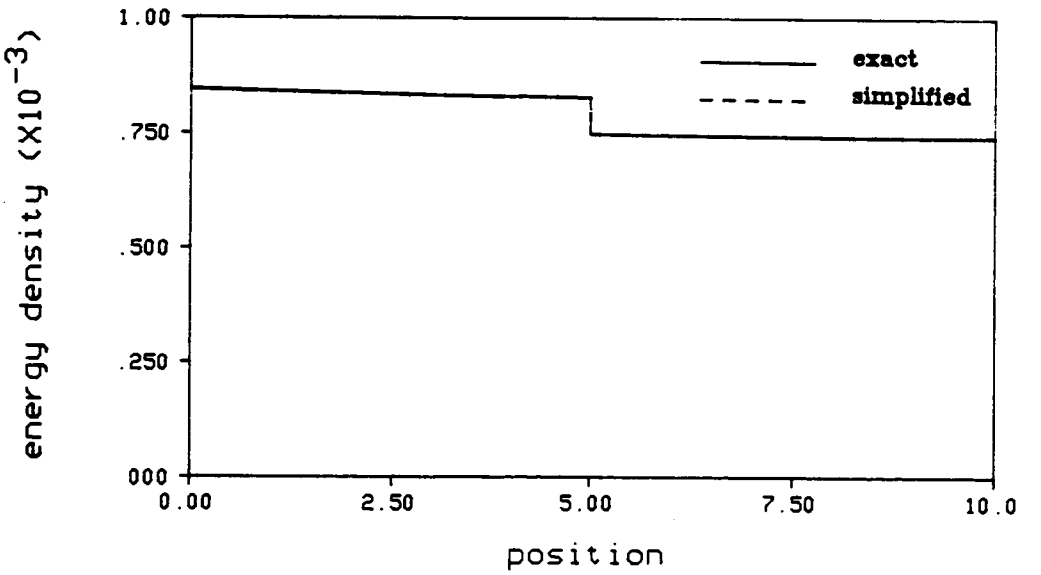

Figure 6.2.5 - Comparison of the Exact and Simplified Energy Density Solutions for the Coupled Rod System Shown in Figure (6.2.1) with ω =12677.79 rad/sec

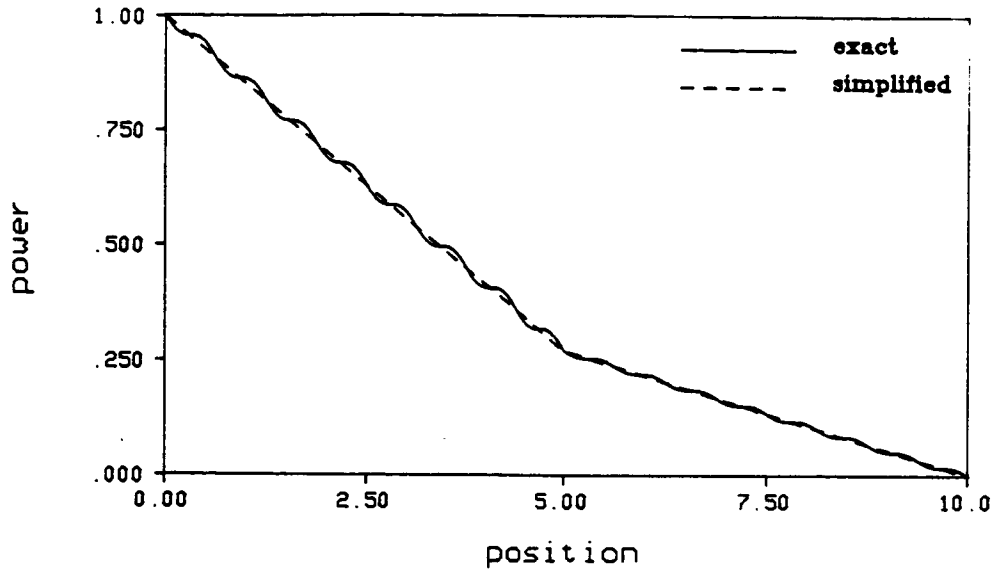

Figure 6.2.6 - Comparison of the Exact and Simplified Power Flow Solutions for the Coupled Rod System Shown in Figure (6.2.1) with ω=25355.58 rad/sec

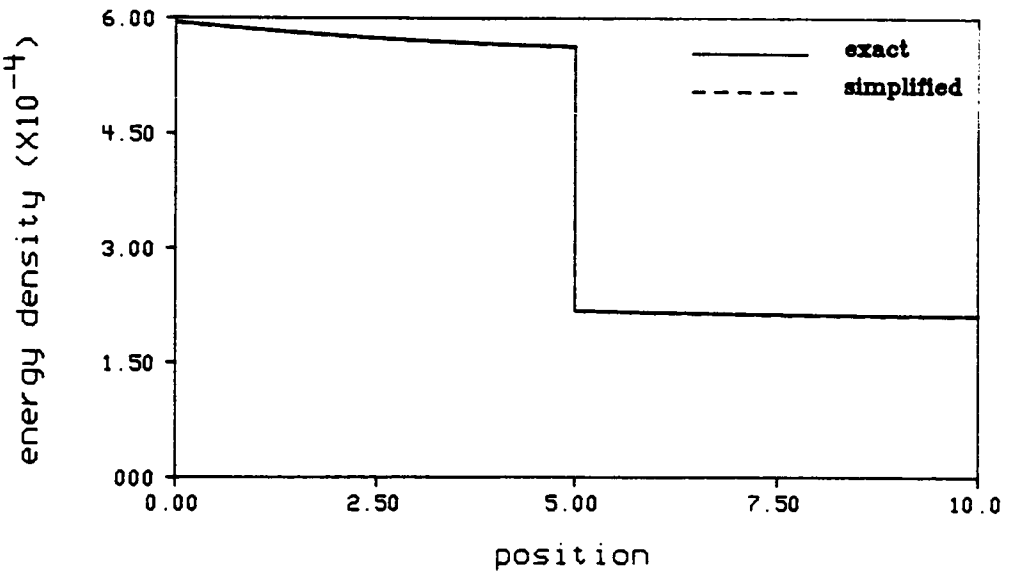

Figure 6.2.7 - Comparison of the Exact and Simplified Energy Density Solutions for the Coupled Rod System Shown in Figure (6.2.1) with ω =25355.58 rad/sec

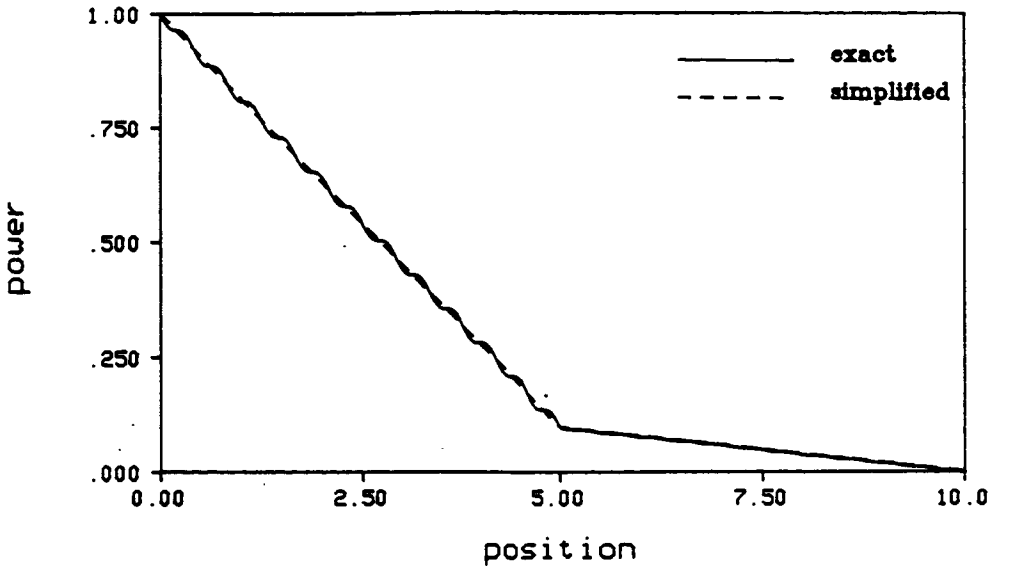

Figure 6.2.8 - Comparison of the Exact and Simplified Power Flow Solutions for the Coupled Rod System Shown in Figure (6.2.1) with ω=38033.37 rad/sec

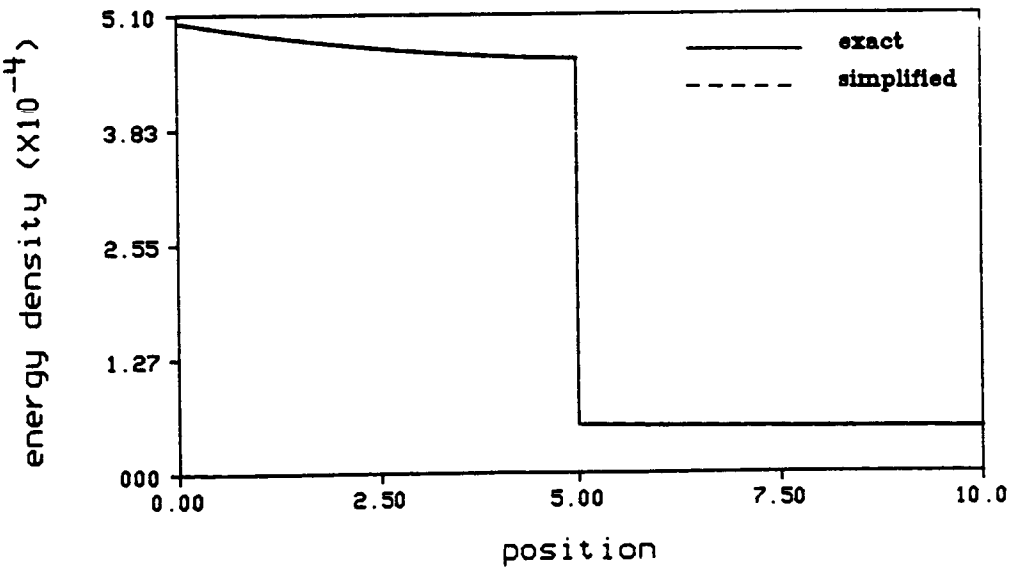

Figure 6.2.9 - Comparison of the Exact and Simplified Energy Density Solutions for the Coupled Rod System Shown in Figure (6.2.1) with ω =38033.37 rad/sec

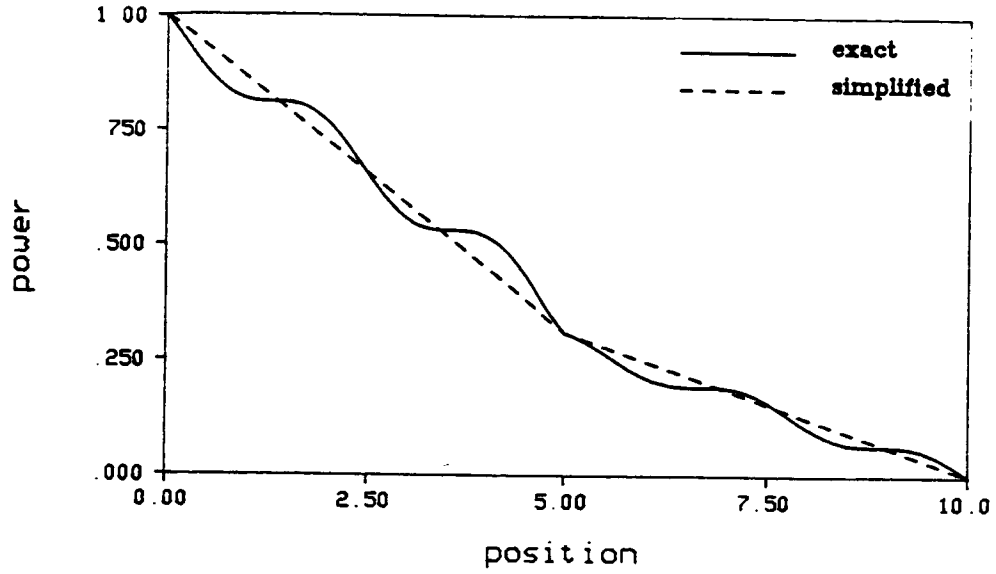

Figure 6.2.10 - Comparison of the Exact and Simplified Power Flow Solutions for the Coupled Rod System Shown in Figure (6.2.1) with ω=7131.26 rad/sec

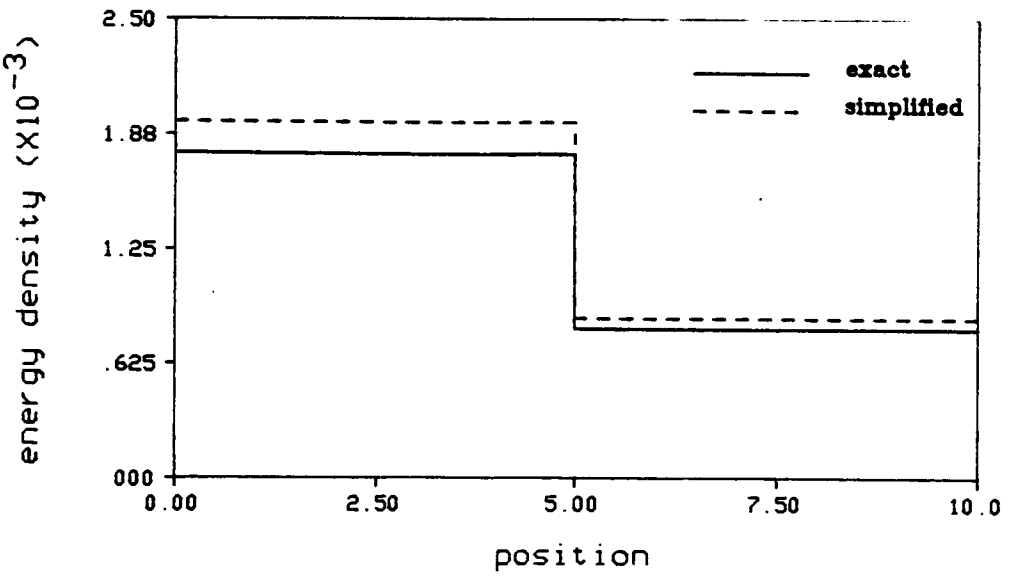

Figure 6.2.11 - Comparison of the Exact and Simplified Energy Density Solutions for the Coupled Rod System Shown in Figure (6.2.1) with ω =7131.26 rad/sec

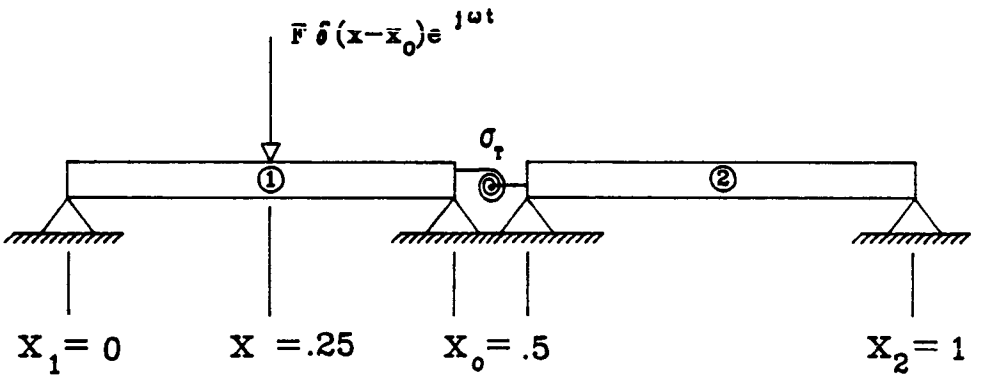

Figure 6.3.1 - Simply Supported, Transversely Vibrating Beams Coupled by a Torsional Spring and Excited by a Harmonic Point Force at x=.25

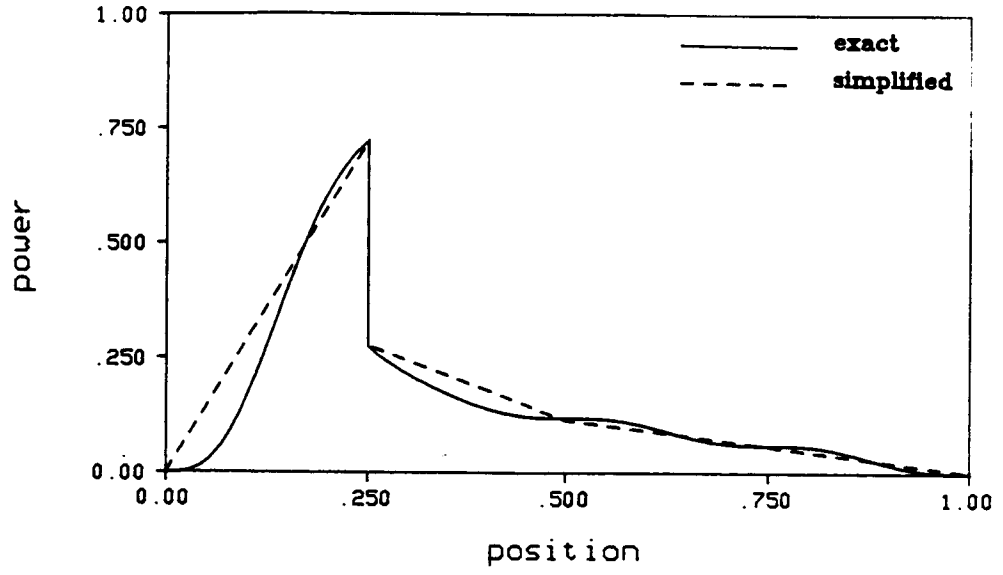

Figure 6.3.2 - Comparison of the Exact and Simplified Power Flow Solutions for the Coupled Beam System Shown in Figure (6.3.1) with ω=2300.00 rad/sec

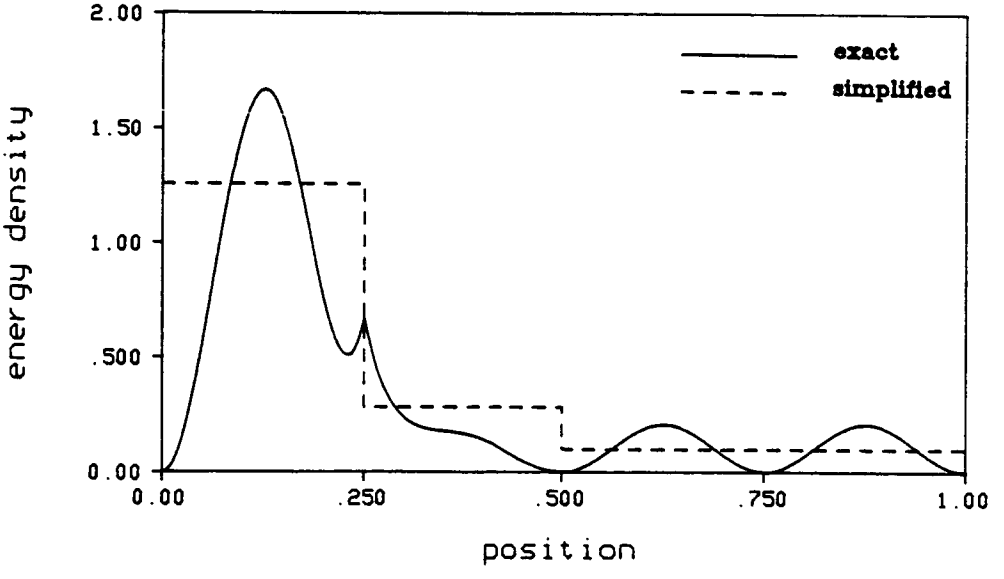

Figure 6.3.3 - Comparison of the Exact and Simplified Energy Density Solutions for the Coupled Beam System Shown in Figure (6.3.1) with ω =2300.00 rad/sec

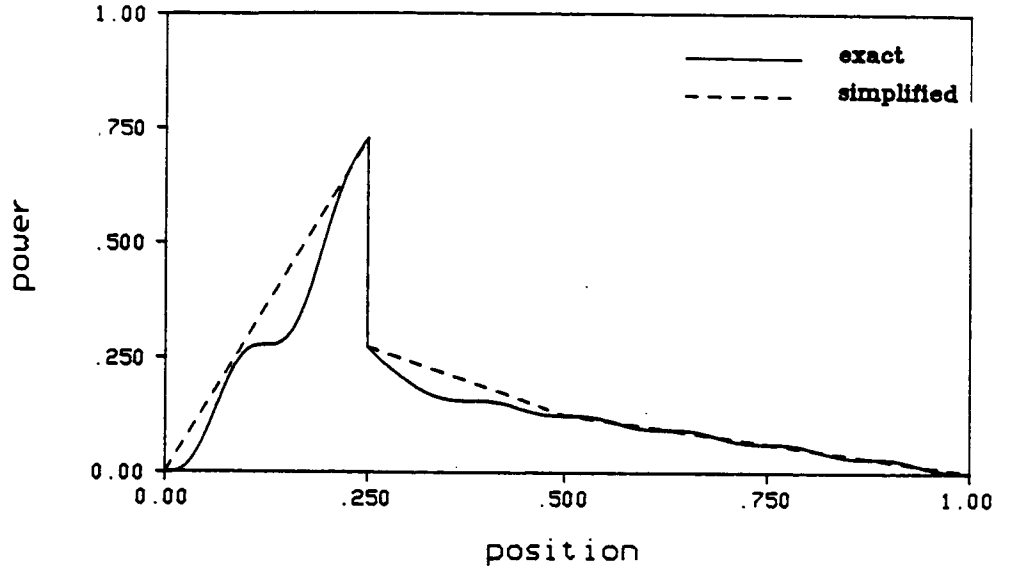

Figure 6.3.4 - Comparison of the Exact and Simplified Power Flow Solutions for the Coupled Beam System Shown in Figure (6.3.1) with ω=9197.80 rad/sec

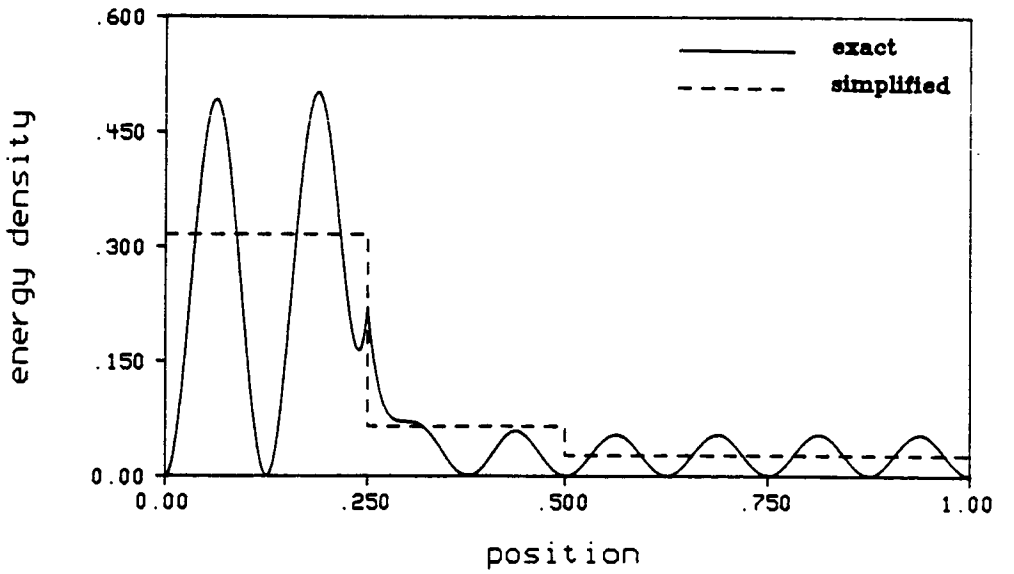

Figure 6.3.5 - Comparison of the Exact and Simplified Energy Density Solutions for the Coupled Beam System Shown in Figure (6.3.1) with ω =9197.80 rad/sec

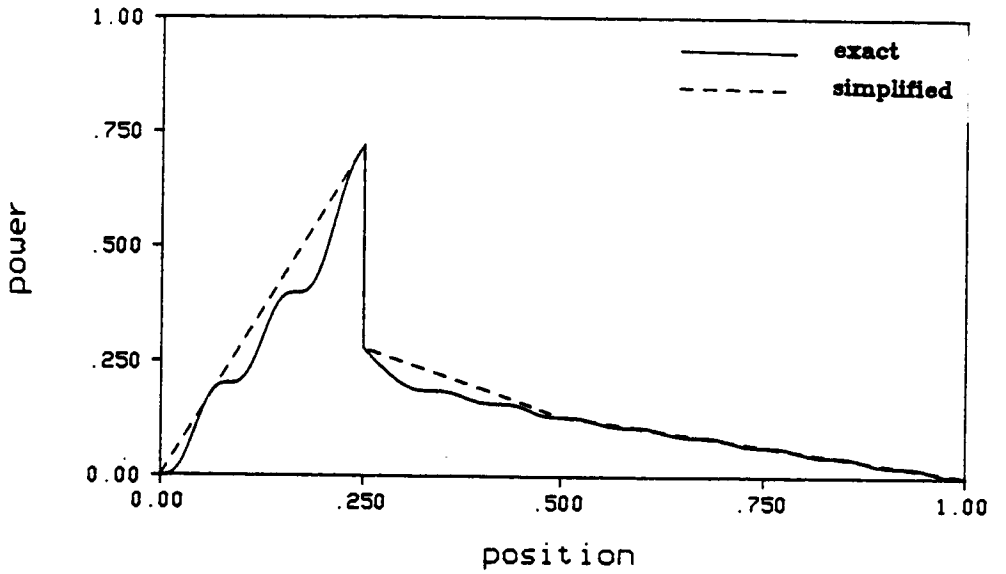

Figure 6.3.6 - Comparison of the Exact and Simplified Power Flow Solutions for the Coupled Beam System Shown in Figure (6.3.1) with ω=20695.5 rad/sec

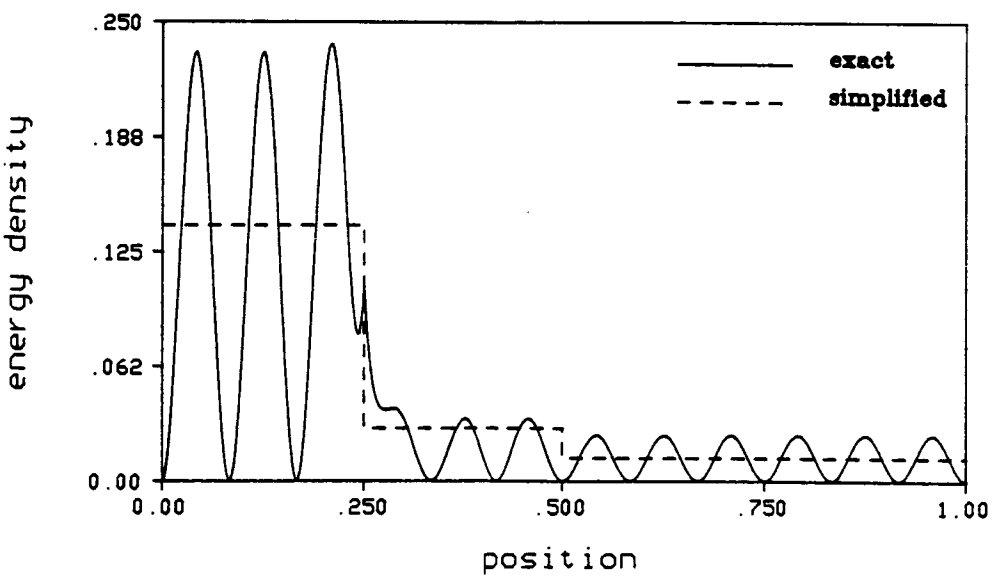

Figure 6.3.7 - Comparison of the Exact and Simplified Energy Density Solutions for the Coupled Beam System Shown in Figure (6.3.1) with ω =20695.5 rad/sec

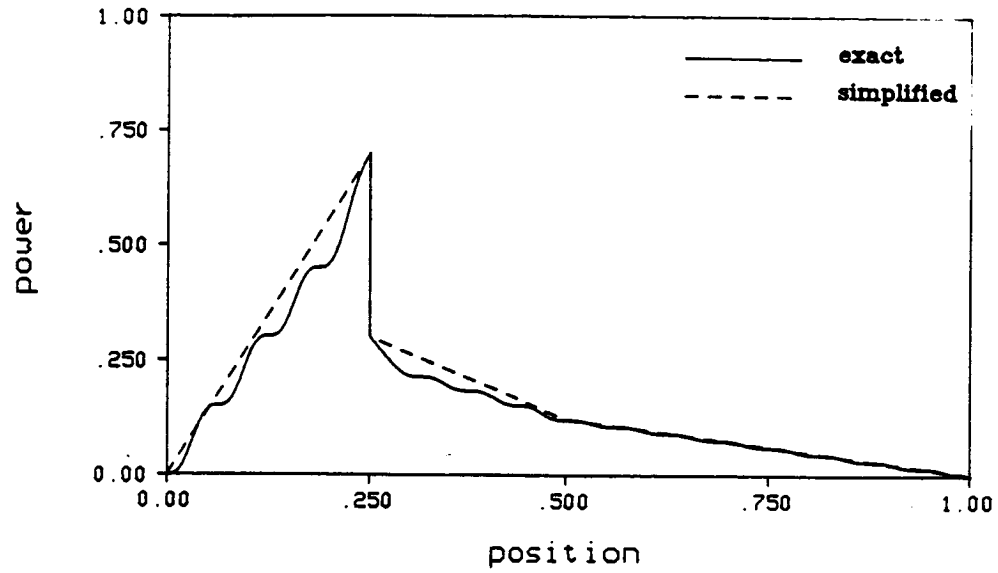

Figure 6.3.8 - Comparison of the Exact and Simplified Power Flow Solutions for the Coupled Beam System Shown in Figure (6.3.1) with ω=36792.0 rad/sec

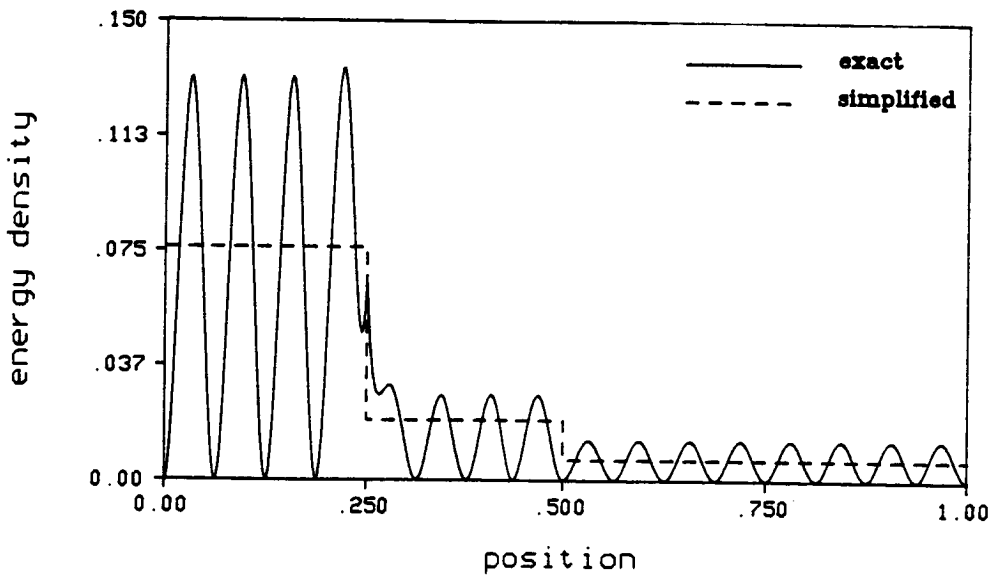

Figure 6.3.9 - Comparison of the Exact and Simplified Energy Density Solutions for the Coupled Beam System Shown in Figure (6.3.1) with ω =36792.0 rad/sec

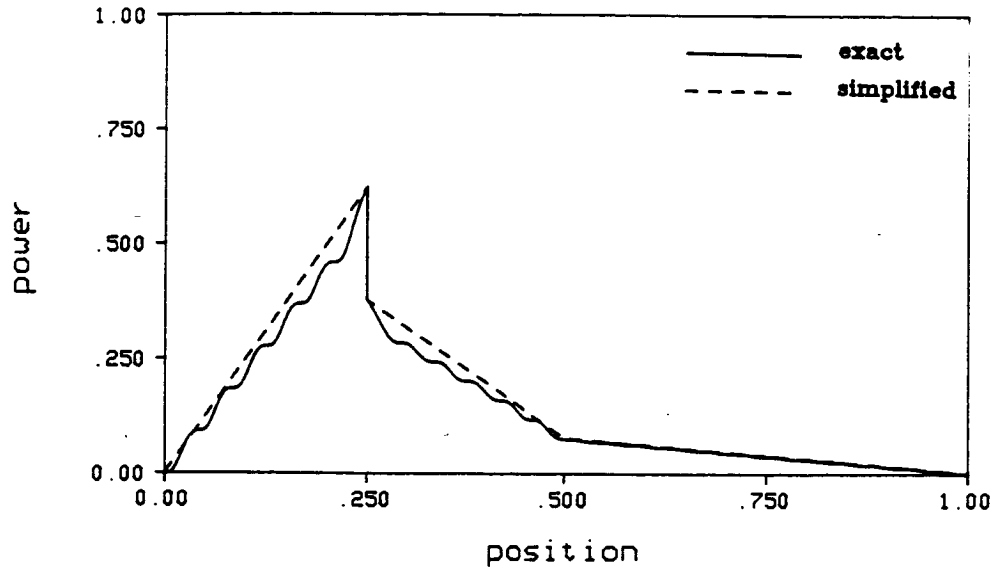

Figure 6.3.10 - Comparison of the Exact and Simplified Power Flow Solutions for the Coupled Beam System Shown in Figure (6.3.1) with ω=82871.88 rad/sec

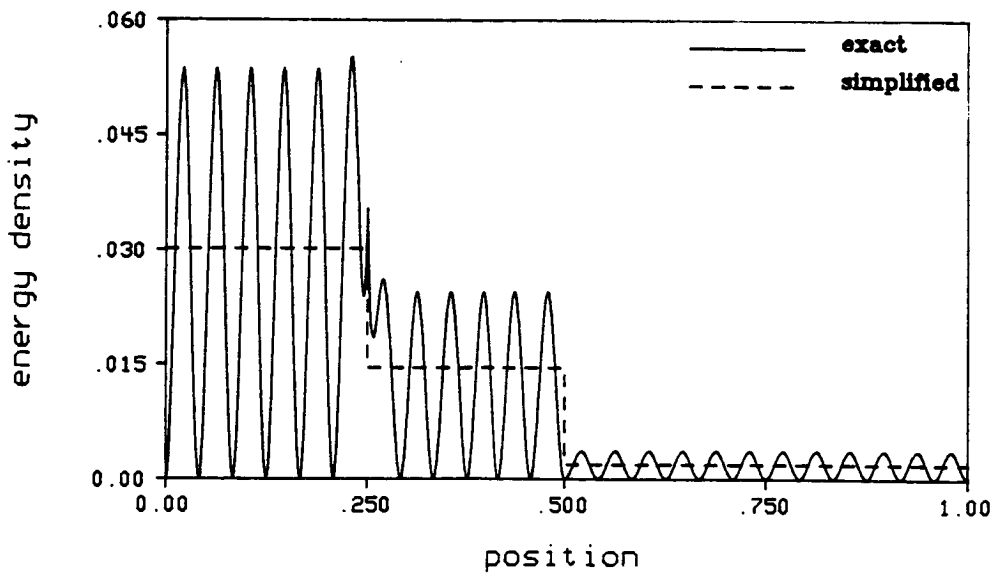

Figure 6.3.11 - Comparison of the Exact and Simplified Energy Density Solutions for the Coupled Beam System Shown in Figure (6.3.1) with ω =82871.88 rad/sec

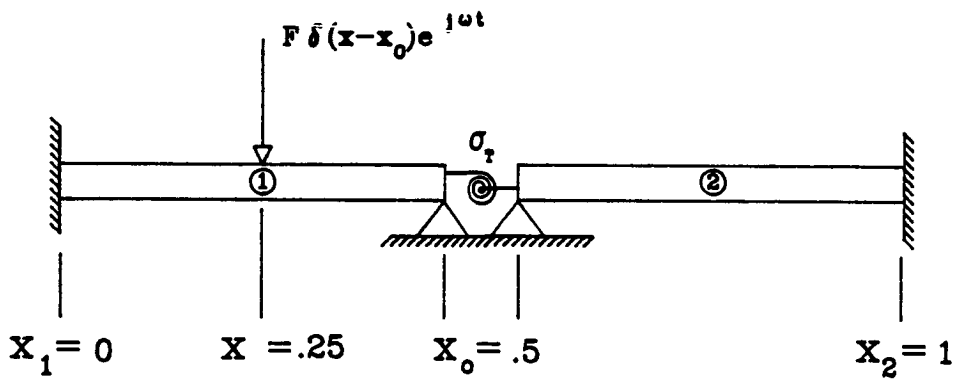

Figure 6.3.12 - Transversely Vibrating Beams Coupled by a Torsional Spring and Excited by a Harmonic Point Force at x=.25

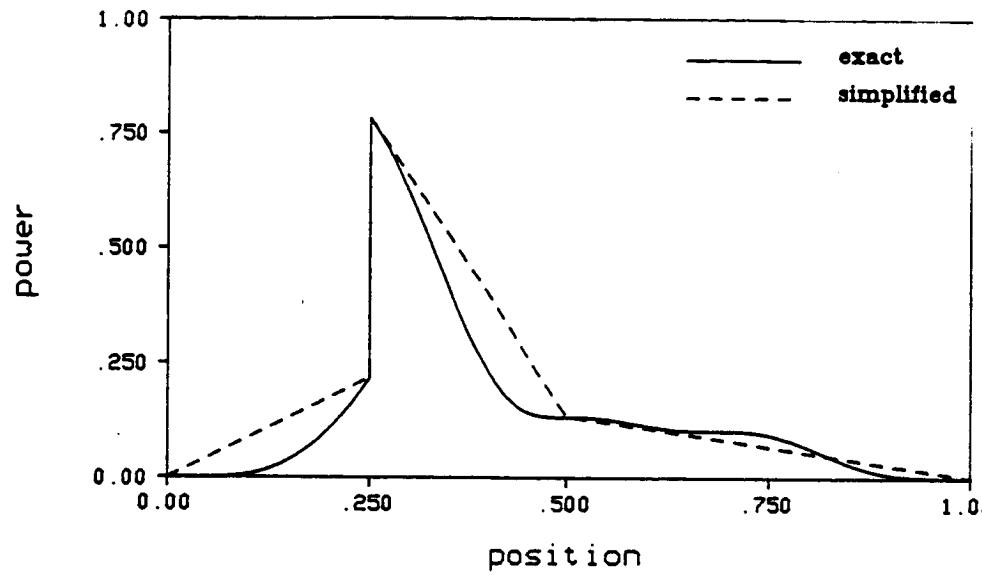

Figure 6.3.13 - Comparison of the Exact and Simplified Power Flow Solutions for the Coupled Beam System Shown in Figure (6.3.12) with ω=2300.00 rad/sec

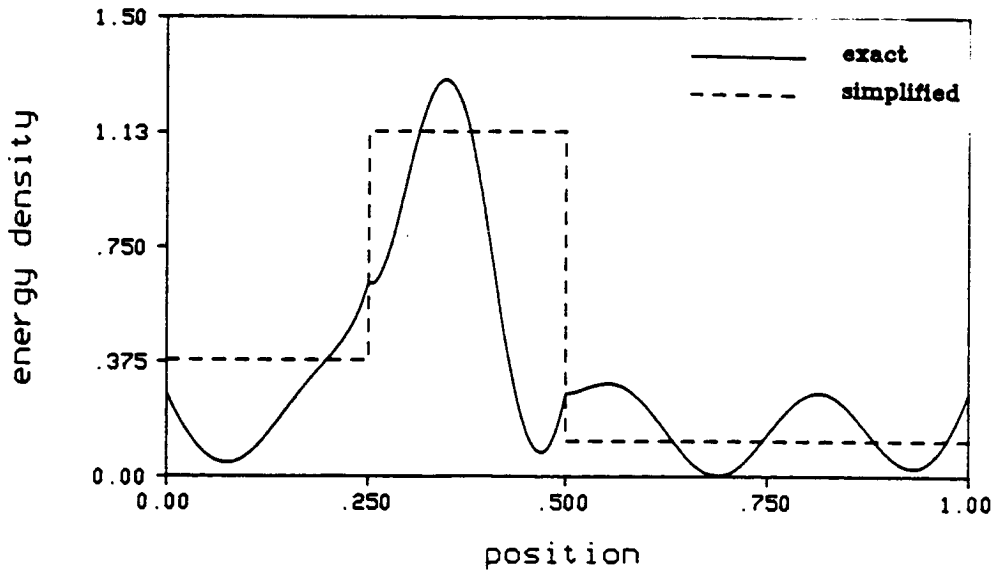

Figure 6.3.14 - Comparison of the Exact and Simplified Energy Density Solutions for the Coupled Beam System Shown in Figure (6.3.12) with ω =2300.00 rad/sec

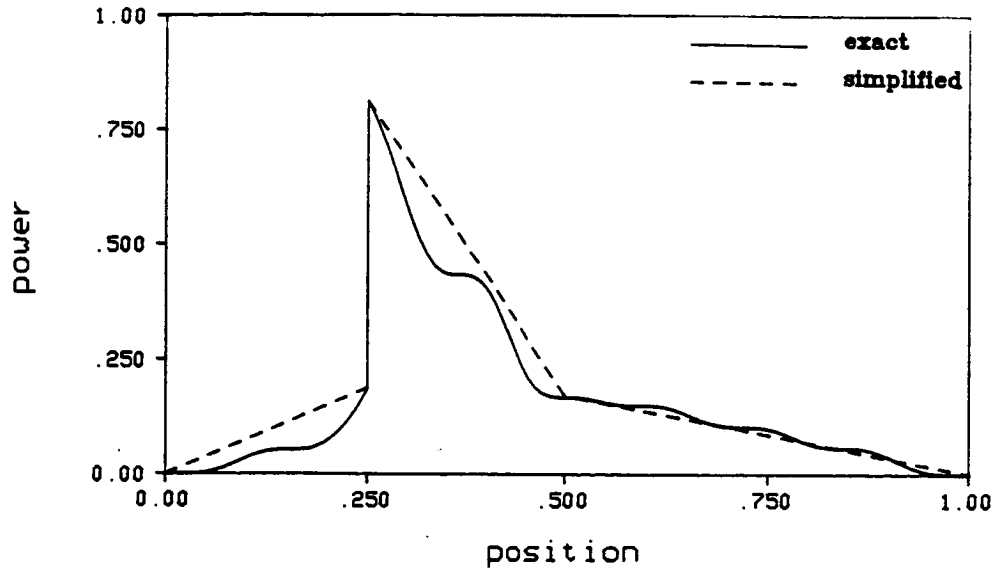

Figure 6.3.15 - Comparison of the Exact and Simplified Power Flow Solutions for the Coupled Beam System Shown in Figure (6.3.12) with ω=9197.80 rad/sec

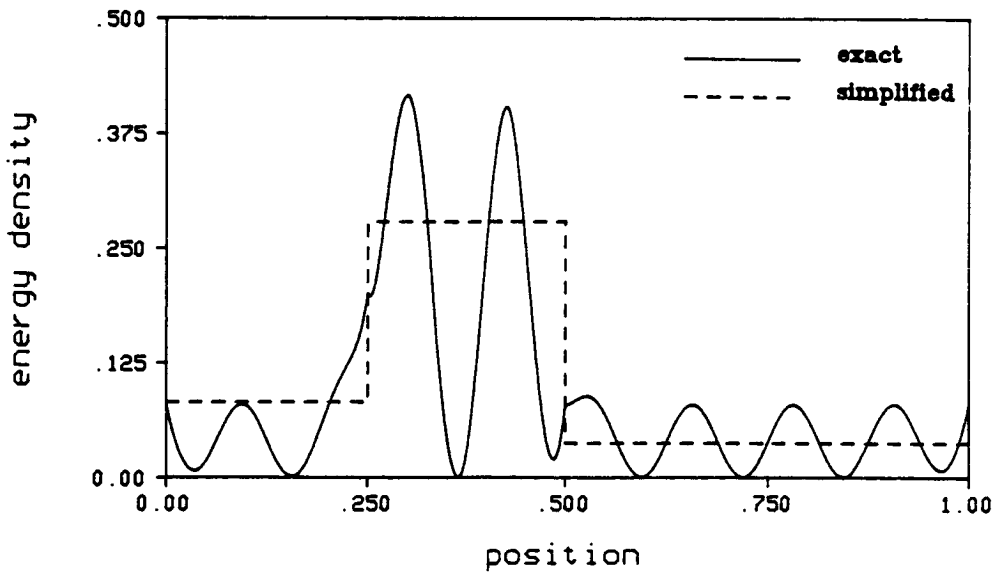

Figure 6.3.16 - Comparison of the Exact and Simplified Energy Density Solutions for the Coupled Beam System Shown in Figure (6.3.12) with ω =9197.80 rad/sec

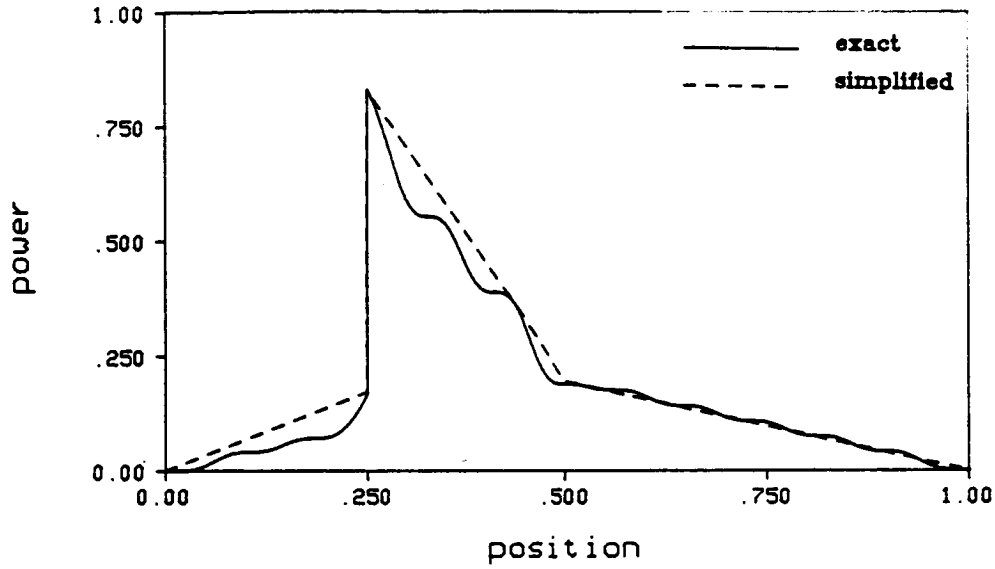

Figure 6.3.17 - Comparison of the Exact and Simplified Power Flow Solutions for the Coupled Beam System Shown in Figure (6.3.12) with ω=20695.5 rad/sec

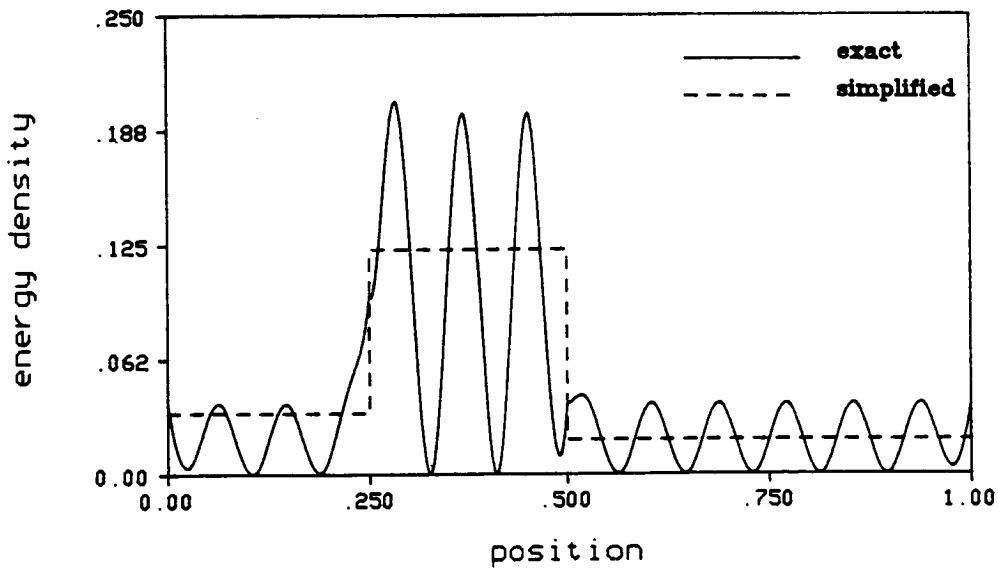

Figure 6.3.18 - Comparison of the Exact and Simplified Energy Density Solutions for the Coupled Beam System Shown in Figure (6.3.12) with ω =20695.5 rad/sec

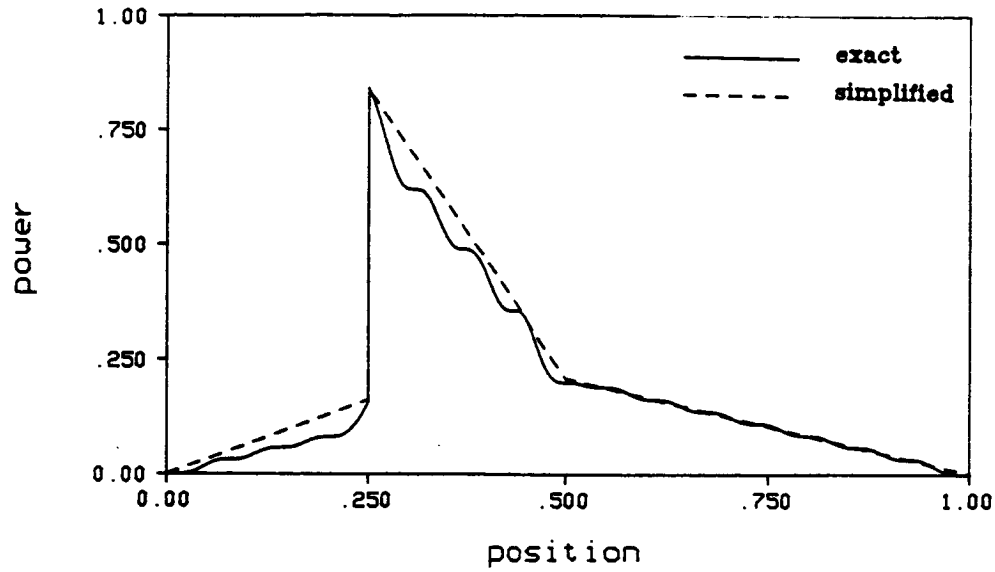

Figure 6.3.19 - Comparison of the Exact and Simplified Power Flow Solutions for the Coupled Beam System Shown in Figure (6.3.12) with ω=36792.0 rad/sec

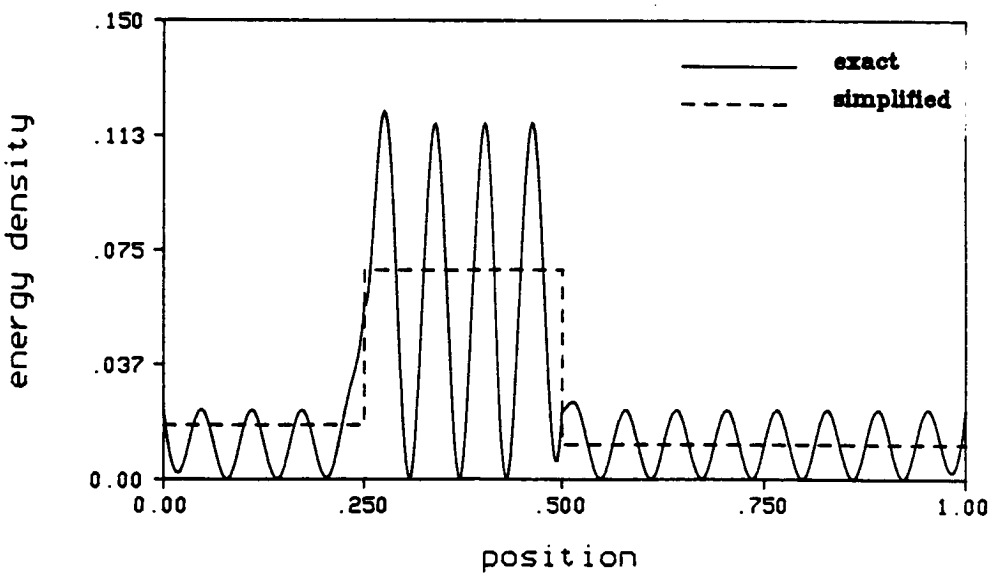

Figure 6.3.20 - Comparison of the Exact and Simplified Energy Density Solutions for the Coupled Beam System Shown in Figure (6.3.12) with ω =36792.0 rad/sec

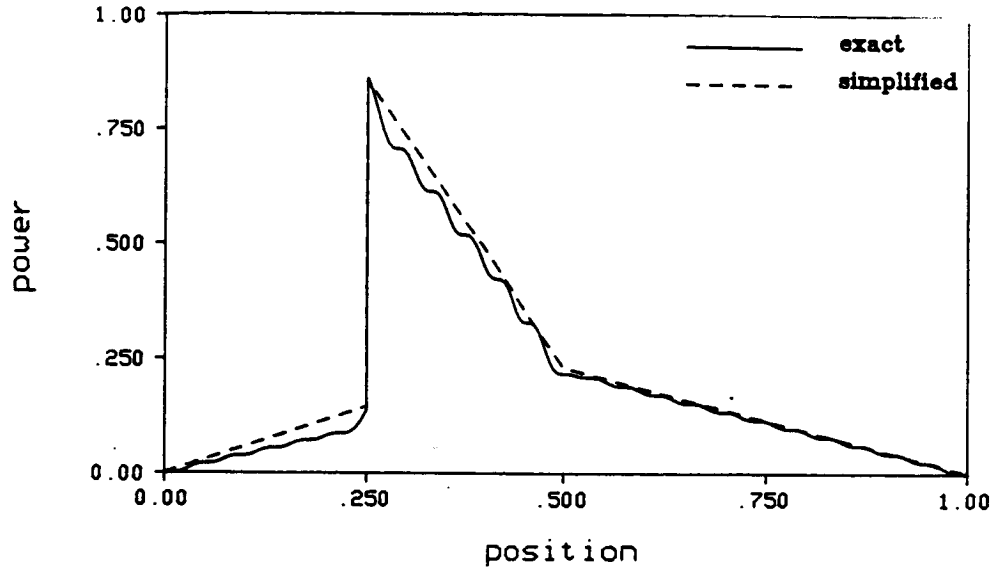

Figure 6.3.21 - Comparison of the Exact and Simplified Power Flow Solutions for the Coupled Beam System Shown in Figure (6.3.12) with ω=82781.88 rad/sec

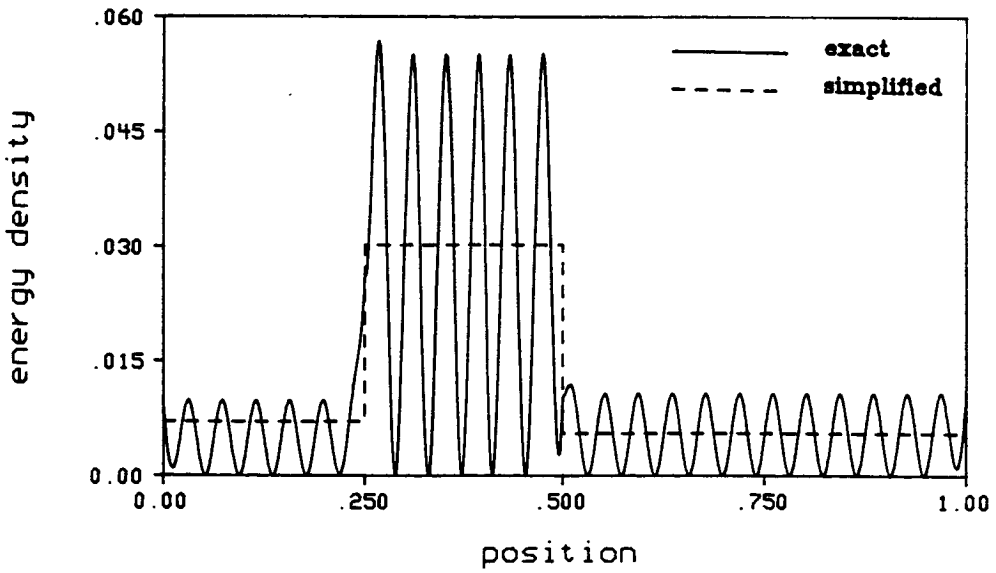

Figure 6.3.22 - Comparison of the Exact and Simplified Energy Density Solutions for the Coupled Beam System Shown in Figure (6.3.12) with ω =82781.88 rad/sec

CHAPTER 7 - CONCLUSIONS AND RECOMMENDATIONS

7.1 Conclusions

In this work, the thermal analogy proposed by Nefske and Sung [2] to model the mechanical power flow in acoustic/structural systems has been investigated. From the classical displacement solutions for harmonically excited, hysteretically damped rods and beams, power flow and energy density equations were derived. Using assumptions based on small structural damping, it was found that the mechanical power flow in rods and beams takes on some of the attributes of thermal power flow in a heat conduction problem.

Chapter 3 investigated the power flow and energy density in a longitudinally vibrating rod. Using the small damping assumption it was found that the local power flow in a rod is proportional to the local gradient in energy density, as shown in equation (3.2.31). The result in equation (3.2.31), along with the power balance on a differential control volume in the rod, led to the development of a Poisson's equation which models the energy distribution in the rod. From the governing Poisson's equation, solutions for the energy density and power flow were calculated.

The hysteretic damping model used in the simplified and exact energy solutions was also discussed in chapter 3. It was found that hysteretic damping,

in an exact analysis, models power dissipation in proportion to the kinetic energy density. The simplified theory models power dissipation in proportion to the total energy density. The difference in how the exact and simplified solutions model power dissipation explains why the exact power flow solution has harmonic components while the simplified power flow solution does not.

Chapter 4 investigated the power flow and energy density in a transversely vibrating beam. The nearfield terms in the displacement solution complicated the beam analysis. To use the thermal analogy it was found that the beam analysis had to be restricted to frequencies where the nearfield terms in the displacement solution were negligible over most of the beam. In an investigation of the power flow in a beam, Nefske and Sung [2] derived a relationship which modeled the local power flow as proportional to the gradient in local energy density. This relationship is shown in equation (4.2.60). The deterministic approach used in this study proved that because of the harmonic spatial variation in energy density, a relationship between the power flow and the gradient in energy density in a beam could be derived only if space averaged values of power flow and energy density were modeled. The correct relationship between power flow and energy density in a beam is shown in equation (4.2.59). Equation (4.2.59) was then used to derive a Poisson's equation which models the spaced averaged energy density distribution in a vibrating beam.

Difficulties encountered when coupling the power flow and energy density solutions for rods and beams were discussed in chapter 5. It was found that

resonant behavior of finite structures complicated the coupling process. The energy solutions have not yet led to an efficient and accurate coupling scheme. However, it was shown that in certain situations, the local energy densities at a coupling location can provide useful information about the dynamic response of coupled structures. Two existing methods of coupling structures were discussed. The first coupling scheme was based on the receptance method. The second method was based on the wave transmission approach. The receptance method allowed coupling of structures driven by single frequency and broadband frequency inputs. The wave transmission approach is a more efficient coupling solution than the receptance method, but it is limited to broadband frequency excitations. Both the receptance method and the wave transmission approach can be numerically implemented.

As discussed in chapter 2, Nefske and Sung did not explicitly prove a relationship between the power flow and energy density in a one dimensional structure. They could not therefore prove under what conditions the new power flow method could be used. The major contribution of this investigation is that it provides the means to determine the conditions for which the new power flow method is valid. In the development of the governing power flow and energy density equations in chapters 3 and 4, each simplifying assumption is discussed and justified. Thus, the validity of each assumption can be individually assessed, allowing one to determine whether or not the new power flow method is applicable to a given physical situation.

Statistical Energy Analysis is a global power flow analysis. It cannot be used to predict spatial variations of energy density and power flow in a given subsystem. The simplified power flow method however, is a local analysis. It can be implemented to describe the local variations in energy density and power flow, which would be particularly useful in cases of multiple local power inputs and local damping treatments. In addition, while SEA is limited to broadband frequency excitation, the simplified power flow solutions can be used in situations where the system response is dominated by resonant behavior.

The power flow examples in chapter 6 proved that the simplified theory could yield accurate predictions of the energy density levels in both rods and beams. From the results in chapter 6, it was concluded that the new power flow method can be used to bridge the mid-frequency range gap where the finite element method is inefficient and Statistical Energy Analysis is unreliable.

7.2 Recommendations

To apply the results for power flow and energy density solutions in chapters 3 and 4, an efficient and accurate coupling scheme must be developed. Work should be continued towards developing a relationship between the local energy densities at a coupling location using the energy relationships developed in section 5.2.

Since the nearfield effects are always important near a discontinuity, it will be necessary to include the nearfield effects when developing local coupling methods for beams. A more complicated analysis of equations (4.2.48) and

(4.2.49) might yield an accurate coupling solution for beams. Perhaps the interactions of two connected beams near a coupling junction can be described by uncoupled farfield and nearfield energy density and power flow expressions.

Once an efficient coupling procedure is developed, the simplified power flow analysis could be easily implemented numerically. Since the governing equations for the simplified power flow analyses are Poisson equations, they are easily solved by a standard heat transfer finite element code as demonstrated by Nefske and Sung.

Finally, power flow equations similar to those developed in chapters 3 and 4 for other types of structures, such as two dimensional plates and three dimensional spaces should be developed. Such studies might provide some insight not found in the one dimensional analyses.

LIST OF REFERENCES

LIST OF REFERENCES

[1] Lu,L.K.H., "Optimum Damping Selection by Statistical Energy Analysis", *Statistical Energy Analysis NCA-Vol.3*, edited by Hsu,K.H., Nefske,D.J., Adnan,A., ASME Winter Annual Meeting, December 13-18, 1987, Boston, MA, pp. 9-14.

[2] Nefske, D.J., Sung, S.H., "Power Flow Finite Element Analysis of Dynamic Systems: Basic Theory and Application to Beams", *Statistical Energy Analysis NCA-Vol.3*, edited by Hsu,K.H., Nefske,D.J., Adnan,A., ASME Winter Annual Meeting, December 13-18, 1987, Boston, MA, pp. 47-54.

[3] Woodhouse,J., "An Introduction to Statistical Energy Analysis of Structural Vibration", *Applied Acoustics*, 14, 1981, pp. 455-469.

[4] Reddy,J.N., *An Introduction to the Finite Element Method*, New York, McGraw-Hill, 1984, pp. 135-140.

[5] Rayleigh, Lord, *Theory of Sound*, New York, Dover Publications Inc., 1945, Vol 2, pp. 192-196.

[6] Lyon,R.H., Maidanik,G., "Power Flow Between Linearly Coupled Oscillators", *J. Acoust. Soc. Am.*, 34(5), 1962, pp. 623-639.

[7] Lyon, R.H., *Statistical Energy Analysis of Dynamical Systems*, Cambridge, MA, MIT Press, 1975.

[8] Cremer,L., Heckl,M., Ungar,E.E., *Structure-Borne Sound*, Berlin, Springer-Verlog, 1973, pp. 282-297.

[9] Maidanik,G., "Some Elements in Statistical Energy Analysis", *J. Sound Vibration*, 52(2), 1977, pp. 171-191.

[10] Fahy,F., *Sound and Structural Vibration: Radiation, Transmission and Response*, London, Academic Press, 1985.

[11] *SEAM'S User Manual*, Cambridge Collaborative Inc., Cambridge, MA, 1986.

[12] R.W. Trendell, L.I.,Yano, *Statistical Energy Analysis Computer User's Guide, COSMIC*, Program Number MFS-27035, November, 1981.

[13] Ranky,M.F., Clarkson,B.L., "Frequency Average Loss Factors of Plates and Shells", *J. Sound Vibration*, 89(3), 1983, pp. 309-323.

[14] Clarkson,B.L., Pope,R.J., "Experimental Determination of Modal Densities and Loss Factors of Flat Plates and Cylinders", *J. Sound Vibration*, 77(4), pp. 535-549.

[15] Scharton,T.D., Lyon,R.H., "Power Flow and Energy Sharing in Random Vibration", *J. Acoust. Soc. Am.*, 43(6), 1968, pp. 1332-1343.

[16] Pinnington,R.J., White,R.G., "Power Flow Through Machine Isolators to Resonant and Non-Resonant Beams", *J. Sound Vibration*, 75(2), 1981, pp. 179-197.

[17] Remington,P.J., Manning,J.E., "Comparison of Statistical Energy Analysis Power Flow Predictions with an Exact Calculation", *J. Acoust. Soc. Am.*, 57(2), 1975, pp. 374-379.

[18] Newland,D.E., "Power Flow Between a Class of Coupled Oscillators", *J. Acoust. Soc. Am.*, 43(3), 1968, pp. 553-559.

[19] Newland,D.E., "Calculation of Power Flow Between Coupled Oscillators", *J. Sound Vibration*, 3(3), 1966, pp. 262-276.

[20] Crandall,S.H., Lotz,R. "On the Coupling Loss Factor in Statistical Energy Analysis", *J. Acoust. Soc. Am.*, 49(1), 1971, pp. 352-356.

[21] Davies,H.G., Wahab,M.A., "Ensemble Averages of Power Flow in Randomly Excited Coupled Beams", *J. Sound Vibration*, 77(3), 1981, pp. 311-321.

[22] Ghering,W.L., Raj,D., "Comparison of Statistical Energy Analysis Predictions with Experimental Results for Cylinder-Plate-Beam Structures", *Statistical Energy Analysis NCA-Vol.3*, edited by Hsu,K.H., Nefske,D.J., Adnan,A., ASME Winter Annual Meeting, December 13-18, 1987, Boston, MA, pp. 81-90.

[23] Brooks,J.E., Maidanik,G., "Loss and Coupling Loss Factor of Two Coupled Dynamic Systems", *J. Sound Vibration*, 55(3), 1977, pp. 315-325.

[24] Bies,D.A., Hamid,S. "In Situ Determination of Loss and Coupling Loss Factors by the Power Injection Method", *J. Sound Vibration*, 70(2), 1980, pp. 187-204.

[25] Goyder,H.G.D., White,R.G., "Vibrational Power Flow From Machines into Built-Up Structures: Parts I-III", *J. Sound Vibration*, 68(1), 1980, pp. 59-117.

[26] Skudrzyk,E.J., "Vibrations of a System with a Finite or an Infinite Number of Resonances", *J. Acoust. Soc. Am.*, 30(12), 1958, pp. 1140-1152.

[27] Belov,V.D., Rybak,S.A., Tartakovskii,B.D., "Propagation of Vibrational Energy in Absorbing Structures", *Soviet Physics Acoustics*, 23(2), 1977, pp. 115-119.

[28] McCormick,C.W., ed. MSC/NASTRAN *User's Manual*, MSR-39, The Macneal-Schwendler Corp., Los Angeles, CA, 1978.

[29] Soedel,W., *Vibrations of Shells and Plates* , New York, Marcel Dekker Inc., 1981.

[30] Kinsler, L.E., Frey, A.R., Coppens, A.B., Sanders,J.V., *Fundamentals of Acoustics*, New York, John Wiley & Sons, 1982, p. 14.

[31] Achenbach, J.D., *Wave Propagation in Elastic Solids*, New York, American Elsevier Publ. Co. Inc., 1973, p. 34.

[32] Lazan,B.,J., *Damping of Materials and Members in Structural Mechanics*, Great Britain, Pergoman Press, 1968, pp. 215-221.

[33] Snowdon, J.C., *Vibration and Shock in Damped Mechanical Systems*, New York, John Wiley & Sons, 1968, pp. 194-200.

[34] Pavic,G., "Measurement of Structure Borne Wave Intensity, Part I: Formulation of Methods", *J. Sound Vibration*, 49(2), 1976, pp. 221-230.

[35] Noiseux,D.U., "Measurement of Power Flow in Uniform Beams and Plates", *J. Acoust. Soc. Am.*, 47(1)II, 1969, pp. 238-247.

[36] Incropera,F.P., DeWitt,D.P., *Fundamentals of Heat and Mass Transfer*, New York, John Wiley & Sons, 1985, pp. 99-103.

[37] Cusheri, J.M., "Power Flow as a Compliment to SEA and Finite Element Analysis", *Statistical Energy Analysis NCA-Vol.3*, edited by Hsu,K.H., Nefske,D.J., Adnan,A., ASME Winter Annual Meeting, December 13-18, 1987, Boston, MA, pp. 55-62.

[38] Lyon,R.H., "The SEA Population Model - Do We Need a New One?", *Statistical Energy Analysis NCA-Vol.3*, edited by Hsu,K.H., Nefske,D.J., Adnan,A., ASME Winter Annual Meeting, December 13-18, 1987, Boston, MA, p. 1.